Properties of heavy hadrons studied with a chiral effective model of diquarks

金, 龍熙

出版情報：Kyushu University, 2023, 博士（理学）, 課程博士
バージョン：
権利関係：

Properties of heavy hadrons studied with a chiral effective model of diquarks

Yonghee Kim

Theoretical Nuclear Physics, Department of Physics
Graduate School of Science, Kyushu University
744, Motooka, Nishi-Ku, Fukuoka 819-0395, Japan

February 9, 2024

Abstract

Quarks are one of the elemental particles, and are the fundamental constituents of matter. Quarks have six types which is called flavor, and they are classified as up (u) and down (d) in first generation, charm (c) and strange (s) in second generation, and top (t) and bottom (b) in third generation. The mass range of these quarks are about $2 - 1.73 \times 10^5$ MeV. In particular, masses of u, d, s quarks are about $2 - 100$ MeV, so that these three are often treated as light quarks ($q = u, d, s$). Light quarks have the approximate flavor symmetry called the chiral symmetry. When this chiral symmetry is spontaneously broken, the light quarks gain masses for about $300 - 500$ MeV. This accounts for the effective mass of quarks when quarks form hadrons. Hence the spontaneous chiral symmetry breaking is the big origin of hadron masses.

Chiral effective theory enables us to recognize the dynamical generation of particle masses from the viewpoint of chiral symmetry breaking. This theory can be constructed for light quarks, and also the group of two light quarks called diquarks. Diquarks are firstly considered in 1960s at the same time with quarks, and nowadays, they are applied as the simplest colorful substructure of hadrons. Diquarks are also studied for the color superconductivity with low temperature and high density, which are frequently considered from 1990s.

For the usage of diquarks, singly heavy baryons composed of one heavy quark ($Q = c, b$) and two light quarks are the good example. They are expected to describe a diquark picture by two light quarks (qq), so that these baryons are also useful to investigate the properties of diquarks. Another hadron which is able to form diquarks as constituents is T_{QQ} tetraquarks. This is composed of two heavy quarks and two light anti-quarks, so that they can recognize as three body systems with one anti-diquark ($\bar{q}\bar{q}$) and two heavy quarks.

In this work, the chiral effective model of diquarks consist of two light quarks are formulated. This model is applied to energy spectra and decay reactions of singly heavy baryons. The theoretical results of these baryons are summarized for comparisons with other data and discussions. Moreover, T_{QQ} tetraquark states are also investigated with this chiral diquark model. The content in this paper is summarized in Refs. [1–4] as below.

- Y. Kim, E. Hiyama, M. Oka, and K. Suzuki, Phys. Rev. D **102**, 014004 (2020), "Spectrum of singly heavy baryons from a chiral effective theory of diquarks"
- Y. Kim, Y. -R. Liu, M. Oka, and K. Suzuki, Phys. Rev. D **104**, 054012 (2021), "Heavy baryon spectrum with chiral multiplets of scalar and vector diquarks"
- Y. Kim, M. Oka, D. Suenaga, and K. Suzuki, Phys. Rev. D **107**, 074015 (2023), "Strong decays of singly heavy baryons from a chiral effective theory of diquarks"
- Y. Kim, M. Oka, and K. Suzuki, Phys. Rev. D **105**, 074021 (2022), "Doubly heavy tetraquarks in a chiral-diquark picture"

Contents

List of Figures

List of Tables

Chapter 1

Introduction

1.1 Quantum chromo-dynamics (QCD)

In the world we live, there are many kinds of matter around us. They are filled with various atoms, which are the basic particles of the chemical elements. In 1911, E. Rutherford and his colleagues conducted the experiment of Coulomb scattering with using the alpha particles, and found the structure of atoms which consist of a nucleus surrounded by orbiting electrons [5]. Moreover, in experimental ways, Rutherford discovered the proton in 1918, and J. Chadwick discovered the neutron in 1932 [6], which are the components of the nucleus. These protons and neutrons are collectively called nucleons. Although the mass of an atom is mostly from a nucleus inside, the size of a nucleus is much smaller than the atom. Nucleons are bounded in this small dense nucleus by the nuclear force based on the strong interaction.

As well as electrons, there are many elemental particles such as quarks and gluons inside nucleons, and also muons and neutrinos for others. About these elemental particles, there are four types of forces working between them: gravitational, electromagnetic, weak and strong interactions. In particular, the unified theory of electromagnetic, weak and strong interactions is the standard model of the elemental particles.

The theoretical physics for the strong interaction is the "quantum chromo-dynamics (QCD)", which is a type of the non-abelian gauge theory with symmetry group $SU(3)$. This theory shows the strong interaction between quarks meditated by gluons. The origin of quarks is the quark model proposed by M. Gell-Mann [7] and G. Zwieg [8, 9] independently in 1964, which explains many newly discovered hadrons as bound states of some constituent particles. Moreover, the color charge as the new quantum number for quarks is introduced by M. Y. Han and Y. Nambu in 1965 [10], which can guarantee the existence of baryons such as Δ^{++} in baryon decuplet [11]. For another quantum number, there are six kinds of quarks called flavor, and are named as "up (u)", "down (d)", "strange (s)", "charm (c)", "bottom (b)", and "top (t)". Properties of each quark are listed in Table 1.1, which are quoted from Particle Data Group (PDG) [12].

1.1.1 QCD Lagrangian

The conventional Lagrangian of QCD is expressed with the quark field q and the gluon field A^a_μ with the indices of space-time $\mu = 0, 1, 2, 3$ and color $a = 1, 2, ..., 8$ as

$$\mathcal{L}_{\mathrm{QCD}} = \sum_{f=u,d,\ldots,t} \bar{q}_f (i\gamma^\mu \mathcal{D}_\mu - m_f) q_f - \frac{1}{4} G^{\mu\nu}_a G^a_{\mu\nu}, \ \bar{q}_f = q^\dagger_f \gamma^0, \tag{1.1}$$

$$G^{\mu\nu}_a = \partial^\mu A^\nu_a - \partial^\nu A^\mu_a + g f_{abc} A^\mu_b A^\nu_c. \tag{1.2}$$

Quark	Mass	Charge	I_z	S	C	B	T
up (u)	$2.16^{+0.49}_{-0.26}$ MeV	$+2/3e$	$+1/2$	0	0	0	0
down (d)	$4.67^{+0.48}_{-0.17}$ MeV	$-1/3e$	$-1/2$	0	0	0	0
strange (s)	$93.4^{+8.6}_{-3.4}$ MeV	$-1/3e$	0	-1	0	0	0
charm (c)	1.27 ± 0.02 GeV	$+2/3e$	0	0	+1	0	0
bottom (b)	$4.18^{+0.03}_{-0.02}$ GeV	$-1/3e$	0	0	0	-1	0
top (t)	$162.5^{+2.1}_{-1.5}$ GeV	$+2/3e$	0	0	0	0	+1

Table1.1 List of quarks, where I_z, S, C, B, T are the third component of isospin, strangeness, charm, bottom and top as quantum number, respectively. u, d, s masses are current quark mass. c and b quark masses are running mass in $\overline{\mathrm{MS}}$ renormalization scheme. t quark mass is $\overline{\mathrm{MS}}$ mass from cross-section measurements.

About the quart part (first term) of Eq. (1.1), $\gamma^i (i = 0, 1, 2, 3)$ shows the Dirac gamma matrices in the four dimensional space-time. $\mathcal{D}_\mu = \partial_\mu + igA^a_\mu T^a$ is the color gauge covariant derivative, where g denotes the dimensionless gauge coupling constant of strong interaction representing the strength of couplings between a quark, an anti-quark, and a gluon. T^a are the generators of $SU(3)$ group expressed with the Gell-Mann matrices λ^a as $T^a = \lambda^a/2$. Also, m_f stands for the current quark mass of each flavor. Showing the color index as $\alpha = R, G, B$, the quark part of Eq. (1.1) is given by

$$\begin{aligned}
&\sum_{f=u,d,\ldots,t} \bar{q}^\alpha_f \left(\delta^{\alpha\beta}\{i\gamma^\mu\partial_\mu - m_f\} - g\gamma^\mu (A^a_\mu T^a)^{\alpha\beta} \right) q^\beta_f \\
&= \sum_{f=u,d,\ldots,t} (\bar{q}^R_f, \bar{q}^G_f, \bar{q}^B_f) \left\{ (i\gamma^\mu\partial_\mu - m_f) \begin{pmatrix} 1 & 0 & 0 \\ 0 & 1 & 0 \\ 0 & 0 & 1 \end{pmatrix} - g\gamma^\mu (A^a_\mu T^a)^{\alpha\beta} \right\} \begin{pmatrix} q^R_f \\ q^G_f \\ q^B_f \end{pmatrix}. \qquad (1.3)
\end{aligned}$$

From this expression, we can see that the terms proportional to the 3-dimensional unit matrix are conserved under the flavor f and color α in a quark q^α_f and an anti-quark $\bar{q}^\alpha_f$. For the other terms where the gluon field $A^a_\mu T^a$ interferes, those quark and anti-quark fields change their colors. Therefore, Eq. (1.3) implies the color transformation of quarks via the absorption and emission of gluons.

Eq. (1.2) represents the strength of gluon field in the gluon part (second term) of Eq. (1.1), where f_{abc} is the structure constant for $SU(3)$ group. In this expression, the third term with the constant f_{abc} indicates that gluons also participate in the strong interaction by their color charges. In detail, the gluon part of Eq. (1.1) can be expressed with gluon fields as

$$\begin{aligned}
-\frac{1}{4}G^{\mu\nu}_a G^a_{\mu\nu} =& -\frac{1}{4}(\partial^\mu A^\nu_a - \partial^\nu A^\mu_a)(\partial_\mu A^a_\nu - \partial_\nu A^a_\mu) \\
& - g f_{abc} A^\mu_b A^\nu_c \partial^\mu A^\nu_a - \frac{g^2}{4} f_{abe} f_{cde} A^\mu_a A^\nu_b A^c_\mu A^d_\nu, \qquad (1.4)
\end{aligned}$$

where the first term shows the non-interacting propagation of gluons, and the second and third terms proportional to g or g^2 corresponds to the self-interaction term of gluons. This self-interaction of gauge fields does not exist in quantum electro-dynamics (QED), because photons do not have their own electric charges and cannot interfere in the electromagnetic interaction themselves. Hence, this becomes the reason why QCD is harder than QED to analyze.

1.1.2 Asymptotic freedom

One of the representative properties of QCD is the "asymptotic freedom". This phenomenon is discovered by D. J. Gross, F. Wilczek , H. D. Politzer, and G. 't Hooft in 1973 [13, 14], after G. 't Hooft proved the renormalizability of Yang-Mills theory (non-abelian gauge theory) in 1971 [15, 16]. This is about the feature of the strong interaction between quarks and gluons, in which its strength becomes weaker as the energy scale increases, in other words, as the corresponding length decreases. Thus, if quarks interact weakly at high energies (momenta) and short distances, the application of perturbative calculation will be allowed. On the contrary, the strong interaction becomes stronger at low energies (momenta) and long distances, so that there are non-perturbative phenomena in the low energy regions and long ranges of QCD. These correlations are inversely related to the electromagnetic interaction in QED.

In concrete, the energy scale μ dependence of the QCD coupling constant, $g(\mu)$, is expressed by the renormalization group equation. When this equation is solved by the perturbative calculation with only the low-dimensional term, the coupling constant in the 1-loop level is given as

$$\alpha_s(\mu) \equiv \frac{g^2(\mu)}{4\pi} \simeq \frac{12\pi}{(33-2N_f)\ln(\mu^2/\Lambda_{\mathrm{QCD}}^2)}. \tag{1.5}$$

Here N_f denotes the number of flavors whose value is 6 when all the observed quarks from u to t is considered. Λ_{QCD} is the integral constant called the "QCD scale" whose value is about 200 MeV, and this constant corresponds to a typical energy scale of the low energy QCD. From Eq. (1.5), we can find that the coupling constant converges to zero when the energy scale increases as $\lim_{\mu\to\infty}\alpha_s(\mu) = 0$, in which the asymptotic freedom is comfirmed. On the other hand, the coupling constant increases as the energy scale decreases, and it diverges to infinity at the point of $\mu = \Lambda_{\mathrm{QCD}}$ as $\lim_{\mu\to\Lambda_{\mathrm{QCD}}}\alpha_s(\mu) = +\infty$. This error implies that the perturbation theory is useless in the low energy QCD.

1.1.3 Color confinement and hadrons

Another properties of QCD is the "color confinement" of quarks and gluons in the low energy regions, which represents that the color-charged particles such as a quark and a gluon cannot be isolated. In other words, quarks and gluons are only observed as the compositions with white color called "hadrons". There are many hadron states, because they can be diversified with the combination of quarks including several quantum numbers such as flavor, spin, and orbital angular momentum. Classification of these various hadrons is generally called "hadron spectroscopy", which is important in the low energy QCD and hadron physics with many unsolved problems.

There are two types of conventional hadrons: One is the "meson" which forms the pair of one quark and one anti-quark ($\bar{q}q$). The other type is the "baryon" which is composed of three quarks (qqq), as well as the "anti-baryon" made from three anti-quarks ($\bar{q}\bar{q}\bar{q}$). In these days, about 200 mesons and 150 baryons are experimentally discovered [12].

Moreover, in principle, it is possible to make many other hadron states with more quarks and anti-quarks, such as "tetraquarks" ($\bar{q}\bar{q}qq$), "pentaquarks" ($\bar{q}qqqq$), "dibaryons" ($\bar{q}\bar{q}\bar{q}qqq$), and so on. Furthermore, "glueballs" (gg, ggg, ...) made by only gluons g or quark-gluon hybrid states ($\bar{q}qg, \ldots$) are allowed as another types of hadron. However, these composite particles are not experimentally identified yet, and they are collectively called "exotic hadrons". From 21st century, some of them are experimentally observed as candidates, which are difficult to explain with meson or baryon pictures.

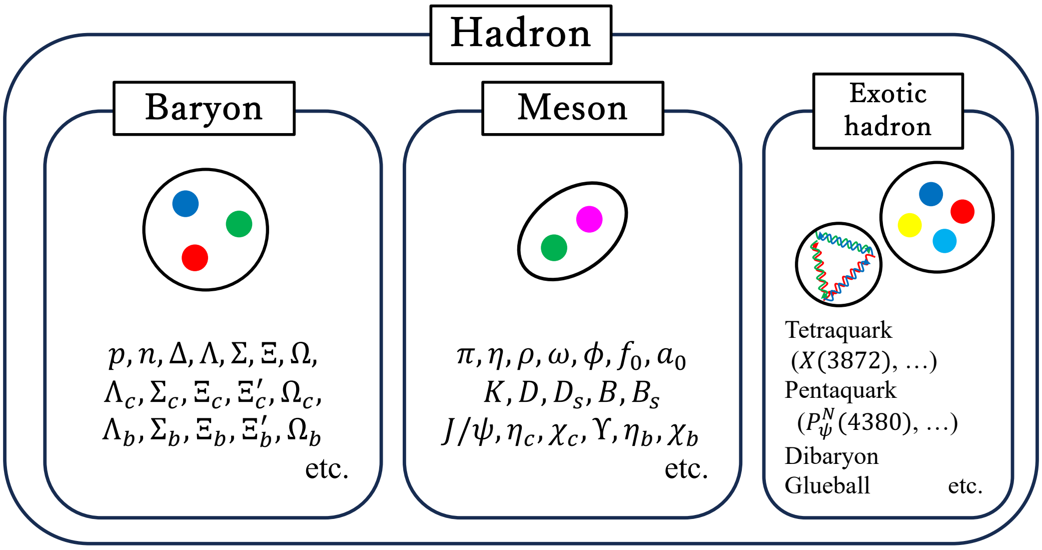

Figure1.1 The schematic picture of the group of hadrons classified into baryons, mesons, and the others (exotic hadrons).

1.1.4 QCD phase diagram

Not only the QCD itself but also the QCD in some external fields, as well as in the vacuum state, is one of interesting subjects. This is equivalent to see the quark matter and its transition in some extreme environments, which is not well known neither theoretically nor experimentally. In Fig. 1.2, the phase diagram of QCD vacuum is simply described, where the external fields are determined by temperature on the vertical axis and density on the horizontal axis. There are three main phases:

Hadron phase
The well-known QCD phase at low temperature and density, where the color confinement is still working to quarks and gluons and thus those elemental particles are restricted to form color singlet hadron states.

Quark-gluon plasma (QGP) phase
The QCD phase at finite temperature, where the elements of hadrons such as quarks and gluons are not confined under the strong interaction. This is near to the environment shortly after the big bang.

Color superconducting phase
The expected QCD phase at low temperature and enough high density, where two quarks condense by forming Cooper pairs and is also called diquark condensate.

For more details about QCD phase diagram, see Ref. [17–23].

1.2 Spontaneous chiral symmetry breaking

The spontaneous chiral symmetry breaking is one of the salient properties of the non-perturbative phenomenon in low energy QCD, which mainly acts to the mass generation

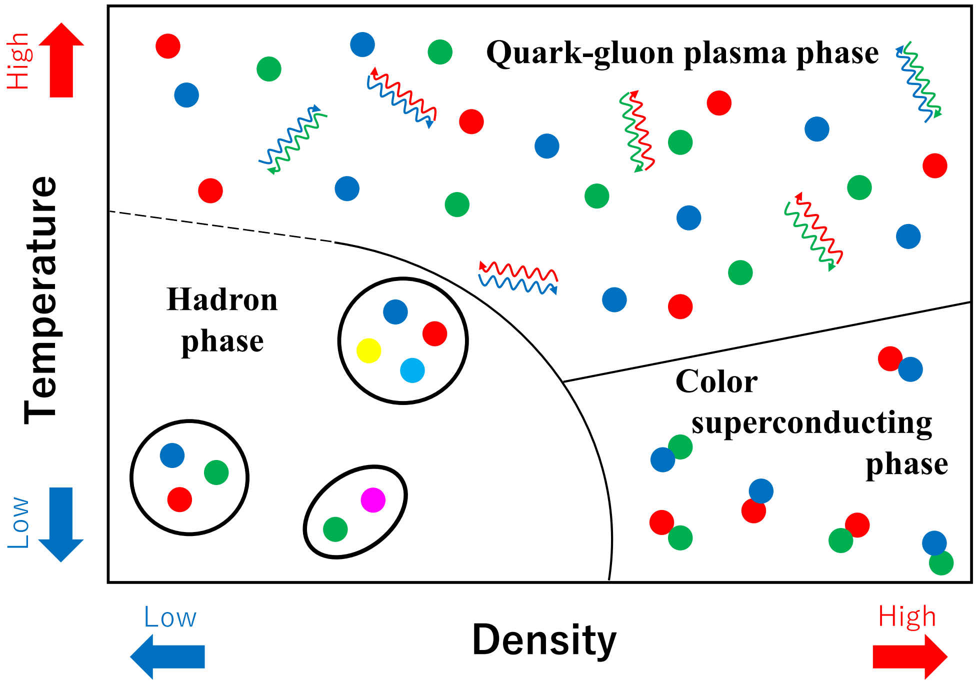

Figure1.2 The outline of expected QCD phase diagram. The dotted and solid border lines between each phase are the crossover line and the first-order line, where the phase transition occurs continuously or discontinuously, respectively.

of quarks inside hadrons. It is apparently seen in nucleons, where mostly 99 percent of nucleon masses (~ 940 MeV) are from this phenomenon and the total mass of three u, d quarks is only about 10 MeV. As these u, d quarks inside hadrons, the effect of spontaneous chiral symmetry breaking becomes larger as the quark mass becomes lighter.

About the masses of quarks, it is conventional to classify the flavor of quarks into light and heavy ones on the basis of the non-perturbative scale of dynamical chiral symmetry breaking which is around 1 GeV [24, 25]. Therefore, according to Table 1.1, it comes down that u, d and s quarks, whose current quark masses are lighter than 1 GeV, are conventionally classified to the "light" quarks in which the spontaneous chiral symmetry breaking is dominant. On the other hand, about the c, b, and t quarks whose current quark masses are heavier than 1 GeV, they are conventionally called the "heavy" quarks in which the chiral symmetry breaking induced by the bare quark masses, also called the "explicit" chiral symmetry breaking, is dominant.

1.2.1 Chiral symmetry

Chiral symmetry is an approximate symmetry which holds for light quarks ($q = u, d, s$). This symmetry appears when the quark masses m_f vanishes from the QCD Lagrangian (1.1). To consider about this symmetry, quarks are classified into the "right-handed" and "left-handed" particles, q_R and q_L. With the quark field q, these two types are expressed with the chiral projection operators, P_R and P_L, defined as below.

$$\begin{aligned} &q = q_R + q_L, \\ &q_{R/L} \equiv P_{R/L}q = \frac{1 \pm \gamma_5}{2}q,\ \gamma_5 = i\gamma^0\gamma^1\gamma^2\gamma^3, \\ &P_{R/L}^2 = P_{R/L},\ P_R P_L = 0,\ P_R + P_L = I_4. \end{aligned} \tag{1.6}$$

About γ_5, its square is $(\gamma_5)^2 = I_4$ where I_n denotes the n-dimensional unit matrix, so that the eigenvalues of γ_5 becomes ± 1. These two eigenvalues ± 1 are called "chirality", and the right and left-handed quarks are the eigenvectors of γ_5 since $\gamma_5 q_{R/L} = \pm q_{R/L}$. In other words, these right and left-handed quarks have the positive and negative chirality, respectively. Also, the product of two different chiral projection operators is $P_R P_L = 0$, so that these right and left components are orthogonal each other.

About the type of chirality ± 1 associated to the right and/or left-handed quarks, this is similar to the physical quantity called "helicity". The helicity h of a particle stands for the direction of spin vector $\boldsymbol{s}$ based on the direction of momentum vector $\boldsymbol{p}$, which is expressed as $h = (\boldsymbol{s} \cdot \boldsymbol{p})/|\boldsymbol{s}||\boldsymbol{p}|$. In particular, the helicity takes the positive value ($h = +1$) when the directions of vectors $\boldsymbol{s}$ and $\boldsymbol{p}$ are the same, and it becomes negative ($h = -1$) when these vectors are in opposite direction. This sign of helicity resembles to that of chirality showing whether a particle is right or left-handed.

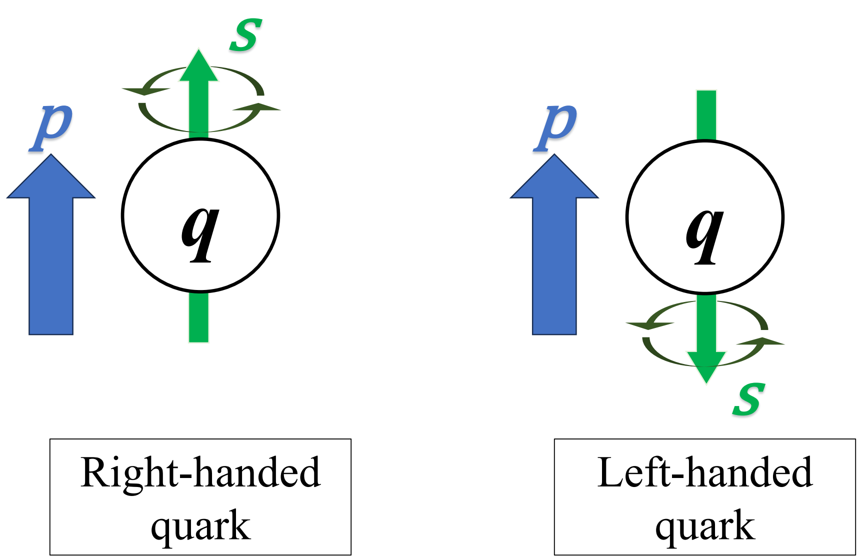

Figure1.3 Right-handed and left-handed quarks distinguished by the helicity. The vectors p and s denote the momentum and spin, respectively.

When the particle is massless ($m_f \to 0$), the sign of chirality and helicity can be identified with each other. This is because the massless particle can move with the fastest speed of light, so that the relation between spin and momentum directions are the same for all observers. This idealized limit of particle mass, where helicity is regarded as chirality, is called "chiral limit". With this limit, we can see the right and left-handed particles as the different types from each other. Hence, the chiral symmetry is the approximate symmetry for right and left-handed quarks appearing by the chiral limit (massless particle) assumption.

For each of right and left-handed quark $q_{R/L}$, the chiral transformation is defined as

$$\mathrm{Ch}: q_{R/L} \to U_{R/L} q_{R/L} \ , \ U_{R/L} = \exp(i\theta^a_{R/L} T^a) \in U(N_f)_{R/L}, \tag{1.7}$$

where the transformation matrix $U_{R/L}$ is the $N_f \times N_f$ unitary matrix in $U(N_f)_{R/L}$ group with N_f flavor, meaning the rotation of the right and left-handed quarks $q_{R/L}$ independently in the flavor space. The number of flavors is often chosen as $N_f = 2$ for u, d quarks or $N_f = 3$ for u, d, s quarks. In the chiral limit ($m_f \to 0$), the quark part of QCD Lagrangian is written with $q_{R/L}$ as

$$\mathcal{L}_{\text{quark}} = \sum_f \left[i\bar{q}_{f,R}\gamma^\mu \mathcal{D}_\mu q_{f,R} + i\bar{q}_{f,L}\gamma^\mu \mathcal{D}_\mu q_{f,L} \right]. \tag{1.8}$$

We can find from this expression that the QCD Lagrangian without the mass term is invariant under the chiral transformation in Eq. (1.7). On the other hand, if the mass term for light quarks exists as in reality, the QCD Lagrangian becomes

$$\mathcal{L}_{\text{quark}} = \sum_f \left[i\bar{q}_{f,R}\gamma^\mu \mathcal{D}_\mu q_{f,R} + i\bar{q}_{f,L}\gamma^\mu \mathcal{D}_\mu q_{f,L} - m_f(\bar{q}_{f,R} q_{f,L} + \bar{q}_{f,L} q_{f,R}) \right], \tag{1.9}$$

in which its Lagrangian is not invariant under the chiral transformation (1.7) because of the mixture of right and left-handed quark fields in the mass term. Thus, Eq. (1.9) implies the explicit chiral symmetry breaking caused by the existence of current quark masses ($m_f \neq 0$).

1.2.2 Chiral condensation

Even if the chiral symmetry is satisfied by the chiral limit, the chiral symmetry is spontaneously broken in the ordinary vacuum state, which leads to the dynamical mass generation of hadrons. At this time, the constituent quarks inside hadrons earn masses and become heavier than those current quark masses. The origin of the spontaneous chiral symmetry breaking is "chiral condensation" with the order parameter $\langle \bar{q}q \rangle$. This symbol stands for the vacuum expectation value (VEV) of scalar mesons composed of one right(left)-handed quark and one left(right)-handed anti-quark, whose value is finite as

$$\langle \bar{q}q \rangle = \langle \bar{q}_{f,R} q_{f,L} + \bar{q}_{f,L} q_{f,R} \rangle \neq 0, \tag{1.10}$$

in the low energy region of the QCD vacuum. This implies that the spontaneous chiral symmetry breaking occurs by the vacuum where the objects expressed as $\langle \bar{q}_{R/L} q_{L/R} \rangle$ are embedded and is not completely an empty space. In other words, the dynamical mass of a quark is generated by the continuous process of collisions between a quark $q_{R/L}$ and the chiral condensate $\langle \bar{q}_{R/L} q_{L/R} \rangle$ inside the low energy QCD vacuum.

On the other hand, the chiral symmetry tends to be restored and not broken in an extreme environment such as high temperature and/or high density. In terms of the chiral condensation, the VEV of scalar meson approaches toward zero as $\langle \bar{q}q \rangle \to 0$ with the increase of temperature and/or density. The transition of parameter $\langle \bar{q}q \rangle$ from low to high temperature is investigated by the lattice QCD simulations [26, 27]. From the viewpoints of baryon density, experimental measurements are conducted for looking into the change of $\langle \bar{q}q \rangle$ [28, 29]. The change of chiral condensation with the order parameter $\langle \bar{q}q \rangle$ is simply described as the function of temperature and density in Fig. 1.4.

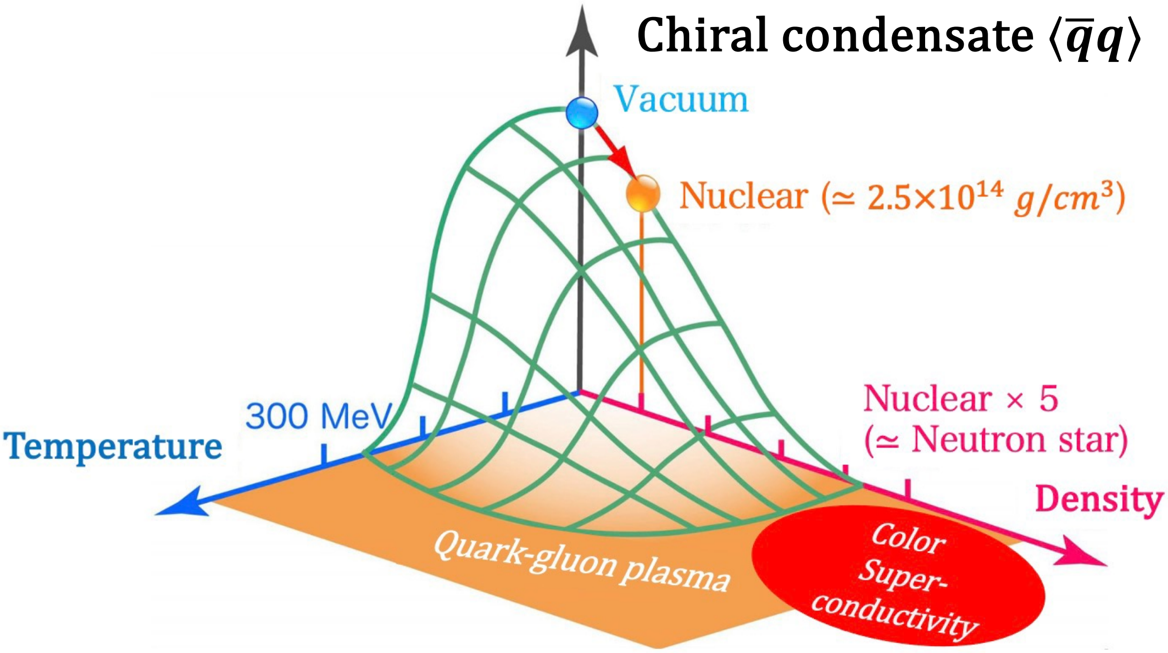

Figure1.4 The expected variation of chiral condensation with the order parameter $\langle \bar{q}q \rangle$ based on temperature and density, quoted from the homepage of nuclear experiment laboratory in Kyushu University (https://ne.phys.kyushu-u.ac.jp/research/spin/).

1.2.3 Nambu-Goldstone boson

As in Eq. (1.7), chiral transformation is defined with the unitary group $U(N_f)$ for each right and left-handed quark. This group is isomorphic to the product of a special unitary group and a complex phase, which is expressed as $U(N_f) \cong SU(N_f) \times U(1)$. Moreover, the $U(1)$ phase transformation in both right and left-handed quarks are identified to the "vector" and "axial-vector" transformation. They are written as

$$\mathrm{V}: \ q \to e^{i\theta_V} q, \ \ \mathrm{A}: \ q \to e^{i\theta_A \gamma_5} q, \tag{1.11}$$

which is equal to the definition $\theta_V \equiv (\theta_R + \theta_L)/2$ and $\theta_A \equiv (\theta_R - \theta_L)/2$. Therefore, the $U(1)_R \times U(1)_L$ group is isomorphic to the $U(1)_V \times U(1)_A$ group, and symmetries of QCD Lagrangian in the chiral limit is decomposed as

$$\begin{aligned} U(N_f)_R \times U(N_f)_L &\cong SU(N_f)_R \times SU(N_f)_L \times U(1)_R \times U(1)_L \\ &\cong SU(N_f)_R \times SU(N_f)_L \times U(1)_V \times U(1)_A. \end{aligned} \tag{1.12}$$

In these groups, $SU(N_f)_R \times SU(N_f)_L$ denotes the usual chiral symmetry, which breaks spontaneously as

$$SU(N_f)_R \times SU(N_f)_L \to SU(N_f)_V, \tag{1.13}$$

in low temperature and low density. Here the remained $SU(N_f)_V$ group shows the flavor symmetry for quarks without considering left or right-handed. According to the Nambu-Goldstone theorem, there are some massless Nambu-Goldstone (NG) bosons [30–32] which appears as the same number as the reduced number of invariant generators by the spontaneous symmetry breaking, $N_f^2 - 1$.

In the case of $N_f = 2$, there are $N_f^2 - 1 = 3$ NG bosons which correspond to the isotriplet pions $(\pi^{\pm}, \pi^0)$. Although they are not completely massless with the experimental mass value 140 MeV due to the explicit chiral symmetry breaking by the small bare u, d quark masses, they are much lighter than the other mesons which are heavier than about 500 MeV.

In the case of $N_f = 3$, not only pions but also kaons $(K^{\pm}, K^0, \bar{K}^0)$ and an eta meson (η) holds for NG bosons, whose total number is $N_f^2 - 1 = 8$. However, kaons and an eta meson are heavier than pions because s quark is much heavier than u, d quarks. This indicates the necessity of considering the explicit chiral symmetry breaking when the s quark is used in the chiral $SU(3)_R \times SU(3)_L$ system.

The NG bosons are frequently used in the chiral effective theory which is the theoretical method to describe the spontaneous chiral symmetry breaking in QCD. This theory deals with the interaction of light quarks and gluons in the low energy region, but also that of hadrons such as pseudoscalar and scalar mesons. This is because the basic degrees of freedom approaches from quarks to hadrons in the low energy regime. In particular, pions and sigma mesons are related to NG bosons and chiral condensate $\langle \bar{q}q \rangle$, respectively.

1.2.4 Chiral $U(1)_A$ anomaly

For the other groups in Eq. (1.12), $U(1)_V$ symmetry stands for the total number of all left and right-handed quarks, which is generally conserved in QCD. On the other hand, the $U(1)_A$ symmetry is associated to the difference between the numbers of right and left-handed quarks. About this symmetry, it is explicitly broken by the quantum anomaly effect, which means that the symmetry satisfied in classical physics comes out to be failed in quantum physics. In particular, the anomaly effect breaking the $U(1)_A$ symmetry is called "chiral anomaly". The image of the chiral $U(1)_A$ anomaly is that, in the quantum world, both the numbers of left and right-handed bolts are changing before and after with keeping their total number by the $U(1)_V$ symmetry conservation.

The chiral anomaly effect is expressed with the non-conservation of axial-vector current J_A^μ, which represents the variation of difference of right and left-handed quark numbers. In general, the divergence of this axial-vector current consequently becomes relevant to the strength of gluon field as

$$\partial_\mu J_A^\mu \propto \frac{g^2}{16\pi^2} \epsilon_{\mu\nu\rho\sigma} G_a^{\mu\nu} G^{a,\rho\sigma} \neq 0, \tag{1.14}$$

with the chiral limit. Here, $\epsilon_{\mu\nu\rho\sigma}$ denotes the Levi-Civita symbol with $\epsilon_{0123} = 1$. From this non-conserving current $\partial_\mu J_A^\mu \neq 0$, the $U(1)_A$ symmetry breaking is confirmed even when the chiral $SU(N_f)_R \times SU(N_f)_L$ symmetry is satisfied.

In hadron physics, it is famous that the chiral $U(1)_A$ anomaly plays a key role in the "$\eta - \eta'$ puzzle" which is known as the $U(1)_A$ problem [33]. This mystery is about the η' meson, whose mass value is about 958 MeV and is quite heavy compared with the other pseudoscalar mesons such as pions ($\simeq$ 140 MeV), kaons ($\simeq$ 500 MeV), and an eta meson ($\simeq$ 550 MeV). It is inconsistent to treat the η' meson as the NG boson appearing by the spontaneous $U(1)_A$ symmetry breaking due to its heavy mass. However, this problem can be resolved if the $U(1)_A$ symmetry is explicitly broken by the chiral anomaly effect.

Including the $\eta - \eta'$ puzzle, the chiral $U(1)_A$ anomaly can be a dramatic solution to explain properties of hadrons. For another example of the importance of chiral anomaly, the mass relation of scalar mesons are discussed with this effect in Ref. [34]. This paper proposes that the origin of the heaviness of $a_0(980)$ meson comes from the $U(1)_A$ anomaly, and the mystery of $a_0(980)$ which is heavier than $K_0^*(700)$ meson can be explained. Without the chiral $U(1)_A$ anomaly, it makes a contradiction between theoretical and experimental mass values of these scalar mesons, because $K_0^*(700)$ becomes heavier than $a_0(980)$ by the naive counting of the number of strange quarks.

1.2.5 Chiral partner structure

The spontaneous chiral symmetry breaking is the big origin of masses for light quarks. By the dynamical mass generation due to its symmetry breaking, the current quark masses become the constituent quark masses which is appropriate to the observed hadron masses. For example, the bare u, d quark masses are only about $2 - 5$ MeV whereas those constituent quark masses are about 350 MeV, so that its effective mass value is heavy enough to be the mass of nucleon with three u, d quarks. Thus the chiral symmetry and its spontaneous breaking is one of the most important properties of QCD relevant to the low energy hadron physics.

From the viewpoints of chiral symmetry, not only the quark mass generation but also the "chiral partner structure" is one of the prominent feature, which is useful to the hadron spectroscopy. This partner stands for two states whose masses are degenerate when the chiral symmetry is not broken, and have the same total spin but have the opposite, even and odd parity. One of the example of chiral partner is the ground state of pions π with spin-parity $J^P = 0^-$ and that of sigma mesons σ, also known as $f_0(500)$, with 0^+. For another, the ground state of $\rho(700)$ mesons with 1^- and that of $a_1(1260)$ mesons with 1^+ are the chiral partner by the vector and axial-vector mesons. For baryons, the ground state of nucleons with $1/2^+$ and the $N(1535)$ resonant states with $1/2^-$ is expected to be its partner.

For the simple proof of the existence of chiral partner structure, we consider the quark part of QCD Lagrangian in the one flavor system, written as

$$\mathcal{L}_{\text{quark}(1f)} = \bar{q}(i\gamma^\mu \partial_\mu - m_q)q, \tag{1.15}$$

where m_q denotes the quark mass. Considering a massless quark by the chiral limit ($m_q \to 0$), this Lagrangian is invariant under vector and axial-vector transformations in Eq. (1.11), and those corresponding Noether currents are expressed as

$$j_V^\mu \equiv \bar{q}\gamma^\mu q, \; j_A^\mu \equiv \bar{q}\gamma^\mu \gamma_5 q. \tag{1.16}$$

On the other hand, chiral transformations in Eq. (1.7) are equivalent to the vector and axial-vector transformations because of $U(1)_R \times U(1)_L \cong U(1)_V \times U(1)_A$, meaning that the Lagrangian in Eq. (1.15) is also invariant under the chiral transformations. The corresponding Noether currents to the chiral transformations are given by

$$j_R^\mu \equiv \bar{q}_R \gamma^\mu q_R, \; j_L^\mu \equiv \bar{q}_L \gamma^\mu q_L, \tag{1.17}$$

so that there are four Noether charges related to these four currents given as

$$Q_{R/L} \equiv \int d\boldsymbol{x}\; j_{R/L}^{\mu=0} = const.\ , \; Q_{V/A} = Q_R \pm Q_L = const.\ . \tag{1.18}$$

Here $Q_{R/L}$ indicates the number of right/left handed quarks, and $Q_{V/A}$ are total and difference of those right and left quark numbers. In the condition where the chiral symmetry is satiefied, both Q_V and Q_A come out to be conserved charges, so that they can commute with Hamiltonian H. Also, these charges are Lorentz scalar so that they remain invariant under the spatial rotations. Therefore, both Q_V and Q_A can also commute with the angular momentum operator J.

$$[H, Q_{V/A}] = 0, \ [J, Q_{V/A}] = 0. \tag{1.19}$$

Here the symbol [ ] in Eq. (1.19) stands for the commutation operator. However, under the spatial inversion, only Q_V can commute with the parity operator P, while Q_A anticommutes with P because of the γ_5 matrix inside its charge.

$$\begin{aligned} PQ_V P^{-1} &= Q_V, \\ PQ_A P^{-1} &= -Q_A. \end{aligned} \tag{1.20}$$

Using these Noether charges Q_V and Q_A, here we consider two hadron states written as $Q_V|m, j, \pi\rangle$ and $Q_A|m, j, \pi\rangle$, where $|m, j, \pi\rangle$ shows the state with mass m, total spin j, and parity π. According to Eqs. (1.19) and (1.20), these two states have the same mass and total spin, but have the opposite parity. As a consequence, when the chiral symmetry is not broken, we can say that there are two states where the masses are degenerate, total spins are the same, and parities are reversed with each other, meaning the chiral partner structure.

One of the important feature of the chiral partner structure is "chiral invariant mass", which is the degenerate mass of two hadron states that appears when the chiral symmetry is not broken. This means, if we recognize its mass value, we can estimate the change of two hadron states in the chiral symmetry restored phase, such as the extreme environment with high temperature and/or high density. For example, according to Refs. [35, 36], the masses of $\rho(700)$ and $a_1(1260)$ mesons are expected to be degenerate with the chiral invariant mass given as about $500 - 700$ MeV, and these two mesons are expected to become lighter in the chiral symmetry restored phase.

Also, the chiral partner structure can be applied to the prediction of one obscure state from the other well-known state. For instance, in Ref. [37], the excited states of Λ_c baryons with spin-parity $1/2^-$ and $3/2^-$ are expected to be exist with those masses of about 3100 MeV, which is not experimentally given yet. This prediction is from the ground state of Λ_c baryon whose spin-parity and mass are $1/2^+$ and about 2286 MeV. Similarly, in Refs. [38, 39], masses and decay widths of excited singly heavy baryon states with negative parity are derived from those baryons in ground states.

1.3 Diquarks

Diquarks are the hypothetical particles consist of two quarks. Since the quark model proposed by Murray Gell-Mann and George Zweig [7–9], the existence of diquarks are implied as a building block of hadrons, as well as single quarks.

In the hadron phase where both temperature and baryon density is low, diquarks are considered as the element of hadrons. For baryons, they are often described as the quark-diquark picture to invesigate those energy spectra and decays [40–49]. For mesons, especially for excited scalar meson states, some researches assume them to be in the tetraquark states, and the diquark–anti-diquark picture is applied in these works to analyze those states [50–57]. For the others, diquarks are applied for the cluster model of exotic hadrons which are composed of four or more quarks and anti-quarks [25, 58–71]. In another field, diquarks are expected to appear as the diquark condensate in the color superconducting phase [72–84]. This phase appears when the temperature is not too high as below 10^{12} kelvins, and the matter is as dense as or denser than that of the core of neutron stars. In this phase, quarks are correlated to form Cooper pairs and condense, which is similar to electrons in metals with low temperature [85, 86]. Therefore, from these explanations, diquarks are involved in phases from low to high baryon density and within the low temperature, so that diquarks are an important subject in high energy physics, elementary particle physics, astrophysics and so on.

Now, let us consider the diquark which is composed of two light quarks as "qq". Similar to quarks, this type of diquarks have three degrees of freedom called color, flavor, and spin. Also, there is the orbital angular momentum between two constituent quarks as the additional degree of freedom for diquarks. These four features of diquarks must be totally anti-symmetric, since the constituent quarks are fermions which are obedient to Pauli's principle.

About the symmetries of these four quantum numbers, diquarks are the group of two quarks with each color represented by $\mathbf{3}$ triplet, so that the color expression of diquark itself is given by $\mathbf{3}\otimes\mathbf{3} = \bar{\mathbf{3}}\oplus\mathbf{6}$. This shows that there are two kinds of color representations for diquarks, classified into the color anti-triplet $\bar{\mathbf{3}}$ type and the sextet $\mathbf{6}$ type. Here if a diquark connects to one quark and forms a baryon, these diquark and quark should be color singlet $\mathbf{1}$ to form an observable baryon. Considering the color product of diquarks with each $\bar{\mathbf{3}}$ and $\mathbf{6}$, the color representation of diquark-quark system is given by

$$(\text{diquark's color}) \otimes (\text{quark's color}) = \begin{cases} \bar{\mathbf{3}} \otimes \mathbf{3} = \mathbf{1} \oplus \mathbf{8} \\ \mathbf{6} \otimes \mathbf{3} = \mathbf{8} \oplus \mathbf{10} \end{cases} . \tag{1.21}$$

Therefore, only the color anti-triplet $\bar{\mathbf{3}}$ diquarks are permitted to be the components of color singlet $\mathbf{1}$ baryons. Moreover, the color-Coulomb interaction between two quarks is proportional the inner product of Gell-Mann matrices, $(\boldsymbol{\lambda}_i \cdot \boldsymbol{\lambda}_j)$. The value of this operator for each color of diquarks is given by

$$(\boldsymbol{\lambda}_i \cdot \boldsymbol{\lambda}_j) = \begin{cases} -8/3 & (\text{color } \bar{\mathbf{3}} \text{ diquarks}) \\ +4/3 & (\text{color } \mathbf{6} \text{ diquarks}) \end{cases} . \tag{1.22}$$

Therefore, the color anti-triplet $\bar{\mathbf{3}}$ diquarks with the negative value of $(\boldsymbol{\lambda}_i \cdot \boldsymbol{\lambda}_j)$ have the attractive interaction between two quarks including the color confinement interaction, and they take form better than the color sextet $\mathbf{6}$ diquarks. From now on, we only consider about diquarks with color $\bar{\mathbf{3}}$ representation.

Next we consider the flavor of diquarks. In the three flavor system with $q = u, d, s$ light quarks, the flavor expression of diquarks is written as $\mathbf{3}\otimes\mathbf{3} = \bar{\mathbf{3}}\oplus\mathbf{6}$, same as the color. In each representation of flavors, the allowed combinations of two quarks are different from each diquark as

I. Flavor $\bar{\mathbf{3}}$ diquarks: $[ud]$, $[ds]$, and $[su]$.
II. Flavor $\mathbf{6}$ diquarks: $\{ud\}, \{ds\}, \{su\}, \{uu\}, \{dd\}$, and $\{ss\}$.

Here the symbol $\{\ \}$ for flavor $\mathbf{6}$ diquarks denotes the anti-commutation operators. Because of these operators, only the flavor $\mathbf{6}$ symmetric diquarks are allowed to take two same quarks such as $\{uu\}, \{dd\}$, and $\{ss\}$.

For the spin of diquarks, quarks have the spin $1/2$, so that diquarks have two types of spin as $1/2\otimes 1/2 = 0 \oplus 1$, showing the anti-symmetric spin singlet (0) and the symmetric spin triplet (1). Lastly, the orbital angular momentum between two quarks inside a diquark is restricted to be either even ($L = S, D, ...$) or odd ($L = P, F, ...$) by the parity, because the symmetries of parity and the other three quantum numbers needs to be totally anti-symmetric by the Pauli's principle.

Diquark	Operator	J^P	Color	Flavor	$^{2s+1}L_J$
Scalar diquark	$(q^T C\gamma^5 q)^{\overline{3}}_A$	0^+	$\overline{3}$	$\overline{3}$	$^1S_0$
Pseudoscalar diquark	$(q^T Cq)^{\overline{3}}_A$	0^-	$\overline{3}$	$\overline{3}$	$^3P_0$
Vector diquark	$(q^T C\gamma^\mu\gamma^5 q)^{\overline{3}}_A$	1^-	$\overline{3}$	$\overline{3}$	$^3P_1$
Axial-vector diquark	$(q^T C\gamma^\mu q)^{\overline{3}}_S$	1^+	$\overline{3}$	6	$^3S_1$
Tensor diquark	$(q^T C\sigma^{\mu\nu} q)^{\overline{3}}_S$	$1^+, 1^-$	$\overline{3}$	6	$^3D_1, ^1P_1$

Table1.2 Operators and properties of diquarks with color $\bar{3}$ representation expressed as the superscript in each operator. The subscript A and S of diquark operators stand for the flavor anti-symmetric and symmetric, respectively.

As a consequence, the diquarks belonging to the color $\bar{\mathbf{3}}$ representation can be defined as in Table 1.2 [87]. Five types of diquarks are summarized in this table, in which those operators are expressed with two quark fields q and the product of some gamma matrices. Here $C = i\gamma^0\gamma^2$ is the charge conjugation operator included for the Lorentz covariance of diquark operators.

In Table 1.2, there are two diquarks whose orbital angular momenta are in S wave state. In particular, the scalar diquark with $\bar{\mathbf{3}}$ anti-symmetric color and flavor is often called the "good" diquark, which has the most attractive interaction between two constituent quarks and is the most stable state of all diquarks. Also, the axial-vector diquark with color $\bar{\mathbf{3}}$ and flavor $\mathbf{6}$ representations is often called the "bad" diquark, and is the stable diquark next to the good diquark. The idea of these good and bad expressions for scalar and axial-vector diquarks has been started by R. L. Jaffe and F. Wilczek to attract attention in the context about descriptions of pentaquarks in Refs. [59, 60]. As these two diquarks are attractive than others, they are frequently investigated by the lattice QCD simulation such as the mass and the size [88–97]. For instance, the mass difference between these diquarks with no constituent s quark is predicted to be about 200 MeV. Also, the strong attraction of scalar diquarks are confirmed in many researches.

1.4 Singly heavy baryons

Since baryons are composite particles with three quarks, some of them are well regarded as the quark–diquark two body systems. One of the baryon that is expected to form a diquark substructure is "singly heavy baryon" which includes one heavy quark Q and two light quarks qq. This is because the color Coulomb and spin-dependent interaction between two quarks become weaker when the quark masses increase, so that the attraction between two light quarks is stronger than that between a light quark and a heavy quark. Therefore, two attractive light quarks can be regarded as a diquark surrounding a remained heavy quark, and singly heavy baryons can be treated as the diquark–heavy-quark two body systems as described in Fig. 1.5. From this reason, in an experimental way, the J-PARC E50 experiment is planning to use a singly charmed baryons to investigate the diquark correlation formed by two light quarks inside those baryons [98].

Note that, in hadron physics, the heavy quark generally represents charm and bottom quarks ($Q = c, b$). Although top quark (t) is also heavy, it is the only quark that is heavier

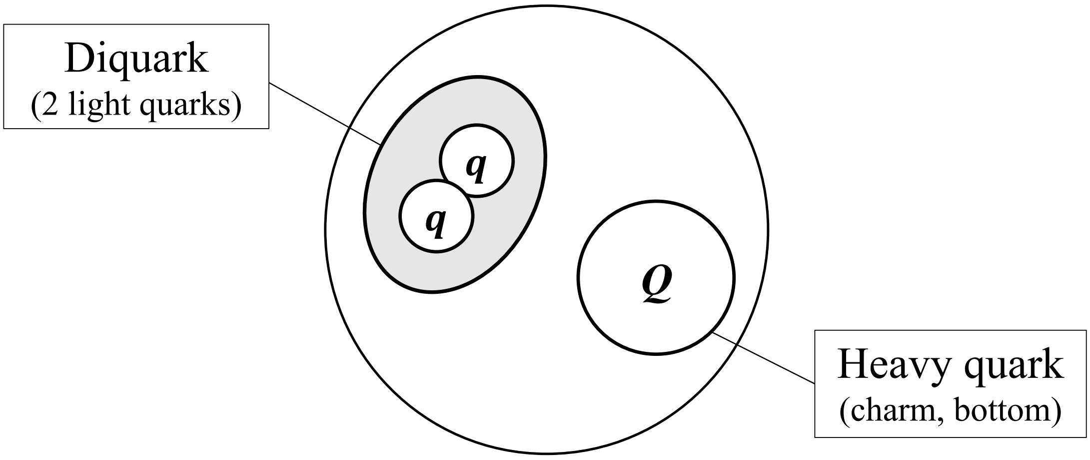

Figure1.5 Structure of singly heavy baryons as the diquark–heavy-quark picture.

than a W boson and it mostly decays to a W boson and a bottom quark affected by the weak interaction. From this weak decay, the lifetime of top quark is known as about 0.5×10^{-24} second, which is shorter than the typical strong interaction time scale defined as 10^{-23} second. Therefore, top quarks are expected to decay to bottom quarks before they behave as the constituent of t-flavored hadrons [99].

Singly heavy baryons, in general, are expressed as $\Lambda_Q, \Sigma_Q, \Xi_Q, \Xi'_Q$, and Ω_Q. The difference of these symbols comes from flavor, spin, and isospin of constituent quarks. In detail, the subscript Q stands for a heavy quark inside those baryons, and the main part is defined by the structure of two light quarks. In the way of diquark–heavy-quark two body system, singly heavy baryons in the ground states are expressed with scalar diquarks with $\bar{\mathbf{3}}$ anti-symmetric flavor $[qq]$ or axial-vector diquarks with $\mathbf{6}$ symmetric flavor $\{qq\}$, as summarized in Table 1.3. Here the Λ_Q and Ξ_Q baryons contain a scalar diquark with spin 0, so that it combines with a remained heavy quark to form the $J^P = 1/2^+$ states. On the other hand, the Σ_Q, Ξ'_Q, and Ω_Q baryons have an axial-vector diquark with spin 1, and combines with a heavy quark to form $J^P = 1/2^+$ or $3/2^+$ states. For more details about the ground state of singly heavy baryons, see those weight diagrams in Figs. 1.6 and 1.7.

Singly heavy baryon	Λ_Q	Σ_Q	Ξ_Q	Ξ'_Q	Ω_Q
Constituents	ud	nn	ns	ns	ss
Flavor	$\bar{\mathbf{3}}$	$\mathbf{6}$	$\bar{\mathbf{3}}$	$\mathbf{6}$	$\mathbf{6}$
Spin	0	1	0	1	1
Isospin	0	1	1/2	1/2	0

Table1.3 Diquark properties in the ground states of singly heavy baryons, where $n = u, d$ in flavor denotes the light quarks except s quarks.

From the experimental points of view, there are about 30 discovered states for both singly charmed and bottom baryons, respectively. In particular, Fig. 1.8 quoted from

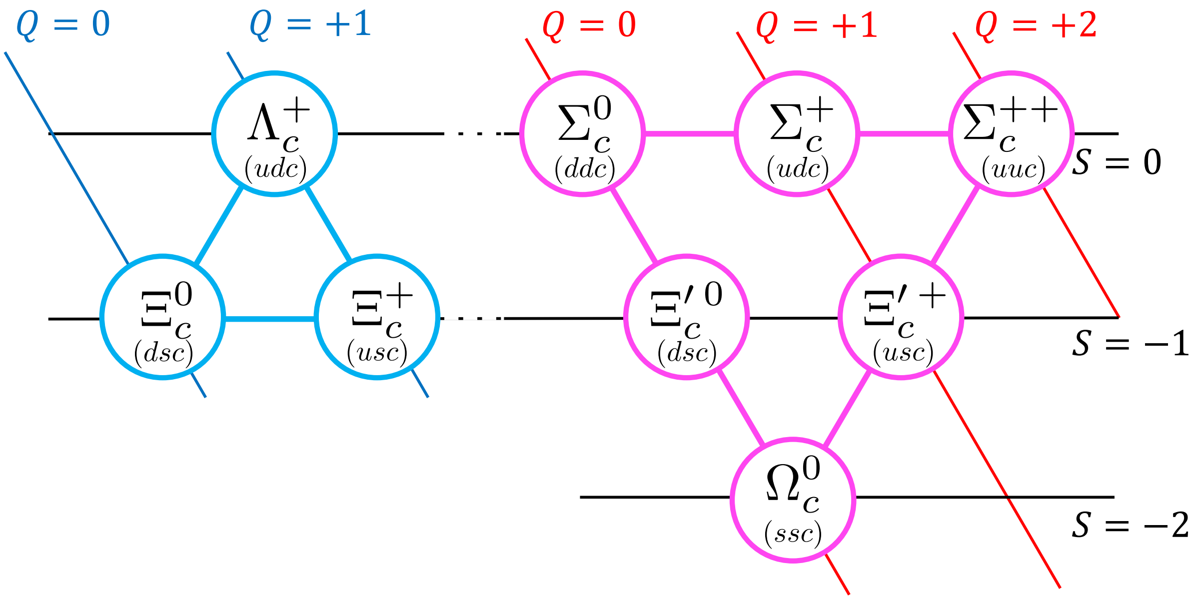

Figure1.6 The weight diagrams of the flavor $\bar{\mathbf{3}}$ and $\mathbf{6}$ ground state representation for singly charmed baryons, where Q and S are the electrical charge and strangeness, respectively.

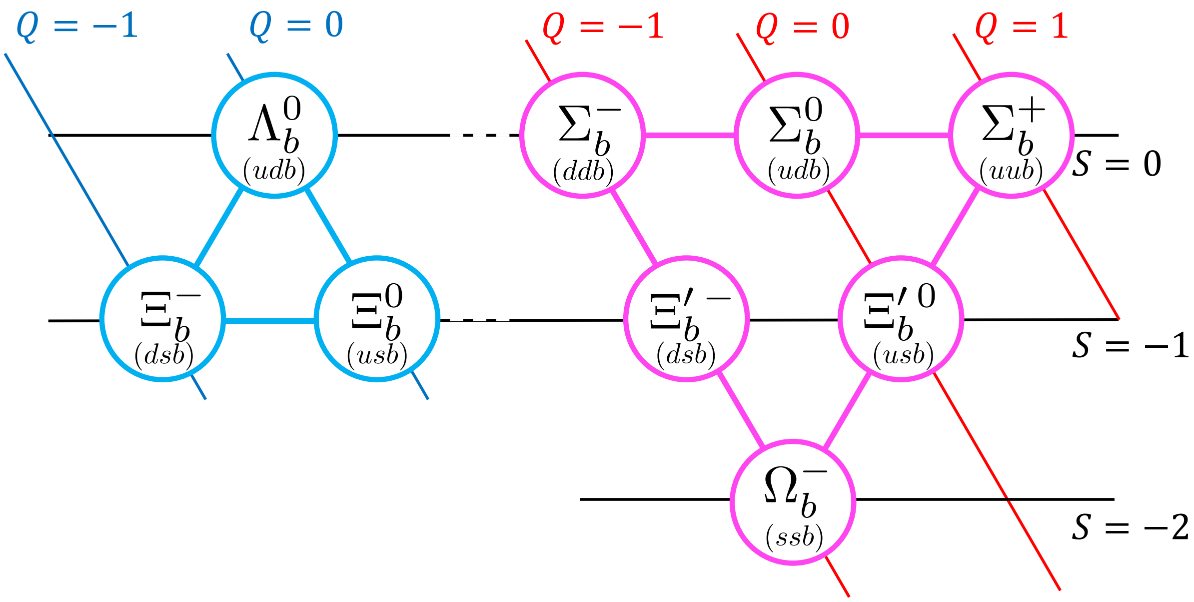

Figure1.7 The weight diagrams of the flavor $\bar{\mathbf{3}}$ and $\mathbf{6}$ ground state representation for singly bottom baryons, where Q and S are the electrical charge and strangeness, respectively.

Ref. [12] shows the energy spectrum of the observed singly heavy baryons whose total spin and parity J^P is given. However, for most of states, those spin and parity are not determined experimentally but are almost the expectation from the quark model. About the number of experimental data, singly charmed baryons with red solid lines have more than singly bottom baryons with blue solid lines. Note that Ξ_Q and Ξ'_Q baryons are placed together in the same spectra because of the flavor mixture.

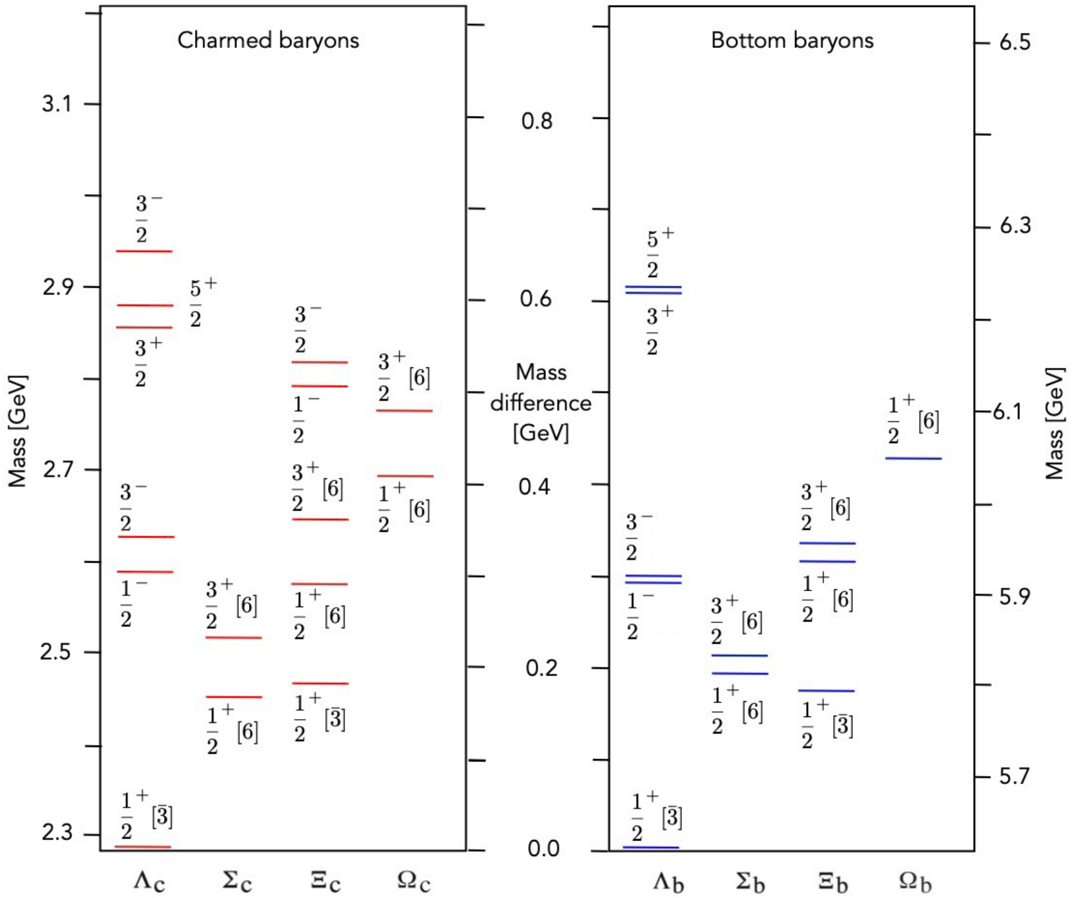

Figure1.8 Energy spectrum of the observed singly heavy baryons whose spin-parity J^P states are known or presumed in Ref. [12]. The flavor symmetry assignments are given in the square brackets [ ] for ground states. The Ξ_Q and Ξ'_Q are in the same line, and the isospin triplet of Σ_Q and doublet of $\Xi_Q^{(\prime)}$ are nearly degenerate.

Comparing charmed and bottom baryons in these spectra, we can find that the structure of lines and quantum numbers is similar to each other, which implies that the strength of color confinement is weakly dependent on the difference of heavy quark flavor. For instance, in the ground state, the mass difference between $\Lambda_c(1/2^+)$ and $\Xi_c(1/2^+)$ is approximately the same as that between $\Lambda_b(1/2^+)$ and $\Xi_b(1/2^+)$. Also, the mass splitting between $\Lambda_c(1/2^+)$ and $\Omega_c(1/2^+)$ is close to that between $\Lambda_b(1/2^+)$ and $\Omega_b(1/2^+)$.

In the excited states of Λ_Q baryons, there are two pairs in which those mass differences are relatively small: One is the states with spin-parity $1/2^-$ and $3/2^-$ which are expected to be the P-wave orbital excitations. The other pair is spin-parity $3/2^+$ and $5/2^+$ states and are the candidates for D-wave orbital excitations. Comparing the energy spectra of Λ_c and Λ_b, the excited energies of those pairs based on the ground state are similar to each other. However, about two states in each pair, the mass splitting between two Λ_c excited states is larger than that between two Λ_b states. For example, the mass difference between

$\Lambda_c(1/2^-)$ and $\Lambda_c(3/2^-)$ is about 50 MeV, but that between $\Lambda_b(1/2^-)$ and $\Lambda_b(3/2^-)$ is only about 10 MeV and is almost degenerate. In general, these pair of two states are called the "heavy-quark spin doublet", in which masses of these two states approach by the increase of constituent heavy quark mass. This phenomenon is induced by the "heavy-quark spin symmetry" which indicates that the spin of heavy quark is conserved when the heavy quark mass approaches infinity [100–106]. Therefore, the mass splitting by the spin dependent force becomes smaller for singly bottom baryons rather than charmed baryons. For the other baryons, the ground states of $\Sigma_{c(b)}(1/2^+)$ and $\Sigma_{c(b)}(3/2^+)$, and also the ground states of $\Xi'_{c(b)}(1/2^+)$ and $\Xi'_{c(b)}(3/2^+)$ are heavy quark spin doublets. Moreover, $\Omega_{c(b)}(1/2^+)$ and $\Omega_{c(b)}(3/2^+)$ in the ground states can be the heavy quark spin doublet, but $\Omega_b(3/2^+)$ is not discovered yet.

1.5 Purpose of the present research

The main purpose of hadron physics is to understand properties of hadrons from the viewpoints of QCD. For this research, chiral symmetry and its spontaneous breaking is one of the most important features to see hadrons in the low energy region. One of the theoretical methods to look into hadrons from the viewpoints of chiral symmetry breaking is the "chiral effective theory", such as the "Linear sigma model" introduced by M. Gell-Mann and M. Levy [107], and also the "NJL model" by Y. Nambu and G. Jona-Lasinio [108]. Chiral effective theory induces the low energy theorems, and many problems about properties of hadrons are theoretically explained by them.

For another perspective about the research of hadrons physics, diquarks are frequently used as the building blocks of hadrons. For example, singly heavy baryons can be described as the diquark–heavy-quark two body systems as in Fig. 1.5. In this case, we can predict the features of unknown singly heavy baryons from diquark properties. In detail, if the interaction between a constituent diquark and a heavy quark is determined, we can solve this two body system by the Schrödinger equation with the diquark–heavy-quark potential term, and can analyze singly heavy baryons from its diquark data. Also, in the opposite way, we can predict the features of diquarks from the well-known singly heavy baryons such as those ground states. As diquarks are the colorful object and cannot observed directly in an experimental way, singly heavy baryons are helpful to investigate diquarks with the color antitriplet $\bar{\mathbf{3}}$ structure. Hence, diquarks and singly heavy baryons are the best pair to look into each other.

There are many kinds of chiral effective theories such as for mesons, baryons, and the other multiquark system. Most of hadrons with various color-singlet structures are discussed in those researches and reviews. However, about diquarks as elements of hadrons, there are less research with the use of chiral effective theory, though both diquarks and chiral symmetry breaking are essential strategies to solve properties of hadrons in low energy QCD. In detail, the firstly constructed chiral effective model for diquarks is in Ref. [25] proposed in 2004, where diquarks as building blocks of tetraquarks and pentaquarks are discussed. Furthermore, the first research of diquarks with using the linear sigma model [107] is in Ref. [87] proposed in 2020, where the naive spectrum of Λ_c and Ξ_c baryons are proposed from constituent diquark masses. Among various systems of hadrons and quarks, there are few chiral effective theory for diquarks which work as the composition of hadrons.

In the present research, to understand the feature of diquarks connected with the chiral symmetry breaking, we construct the "chiral effective model of diquarks" with using the linear sigma model [107]. Using this model, we can investigate relations and variations of diquarks from the viewpoints of chiral symmetry breaking. This model also makes us possible to see the change of diquark properties from a perspective of chiral condensation.

For the chiral effective model of diquarks in this work, we consider the Lagrangian including diquarks as basic fields and satisfying the chiral $SU(3)_R \times SU(3)_L$ symmetry with $N_f = 3$ flavor system. In particular, we derive the formula which represents the dynamical generation of diquark masses by the explicit chiral symmetry breaking. We also look into the relation of diquarks with various structures and quantum numbers, as well as the change of those diquarks by the chiral symmetry restoration.

After constructing the chiral effective model of diquarks, we apply this model to hadrons which include diquarks as elements. Singly heavy baryons with diquark–heavy-quark pictures, described as in Fig. 1.5, is the main theme of this research. In particular, we investigate the energy spectra and decay reactions of those heavy baryons with considering a constituent diquark based on the chiral effective model and diquark–heavy-quark interaction.

For the additional research, we look into the T_{QQ} tetraquarks with one anti-diquark as an element of those exotic hadrons. In this case, T_{QQ} tetraquarks are regarded as the three body systems composed of two heavy quarks and one light anti-diquark as in Fig. 1.9. In particular, we investigate the existence of T_{QQ} tetraquark bound states, and compare our results with the recent experimental data and other theoretical predictions.

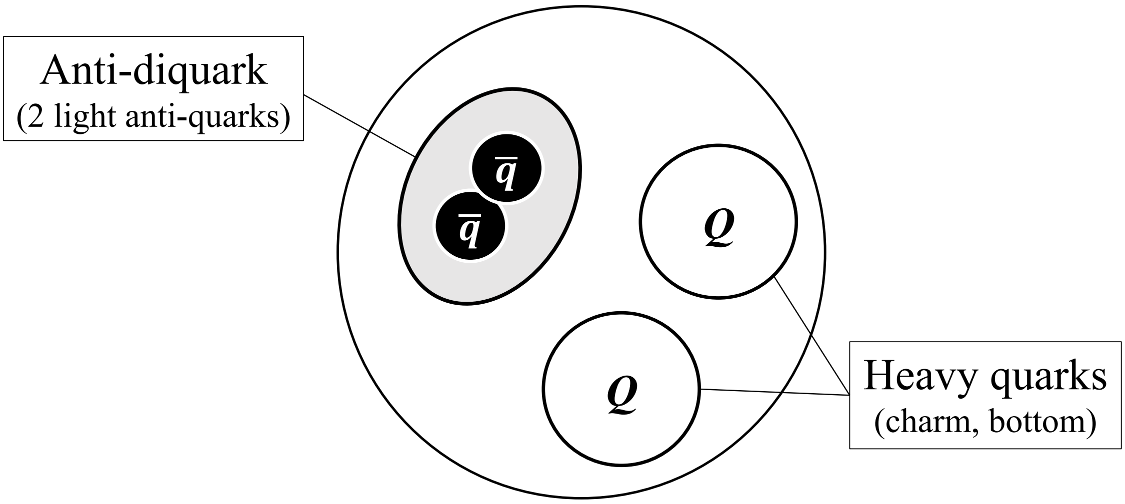

Figure1.9 Structure of T_{QQ} tetraquarks as the heavy-quark–heavy-quark–anti-diquark picture.

This dissertation is organized as follows. In chapter 2, we explain the linear sigma model we apply in this research, and formulate the chiral effective model for various diquarks. In chapter 3, we introduce the calculation method to compute few body systems with a diquark or an anti-diquark element. In chapter 4, we firstly construct the diquark–heavy-quark potential models and determine parameters in these potentials. After this, we show numerical results of the energy spectra for singly heavy baryons based on a diquark–heavy-quark description. In chapter 5, we look into one-pion emission decays of singly heavy baryons from the viewpoints of diquarks, and discuss the chiral symmetry restoration which affect these strong decays. In chapter 6, we investigate the existence of T_{QQ} tetraquark bound states from the perspective of anti-diquark picture, and compare our results with those in other various researches. Finally, chapter 7 is devoted to the summary of this present research.

Chapter 2

Chiral effective model of diquarks

In this chapter, we firstly explain one of the most famous model for chiral effective theory called the "Linear sigma model" with the flavor $SU(2)$ and $SU(3)$ systems. Next we construct the chiral effective model of diquarks using the linear sigma model with $SU(3)$ flavor. In this work, there are four types of diquark in this chiral effective model, whose names are "scalar diquark", "pseudoscalar diquark", "vector diquark", and "axial-vector diquark". Their features are summarized in Table 1.2.

2.1 Linear sigma model and chiral symmetry breaking

The linear sigma model is the prototype of an effective theory which implements the idea of chiral symmetry breaking. This model was firstly constructed by M. Gell-Mann and M. Levy [107] for the study of chiral symmetry in the pion-nucleon system, and is extended to the quark-level system [7–9]. In concrete, the chiral effective Lagrangian for the linear sigma model with $SU(2)$ flavor system is written as

$$\begin{aligned} \mathcal{L}_{SU(2)} &= \frac{1}{2}(\partial_\mu \sigma)^2 + \frac{1}{2}(\partial_\mu \boldsymbol{\pi})^2 - V(\sigma, \boldsymbol{\pi}) \\ &\quad + \bar{q} i \gamma^\mu \partial_\mu q - g_s \bar{q}(\sigma + i\gamma_5 \boldsymbol{\tau}\cdot\boldsymbol{\pi}) q, \\ V(\sigma, \boldsymbol{\pi}) &= \frac{\mu^2}{2}(\sigma^2 + \boldsymbol{\pi}^2) + \frac{\lambda}{24}(\sigma^2 + \boldsymbol{\pi}^2)^2. \end{aligned} \tag{2.1}$$

Here q is the massless quark field. $\boldsymbol{\pi} = (\pi_1, \pi_2, \pi_3) \sim \bar{q} i \boldsymbol{\tau} \gamma_5 q$ with the Pauli matrix $\boldsymbol{\tau}$ is an isotriplet of pion fields, and $\sigma \sim \bar{q}q$ is the isosinglet scalar meson field. The coefficient g_s is the quark-meson coupling constant, which is expressed as $g_s = 2\pi/\sqrt{3} (\simeq 3.63)$ according to Refs. [109, 110]. The self-interactions of these meson fields are expressed as in the potential term $V(\sigma, \boldsymbol{\pi})$. Since this Lagrangian $\mathcal{L}_{SU(2)}$ is chiral $SU(2)_R \times SU(2)_L$ invariant, it is also invariant under $SU(2)$ vector and axial-vector transformations. These infinitesimal transformations are given by

$$\mathrm{V}: q \to q - i\boldsymbol{\alpha}\cdot\frac{\boldsymbol{\tau}}{2} q, \quad \boldsymbol{\pi} \to \boldsymbol{\pi} + \boldsymbol{\alpha}\times\boldsymbol{\pi}, \quad \sigma \to \sigma, \tag{2.2}$$

$$\mathrm{A}: q \to q - i\boldsymbol{\beta}\cdot\frac{\boldsymbol{\tau}}{2}\gamma_5 q, \quad \boldsymbol{\pi} \to \boldsymbol{\pi} + \boldsymbol{\beta}\sigma, \quad \sigma \to \sigma - \boldsymbol{\beta}\cdot\boldsymbol{\pi}, \tag{2.3}$$

and those associated Noether currents are written as

$$J_V^{a,\mu} \equiv (\pi \times \partial^\mu \pi)^a + \frac{1}{2}\bar{\psi}\gamma^\mu \tau^a \psi, \tag{2.4}$$

$$J_A^{a,\mu} \equiv (\sigma \partial^\mu \pi^a - \pi^a \partial^\mu \sigma) + \frac{1}{2}\bar{\psi}\gamma^\mu \gamma_5 \tau^a \psi. \tag{2.5}$$

Therefore the correlated Noether charges, and also those from chiral transformation are derived as

$$\mathcal{Q}^a_{V/A} \equiv \int d\boldsymbol{x} J^{a,\mu=0}_{V/A} = const.\ ,\ \ \mathcal{Q}^a_{R/L} = \frac{1}{2}(\mathcal{Q}^a_V \mp \mathcal{Q}^a_A) = const.\ , \tag{2.6}$$

which is similar to Eq. (1.18). In particular, two Noether charges from chiral transformation have the commutation relations expressed as

$$[\mathcal{Q}^a_L, \mathcal{Q}^b_L] = i\epsilon_{abc}\mathcal{Q}^c_L,\ [\mathcal{Q}^a_R, \mathcal{Q}^b_R] = i\epsilon_{abc}\mathcal{Q}^c_R,\quad [\mathcal{Q}^a_L, \mathcal{Q}^b_R] = 0. \tag{2.7}$$

Therefore, we can confirm that these Noether charges appearing from the $SU(2)$ symmetry is separated as $SU(2)_R \times SU(2)_L$.

The chiral $SU(2)_R \times SU(2)_L$ symmetry is the isomorphism of $O(4)$ symmetry. This is explained by the four dimensional scalar field $\phi = (\sigma, \pi_1, \pi_2, \pi_3)$ transformed by an orthogonal 4×4 matrix R as

$$\begin{aligned} &\phi_i \to R_{ij}\phi_j \simeq \phi_i + \epsilon_{ij}\phi_j, \\ &R_{ij} = \delta_{ij} + \epsilon_{ij},\ \epsilon_{ij} = -\epsilon_{ji}. \end{aligned} \tag{2.8}$$

We can observe from this transformation that the squared length of the vector ϕ, $\phi^2 = \sigma^2 + \boldsymbol{\pi}^2$, is invariant under the four dimensional $O(4)$ rotation. Moreover, the ϵ_{ij} in the rotational operator R corresponds to the vector and axial-vector transformations in Eqs. (2.2) and (2.3) as

$$\epsilon_{ij} = \epsilon_{ijk}\alpha_k,\ \epsilon_{0i} = \beta_i\ (i,j,k = 1,2,3). \tag{2.9}$$

In the linear sigma model, the ground state is determined by the minimum of the potential term $V(\sigma, \boldsymbol{\pi})$ describing the self-interactions of scalar fields. If the parameter μ^2 is negative, the minimum of this potential is located at

$$\sigma^2 + \boldsymbol{\pi}^2 = -\frac{6\mu^2}{\lambda} \equiv \upsilon^2. \tag{2.10}$$

This equation insists that, in the 4-dimensional space formed by σ and $\boldsymbol{\pi}$ scalar fields, there are various vacuum states starting from the point $(\upsilon, 0, 0, 0)$, which are invariant under the $O(3)$ rotation of the last three components. This is often called as "Nambu-Goldstone (NG) phase", and the chiral symmetry is spontaneously broken from $O(4) \cong SU(2)_R \times SU(2)_L$ to $O(3)$ in these ground states. In this situation, we can determine a particular ground state affected by the chiral condensate ($\langle\bar{q}q\rangle \neq 0$) such as

$$\langle\sigma\rangle = \upsilon,\quad \langle\boldsymbol{\pi}\rangle = 0, \tag{2.11}$$

where υ is the VEV of the σ field. By expanding the sigma meson field around this minimum state as $\sigma \to \upsilon + \sigma$, the Lagrangian becomes

$$\begin{aligned} \mathcal{L}'_{SU(2)} &= \frac{1}{2}(\partial_\mu\sigma)^2 + \frac{1}{2}(\partial_\mu\boldsymbol{\pi})^2 + \mu^2\sigma^2 + \frac{\lambda}{24}\upsilon^4 - V'(\sigma, \boldsymbol{\pi}) \\ &\quad + \bar{q}i\gamma^\mu\partial_\mu q + g_s\bar{q}(\sigma + i\gamma_5\boldsymbol{\tau}\cdot\boldsymbol{\pi})q - g_s\upsilon\bar{q}q, \\ V'(\sigma, \boldsymbol{\pi}) &= \frac{\lambda\upsilon}{6}\sigma(\sigma^2 + \boldsymbol{\pi}^2) + \frac{\lambda}{24}(\sigma^2 + \boldsymbol{\pi}^2)^2. \end{aligned} \tag{2.12}$$

We can find that the spontaneous chiral symmetry breaking makes the quark and the scalar meson massive with mass $g_s\upsilon$ and $|\sqrt{2}\mu|$ respectively, while the pions are massless NG bosons which appears by the $O(4) \to O(3)$ symmetry breaking [30–32].

After the spontaneous chiral symmetry breaking, the axial vector current $J_A^{a,\mu}$ will have a new term expressed as "$\upsilon\partial^\mu\boldsymbol{\pi}$", and this is responsible for the matrix element of the weak decay of pion $\pi^+ \to \mu^+ + \nu$,

$$\upsilon\langle 0|\partial^\mu\pi^a|\pi^b(p^\mu)\rangle = if_\pi p^\mu\delta_{ab}. \tag{2.13}$$

From this equation, we can associate the VEV υ with the pion decay constant $f_\pi \simeq 92$ MeV. As a result, the quark mass obtained by the chiral symmetry breaking becomes

$$M_q \equiv g_s\upsilon = g_s f_\pi, \tag{2.14}$$

which is called the Goldberger-Treiman relation [111].

This system of mass generation attributed to the spontaneous chiral symmetry breaking is for the idealized massless quarks. In reality, quarks do have their own finite masses $m_q \neq 0$, so that the chiral symmetry is explicitly broken. However, the masses of light quarks, especially the u, d quarks, are lighter than 10 MeV, which is much smaller than the effective mass appearing from the chiral symmetry breaking, $g_s f_\pi \simeq 3.63 \times 92$ MeV $\simeq 350$ MeV. Hence, it is also important to consider this approximated chiral symmetry which breaks explicitly by the genuine light quark masses. In this occasion, pions that should appear as the massless NG bosons acquire masses. In concrete, the explicit chiral symmetry breaking and the pion masses can be represented by adding the chiral symmetry breaking term,

$$\mathcal{L}^{SB}_{SU(2)} = \epsilon_{SB}\sigma, \tag{2.15}$$

in the Lagrangian (2.1). Then the minimum of the potential $V(\sigma,\boldsymbol{\pi})$ shifts to

$$\upsilon = \sqrt{\frac{6\mu^2}{\lambda}} + \frac{\epsilon_{SB}}{2\mu^2}, \tag{2.16}$$

with the first order of parameter ϵ_{SB}, and the pion masses m_π can be given by

$$m_\pi^2 = \frac{\epsilon_{SB}}{\upsilon} = \frac{\epsilon_{SB}}{f_\pi}. \tag{2.17}$$

Therefore, we can see that the existence of explicit chiral symmetry breaking term $\epsilon_{SB} \neq 0$ gives masses to pions as NG bosons.

2.2 $SU(3)$ Linear sigma model

The linear sigma model can be extended to the $SU(3)$ flavor system for u, d, and s quarks. In this model, The field Σ composed of scalar meson $\tilde{\sigma} \sim \bar{q}q$ and pseudoscalar meson $\tilde{\pi} \sim \bar{q}\gamma_5 q$ is used.

$$\Sigma = \tilde{\sigma} + i\tilde{\pi} = T_a(\tilde{\sigma}_a + i\tilde{\pi}_a). \tag{2.18}$$

Here $T_a = \lambda_a/2$ $(a = 0, 1, ..., 8)$ are the generators of the $U(3)$ symmetry expressed with Gell-Mann Matrices and $\lambda_0 = \sqrt{\frac{2}{3}}\mathrm{diag}(1,1,1)$. This meson field Σ is in the form of $q_L \otimes \bar{q}_R$ under the chiral $SU(3)_R \times SU(3)_L$ space, so that the chiral transformation of Σ can be expressed with operators $U_{R/L}$ belonging to the special unitary group $SU(3)_{R/L}$ as

$$\mathrm{Ch}: \Sigma_{ij} \to (U_L)_{ik}\Sigma_{km}(U_R^\dagger)_{mj}\ ,\ U_{R/L} = \exp(i\theta^a_{R/L}T^a) \in SU(3)_{R/L}. \tag{2.19}$$

Although there are only four mesons for $SU(2)$ version, the $SU(3)$ extended linear sigma model has nine for both scalar and pseudoscalar mesons, containing 18 mesons totally [112, 113].

$$\tilde{\sigma} = \frac{1}{\sqrt{2}} \begin{pmatrix} \frac{1}{\sqrt{2}}(\sigma + a_0^0) & a_0^+ & K^{*+} \\ a_0^- & \frac{1}{\sqrt{2}}(\sigma - a_0^0) & K^{*0} \\ K^{*-} & \bar{K}^{*0} & \zeta \end{pmatrix}, \tag{2.20}$$

$$\tilde{\pi} = \frac{1}{\sqrt{2}} \begin{pmatrix} \frac{1}{\sqrt{2}}\pi^0 + \frac{1}{\sqrt{6}}\eta_8 + \frac{1}{\sqrt{3}}\eta_0 & \pi^+ & K^+ \\ \pi^- & -\frac{1}{\sqrt{2}}\pi^0 + \frac{1}{\sqrt{6}}\eta_8 + \frac{1}{\sqrt{3}}\eta_0 & K^0 \\ K^- & \bar{K}^0 & -\frac{2}{\sqrt{6}}\eta_8 + \frac{1}{\sqrt{3}}\eta_0 \end{pmatrix}. \tag{2.21}$$

Here σ and ζ in the scalar meson $\tilde{\sigma}$ corresponds to the chiral condensate of the u, d quarks and the s quark, respectively. They are concretely written as

$$\begin{aligned} \sigma &= \frac{1}{\sqrt{3}}\sigma_8 + \frac{\sqrt{2}}{\sqrt{3}}\sigma_0, \\ \zeta &= -\frac{2}{\sqrt{6}}\sigma_8 + \frac{1}{\sqrt{3}}\sigma_0. \end{aligned} \tag{2.22}$$

Using the Σ field, the meson part of the Lagrangian is written as [113, 114],

$$\begin{aligned} \mathcal{L}^M_{SU(3)} &= \frac{1}{4}\mathrm{Tr}[\partial_\mu \Sigma^\dagger \partial^\mu \Sigma] - V(\Sigma), \\ V(\Sigma) &= V_0(\Sigma) + V_{anm}(\Sigma) + V_{SB}(\Sigma) + V_{SB-anm}(\Sigma). \end{aligned} \tag{2.23}$$

The first and second terms in $\mathcal{L}^M_{SU(3)}$ show the kinematic part and the potential term, respectively. In the potential term $V(\Sigma)$, $V_0(\Sigma)$ fulfills the $SU(3)_R \times SU(3)_L \times U(1)_V \times U(1)_A$ symmetry, and $V_{anm}(\Sigma)$ only breaks $U(1)_A$ symmetry, which are written as

$$\begin{aligned} V_0(\Sigma) &= m^2 \mathrm{Tr}(\Sigma^\dagger \Sigma) + \lambda_1 [\mathrm{Tr}(\Sigma^\dagger \Sigma)]^2 + \lambda_2 [\mathrm{Tr}(\Sigma^\dagger \Sigma)^2], \\ V_{anm}(\Sigma) &= -B[\det(\Sigma) + \det(\Sigma^\dagger)], \end{aligned} \tag{2.24}$$

where m and B are one mass-dimensional parameters, and $\lambda_{1,2}$ are dimensionless parameters, respectively. The last two of the potential, $V_{SB}(\Sigma)$ and $V_{SB-anm}(\Sigma)$, are terms where the chiral symmetry is explicitly broken by the quark masses. These potentials are expressed with the matrix of the quark mass $\mathcal{M} = \mathrm{diag}(m_u, m_d, m_s)$ as below, in which m_u, m_d, m_s denote the mass of u, d, s quarks.

$$\begin{aligned} V_{SB}(\Sigma) &= -c\ \mathrm{Tr}[\mathcal{M}^\dagger \Sigma + \mathcal{M}\Sigma^\dagger], \\ V_{SB-anm}(\Sigma) &= -kc\ [\epsilon_{abc}\epsilon^{def} \mathcal{M}^a_d \Sigma^b_e \Sigma^c_f + h.c.]. \end{aligned} \tag{2.25}$$

Here c and k are parameters with the mass-dimension two and minus one, respectively. Similar to the $SU(2)$ version, the scalar meson $\tilde{\sigma}$ takes the finite VEV ($\tilde{\sigma} \sim \langle \bar{q}q \rangle \neq 0$) as

$$\langle \Sigma_{ij} \rangle = \langle \tilde{\sigma}_{ij} \rangle = \mathrm{diag}(f_\pi, f_\pi, f_s), \quad \langle \tilde{\pi}_{ij} \rangle = 0. \tag{2.26}$$

From the Goldberger-Treiman relation expressed as Eq. (2.14) in the last section, the VEV related to the u, d quarks are $\langle \tilde{\sigma}_{11} \rangle = \langle \tilde{\sigma}_{22} \rangle = f_\pi \simeq 92$ MeV. Also, the VEV for the s quark is given from kaon version of Goldberger-Treiman relation [111] as $\langle \tilde{\sigma}_{33} \rangle =$

$2f_K - f_\pi \equiv f_s \simeq 128$ MeV [87], where $f_K \simeq 110$ MeV is the kaon decay constant. The pseudoscalar mesons in $\tilde{\pi}$ field are the NG bosons appearing from the symmetry breaking [30–32], in which the VEV of $\tilde{\pi}$ is equal to zero.

Although Eq. (2.23) is the Lagrangian only for the Σ meson field, the quark part for this Lagrangian can be given by [114]

$$\mathcal{L}^q_{SU(3)} = \bar{q}\left[i\gamma^\mu\partial_\mu - g_s T_a(\tilde{\sigma}_a + i\gamma_5\tilde{\pi}_a)\right]q, \tag{2.27}$$

where g_s denotes the quark-meson coupling constant. As in Eq. (2.26), $\tilde{\sigma}$ takes the finite VEV related to the chiral condensate. Then if we exchange this field as $\tilde{\sigma} \to \tilde{\sigma} + \mathrm{diag}(f_\pi, f_\pi, f_s)$, the Lagrangian $\mathcal{L}^q_{SU(3)}$ becomes

$$\mathcal{L}^{q'}_{SU(3)} = \bar{q}\left[i\gamma^\mu\partial_\mu - g_s T_a(\tilde{\sigma}_a + i\tilde{\pi}_a)\right]q + g_s(f_\pi\bar{q}_1 q_1 + f_\pi\bar{q}_2 q_2 + f_s\bar{q}_3 q_3). \tag{2.28}$$

Therefore, the effective quark masses acquired by the chiral symmetry breaking are expressed as $g_s f_\pi \simeq 350$ MeV for u, d quarks, and $g_s f_s \simeq 450$ MeV for s quark.

Same process can be performed to the meson part of Lagrangian $\mathcal{L}^M_{SU(3)}$, in which the potential $V(\Sigma)$ takes the minimum value by inserting $\Sigma = \langle\Sigma\rangle$. Considering the isospin symmetry that masses of u and d quarks are the same, the mass formulae for pion and kaon are given by [113]

$$\begin{aligned} m_\pi^2 &= \frac{2cm_{u,d}}{f_\pi}(1 + kf_s), \\ m_K^2 &= \frac{2c(m_{u,d} + m_s)}{f_\pi + f_s}(1 + kf_\pi), \end{aligned} \tag{2.29}$$

and values of quark condensates are also given as

$$\begin{aligned} \langle\bar{n}n\rangle \equiv \langle\bar{u}u\rangle = \langle\bar{d}d\rangle &= \left\langle \frac{\partial\mathcal{L}^M_{SU(3)}}{\partial m_{u,d}} \right\rangle = -cf_\pi(1 + kf_s), \\ \langle\bar{s}s\rangle &= \left\langle \frac{\partial\mathcal{L}^M_{SU(3)}}{\partial m_s} \right\rangle = -c(f_s + kf_\pi^2). \end{aligned} \tag{2.30}$$

From these expressions, we can give relations to quark condensates with decay constants and meson masses as

$$\begin{aligned} f_\pi^2 m_\pi^2 &= -2m_{u,d}\langle\bar{n}n\rangle, \\ f_K^2 m_K^2 &= -\frac{m_{u,d} + m_s}{2}(\langle\bar{n}n\rangle + \langle\bar{s}s\rangle), \end{aligned} \tag{2.31}$$

which is called the Gell-Mann–Oakes–Renner relation [115].

2.3 Chiral effective Lagrangian for diquarks

In this section, we consider the chiral effective Lagrangian of diquarks on the basis of $SU(3)$ linear sigma model. As diquarks are the main components, we firstly construct some diquark fields made of two quarks, especially the right and left-handed form $q_{R/L}$ defined in Eq. (1.6). The chiral transformations of these two quark fields are given by

$$\begin{aligned} \mathrm{Ch}: q^a_{R,i} &\to (U_R)_{ij} q^a_{R,j}, \quad U_R \in SU(3)_R, \\ \mathrm{Ch}: q^a_{L,i} &\to (U_L)_{ij} q^a_{L,j}, \quad U_L \in SU(3)_L. \end{aligned} \tag{2.32}$$

From these transformations, we can define the chiral transformation of diquark fields [87]. Thus the chiral effective Lagrangian for diquarks based on the $SU(3)$ linear sigma model can be formalized with reference to Eqs. (2.19) and (2.32).

We now construct the chiral effective Lagrangian for scalar diquarks with spin 0 and vector diquarks with spin 1. In concrete, we describe the Lagrangian including the diquark fields and Σ fields as

$$\mathcal{L} = \frac{1}{4}\mathrm{Tr}[\partial_\mu \Sigma^\dagger \partial^\mu \Sigma] - V(\Sigma) + \mathcal{L}_S + \mathcal{L}_V + \mathcal{L}_{S-V}. \tag{2.33}$$

About third and forth terms in Eq. (2.33), $\mathcal{L}_S$ and $\mathcal{L}_V$, they are the Lagrangians only for scalar diquarks and vector diquarks with interaction of Σ field, respectively. The last $\mathcal{L}_{S-V}$ term shows the interaction between scalar and vector diquarks with Σ field. After the construction of effective Lagrangians, we consider the effects of chiral symmetry breaking to diquarks.

2.3.1 Chiral effective Lagrangian for scalar diquarks

At first, we define fields for scalar and pseudoscalar diquarks with the right and left-handed quark fields. According to Table 1.2, we can make two kinds of diquark fields as

$$d^a_{R,i} \equiv \epsilon^{abc}\epsilon_{ijk}(q^{bT}_{R,j} C q^c_{R,k}), \; d^a_{L,i} \equiv \epsilon^{abc}\epsilon_{ijk}(q^{bT}_{L,j} C q^c_{L,k}). \tag{2.34}$$

Here the superscript a, b, c and the subscript i, j, k are for color and flavor components, respectively. We define these fields $d^a_{R/L,i}$ as the right/left-handed diquark fields. These chiral transformations is given by

$$\mathrm{Ch}: d^a_{R,i} \;\to\; d^a_{R,j}(U^\dagger_R)_{ji} \;, \; d^a_{L,i} \;\to\; d^a_{L,j}(U^\dagger_L)_{ji}. \tag{2.35}$$

Next we consider the parity transformation of these right and left-handed diquarks. About the right and left-handed quark fields, these space inversions are given as

$$\mathcal{P} \;:\; q^a_{R,i}(t, \boldsymbol{x}) \to \gamma^0 q^a_{L,i}(t, -\boldsymbol{x}) \;, \; q^a_{L,i}(t, \boldsymbol{x}) \to \gamma^0 q^a_{R,i}(t, -\boldsymbol{x}). \tag{2.36}$$

Therefore, the parity transformation of right and left-handed diquarks is given by

$$\mathcal{P} \;:\; d^a_{R,i} \to -d^a_{L,i}, \;\; d^a_{L,i} \to -d^a_{R,i}. \tag{2.37}$$

Here we describe the scalar and pseudoscalar diquark fields as S^a_i and P^a_i, in which the parity transformation of these fields is given by

$$\mathcal{P} \;:\; S^a_i \to S^a_i \;, \; P^a_i \to -P^a_i. \tag{2.38}$$

As a result, these S_i^a and P_i^a diquark fields are expressed with the right and left-handed types of diquark fields as

$$S_i^a = \frac{1}{\sqrt{2}}(d_{R,i}^a - d_{L,i}^a) \ , \ P_i^a = \frac{1}{\sqrt{2}}(d_{R,i}^a + d_{L,i}^a). \tag{2.39}$$

With these diquark fields in Eq. (2.34) and the Σ meson field, the chiral effective Lagrangian for scalar and pseudoscalar diquarks gives form as

$$\begin{aligned}\mathcal{L}_S = &\mathcal{D}_\mu d_{R,i}(\mathcal{D}^\mu d_{R,i})^\dagger + \mathcal{D}_\mu d_{L,i}(\mathcal{D}^\mu d_{L,i})^\dagger \\ &- m_{S0}^2(d_{R,i}d_{R,i}^\dagger + d_{L,i}d_{L,i}^\dagger) \\ &- \frac{m_{S1}^2}{f_\pi}(d_{R,i}\Sigma_{ij}^\dagger d_{L,j}^\dagger + d_{L,i}\Sigma_{ij}d_{R,j}^\dagger) \\ &- \frac{m_{S2}^2}{2f_\pi^2}\epsilon_{ijk}\epsilon_{lmn}(d_{R,k}\Sigma_{li}\Sigma_{mj}d_{L,n}^\dagger + d_{L,k}\Sigma_{li}^\dagger\Sigma_{m,j}^\dagger d_{R,n}^\dagger),\end{aligned} \tag{2.40}$$

where the superscript for colors is omitted. The mass-dimension of coefficients $m_{S0,S1,S2}$ are all one.

Since the chiral transformation of Σ field is expressed as $\Sigma_{ij} \to (U_L)_{ik}\Sigma_{km}(U_R^\dagger)_{mj}$ in Eq. (2.19), this Lagrangian is certainly chiral invariant. Also, the parity transformation of Σ is given as $\mathcal{P} : \Sigma_{ij} \to \Sigma_{ij}^\dagger$, so that this effective Lagrangian is invariant under the space inversion. However, under the axial vector transformation, the term with coefficient m_{S1}^2 is not invariant, which is responsible for the chiral $U(1)_A$ anomaly effects induced by the instanton [87]. The $U(1)_A$ symmetry breaking of m_{S1}^2 term can be confirmed by Fig. 2.1, where the number of right handed (R) and left handed (L) quarks are not conserved through the interaction vertex m_{S1}^2.

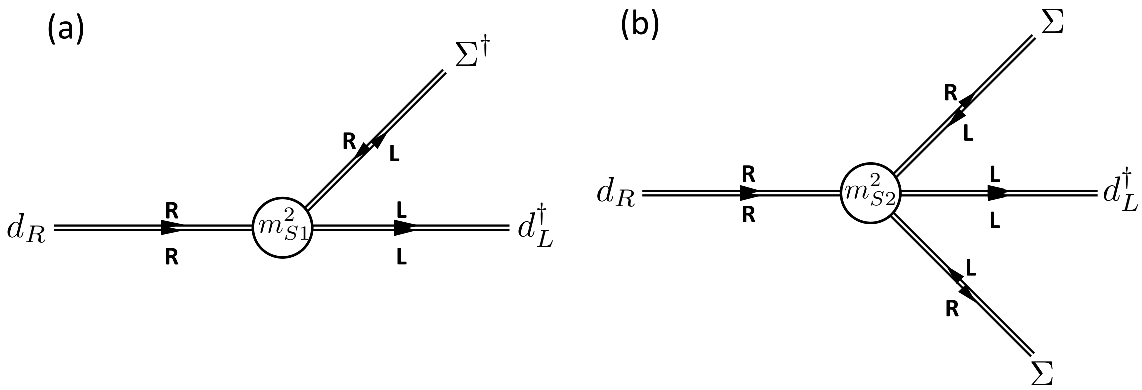

Figure2.1 Quark line representations for the effective Lagrangian $\mathcal{L}_S$ in Eq. (2.40), showing the interaction between scalar diquarks and mesons. The left and right figure describe m_{S1}^2 term and m_{S2}^2 term, respectively.

The first line of Eq. (2.40) shows the kinetic terms, where $\mathcal{D}_\mu = \partial_\mu + igA_\mu^aT^a$ is the color-gauge covariant derivative appearing from diquarks being non-color singlet. The second line with coefficient m_{S0}^2 is the mass term, and the others are the interaction terms with one or two Σ fields. However, we omit terms including $\Sigma\Sigma^\dagger$ or $\Sigma^\dagger\Sigma$, because they do not affect to the mass differences between scalar and pseudoscalar diquarks [87]. Also, we neglect terms including three or more Σ fields.

2.3.2 Mass formulae of scalar diquarks

According to the linear sigma model for quarks explained in the previous section, light quarks aquire effective masses more than 300 MeV by the spontaneous chiral symmetry breaking, which is expressed with the VEV of σ field as $g_s\langle\tilde{\sigma}_{ii}\rangle$. In the case of explicit chiral symmetry breaking, these effective masses are added with the genuine light quark masses $m_i \neq 0$, so that the mass term of quark field becomes as

$$-m_i\bar{q}_i q_i \to -(m_i + g_s\langle\tilde{\sigma}_{ii}\rangle)\bar{q}_i q_i. \tag{2.41}$$

Using the quark mass matrix $\mathcal{M} = \mathrm{diag}\{m_u, m_d, m_s\}$, the effective quark mass matrix $\mathcal{M}_{\mathrm{eff}}$ is written with the VEV of Σ field as

$$\begin{aligned}\mathcal{M} \to \mathcal{M}_{\mathrm{eff}} &= \mathcal{M} + g_s\langle\Sigma\rangle \\ &= \mathrm{diag}\{m_u + g_s f_\pi, m_d + g_s f_\pi, m_s + g_s f_s\}.\end{aligned} \tag{2.42}$$

About u, d quark masses $m_{u,d} \simeq 2, 5$ MeV, they are much lighter than the mass of s quark $m_s \simeq 100$ MeV, and also the effective masses by the chiral symmetry breaking $g_s f_\pi \simeq 350$ MeV, $g_s f_s \simeq 450$ MeV. Neglecting these quark masses as $m_{u,d} \to 0$, the effective quark mass matrix $\mathcal{M}_{\mathrm{eff}}$ is approximated as

$$\mathcal{M}_{\mathrm{eff}} \simeq g_s f_\pi \mathrm{diag}\{1, 1, \check{\mathcal{A}}_{\mathrm{s}}\},\ \check{\mathcal{A}}_{\mathrm{s}} \equiv \frac{f_s}{f_\pi}(1 + \frac{m_s}{g_s f_s}) \simeq 5/3. \tag{2.43}$$

The value of constant $\check{\mathcal{A}}_{\mathrm{s}}$ can be determined by $f_\pi = 92.1$ MeV, $f_s = 2f_K - f_\pi = 128.1$ MeV, $m_s = 93.1$ MeV, and $g_s = 2\pi/\sqrt{3}$ from Refs. [12, 109, 110]. Hence this value is consequently given by $\check{\mathcal{A}}_{\mathrm{s}} = 1.669...$, so that it is well approximated as $\check{\mathcal{A}}_{\mathrm{s}} = 5/3$.

To consider the explicit chiral symmetry breaking effect for the chiral effective Lagrangian (2.40), we firstly replace the Σ field as $\Sigma \to \Sigma + \mathcal{M}/g_s$ to add terms where the chiral symmetry is explicitly broken by the quark masses. Next, we substitute the VEV in Eq. (2.26) to the Σ field which is expressed as $\langle\Sigma\rangle = \mathrm{diag}(f_\pi, f_\pi, f_s)$. The total of this operation is the same as substituting the VEV of Σ field for the explicit chiral symmetry breaking, defined as

$$\langle\Sigma\rangle_{SB} \equiv \mathcal{M}_{\mathrm{eff}}/g_s \simeq f_\pi \mathrm{diag}\{1, 1, \check{\mathcal{A}}_{\mathrm{s}}\}. \tag{2.44}$$

From now on, we use the matrix $f_\pi \mathrm{diag}\{1, 1, \check{\mathcal{A}}_{\mathrm{s}}\}$ for the VEV of Σ field in the situation of considering the explicit chiral symmetry breaking. With this mean field approximation, the Lagrangian for scalar and pseudoscalar diquarks becomes

$$\begin{aligned}\mathcal{L}_S^{SB} &= \mathcal{D}_\mu d_{R,i}(\mathcal{D}^\mu d_{R,i})^\dagger + \mathcal{D}_\mu d_{L,i}(\mathcal{D}^\mu d_{L,i})^\dagger - \mathcal{L}_{Smass}, \\ \mathcal{L}_{Smass} &= m_{S0}^2(d_{R,i}d_{R,i}^\dagger + d_{L,i}d_{L,i}^\dagger) \\ &\quad + (m_{S1}^2 + \check{\mathcal{A}}_{\mathrm{s}} m_{S2}^2)(d_{R,1}d_{L,1}^\dagger + d_{L,1}d_{R,1}^\dagger + d_{R,2}d_{L,2}^\dagger + d_{L,2}d_{R,2}^\dagger) \\ &\quad + (\check{\mathcal{A}}_{\mathrm{s}} m_{S1}^2 + m_{S2}^2)(d_{R,3}d_{L,3}^\dagger + d_{L,3}d_{R,3}^\dagger).\end{aligned} \tag{2.45}$$

Here $\mathcal{L}_{Smass}$ denotes the mass terms. From Eqs. (2.34) and (2.35), the flavor of right and left-handed diquarks $i = 1, 2, 3$ is equivalent to ds, su, ud diquarks, where $i = 1, 2$ have one strange quark and $i = 3$ is non-strange type. The classified mass term $\mathcal{L}_{Smass}$ into each flavor is written as below.

1. For ds, su singly strange diquarks,

$$\mathcal{L}_{Smass(i=1,2)} = \begin{pmatrix} d_{R,i=1,2} \\ d_{L,i=1,2} \end{pmatrix}^\dagger \begin{pmatrix} m_{S0}^2 & m_{S1}^2 + \check{A}_s m_{S2}^2 \\ m_{S1}^2 + \check{A}_s m_{S2}^2 & m_{S0}^2 \end{pmatrix} \begin{pmatrix} d_{R,i=1,2} \\ d_{L,i=1,2} \end{pmatrix}. \tag{2.46}$$

2. For ud non-strange diquark,

$$\mathcal{L}_{Smass(i=3)} = \begin{pmatrix} d_{R,i=3} \\ d_{L,i=3} \end{pmatrix}^\dagger \begin{pmatrix} m_{S0}^2 & \check{A}_s m_{S1}^2 + m_{S2}^2 \\ \check{A}_s m_{S1}^2 + m_{S2}^2 & m_{S0}^2 \end{pmatrix} \begin{pmatrix} d_{R,i=3} \\ d_{L,i=3} \end{pmatrix}. \tag{2.47}$$

In each mass terms Eqs. (2.46) and (2.47), we change diquark fields from the right/left-handed type, $d_{R,i}$ and $d_{L,i}$, to the parity eigenstates, S_i and P_i, by Eq. (2.39). At this time, the 2×2 matrices composed of parameters m_0^2, m_1^2, m_2^2, and $\check{A}_s$ are diagonalized, and these components show the squared masses of scalar and pseudoscalar diquarks. These mass eigenvalues are calculated as

$$\begin{aligned} M_{1,2}(0^+) &= \sqrt{m_{S0}^2 - m_{S1}^2 - \check{A}_s m_{S2}^2}, \\ M_3(0^+) &= \sqrt{m_{S0}^2 - \check{A}_s m_{S1}^2 - m_{S2}^2}, \\ M_{1,2}(0^-) &= \sqrt{m_{S0}^2 + m_{S1}^2 + \check{A}_s m_{S2}^2}, \\ M_3(0^-) &= \sqrt{m_{S0}^2 + \check{A}_s m_{S1}^2 + m_{S2}^2}. \end{aligned} \tag{2.48}$$

These are the mass formulae of scalar and pseudoscalar diquarks from the linear sigma model. For the left side of these equations, the subscript of M and $(0^\pm)$ denote the flavor and spin-parity states of diquarks, respectively.

Moreover, four equations in Eq. (2.48) are totally expressed only by the diquark mass symbols $M_i(J^P)$ as

$$[M_{1,2}(0^+)]^2 - [M_3(0^+)]^2 = [M_3(0^-)]^2 - [M_{1,2}(0^-)]^2. \tag{2.49}$$

To discuss the mass formula in Eq. (2.49), here we consider the scalar diquark as a component of singly heavy baryons. According to Table 1.3, the non-strange ud scalar diquark and the singly strange ds, su scalar diquarks can be an element of Λ_Q and Ξ_Q baryons, respectively. Also, according to Fig. 1.8 from Ref. [12], the experimental masses of Λ_c and Ξ_c baryons in the ground states are 2286.46 MeV and 2469.42 MeV, and those of Λ_b and Ξ_b baryons are 5619.60 MeV and 5794.45 MeV, respectively. Thus, as the Λ_Q baryons are lighter than Ξ_Q baryons with the same heavy quark Q, the mass relation of scalar diquarks is expected to be

$$M_{1,2}(0^+) > M_3(0^+), \tag{2.50}$$

in which a ds or su diquark is heavier than a ud diquark. Hence both side of Eq. (2.49) are positive. However, this expectation for scalar diquark masses brings about the peculiar feature for pseudoscalar diquarks. That is, from Eqs. (2.49) and (2.50), the mass relation for pseudoscalar diquarks becomes

$$M_{1,2}(0^-) < M_3(0^-), \tag{2.51}$$

unless diquarks are not tachyonic. This inequality shows that a ud pseudoscalar diquark is heavier than a ds or su pseudoscalar diquark, which is inversely different from the scalar diquark masses. As a consequence, whereas u, d quarks are lighter than s quark, the pseudoscalar diquark takes the big mass value with containing no s quark rather than one.

A

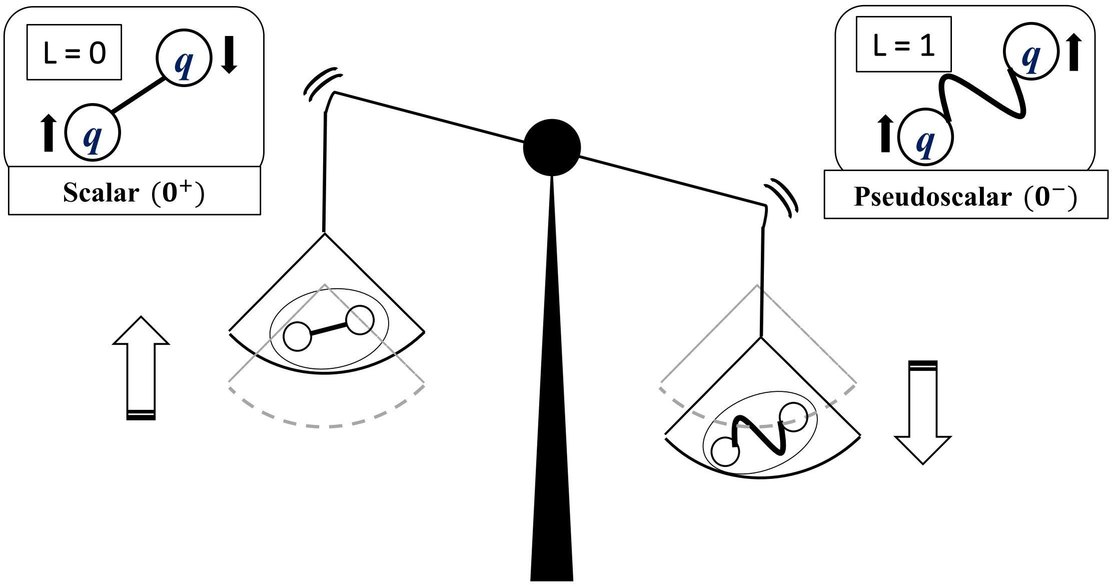

Figure2.2 Chiral partner structure by the scalar and pseudoscalar diquarks. The masses of these diquarks are degenerate to m_{S0} in case that the chiral symmetry is satisfied in the chiral limit. When the chiral symmetry breaks, the scalar diquark becomes lighter than the pseudoscalar diquark.

The explicit chiral symmetry breaking consequently induced the mass equation and relation for scalar and pseudoscalar diquarks as Eqs. (2.48) and (2.49). However, if the chiral symmetry is not broken with massless quarks, the VEV of scalar meson field becomes $\langle\tilde{\sigma}\rangle = 0$. Therefore, from $\langle\Sigma\rangle = 0$, the parameters m_{S1}^2 and m_{S2}^2 in mass formulae are all erased, and scalar and pseudoscalar diquarks are all degenerate to the chiral invariant mass m_{S0}. This indicates that scalar and pseudoscalar diquarks are the chiral partner which have same spin 0 but have different parity.

2.3.3 Chiral effective Lagrangian for vector diquarks

In this subsection, firstly, we define the field showing the vector and axial-vector diquarks. According to Table 1.2, we can make the diquark field expressed as

$$d_{ij}^{a,\mu} \equiv \epsilon^{abc}(q_{L,i}^{bT} C\gamma^\mu q_{R,j}^c) = \epsilon^{abc}(q_{R,j}^{bT} C\gamma^\mu q_{L,i}^c). \tag{2.52}$$

The superscript a, b, c and the subscript i, j, k represent the color and flavor, respectively, and this vector field consists both right and left-handed quarks. We call this field $d_{ij}^{a;\mu}$ as chiral vector diquark field, in which this chiral transformation is given by

$$\begin{aligned} \mathrm{Ch} &: d_{ij}^{a,\mu} \to U_{L,ik}\; d_{km}^{a,\mu}\; U_{R,mj}^{T}, \\ (\mathrm{Ch} &: d_{ij}^{a,\mu\dagger} \to U_{R,ik}^{T\dagger}\; d_{km}^{a,\mu\dagger}\; U_{L,mj}^{\dagger}). \end{aligned} \tag{2.53}$$

Vector diquark and axial-vector diquark fields, $V_{ij}^{a,\mu}$ and $A_{ij}^{a,\mu}$, are expressed with this field. Considering the parity transformation of the chiral vector diquark field, it is given by

$$\mathcal{P} \;:\; d_{ij}^{a,\mu} \to -d_{\mu,ij}^{a}, \tag{2.54}$$

because of the space inversion of right and left-handed quark expressed as $\mathcal{P}:\; q_{R,i}^{a}(t,\boldsymbol{x}) \to \gamma^0 q_{L,i}^{a}(t,-\boldsymbol{x})$ and $\mathcal{P}:\; q_{L,i}^{a}(t,\boldsymbol{x}) \to \gamma^0 q_{R,i}^{a}(t,-\boldsymbol{x})$, according to Eq. (2.36). On the other hand, the parity transformation of $V_{ij}^{a,\mu}$ and $A_{ij}^{a,\mu}$ fields is expressed as

$$\mathcal{P} \;:\; V_{ij}^{a,\mu} \to V_{\mu,ij}^{a} \;,\; A_{ij}^{a,\mu} \to -A_{\mu,ij}^{a}. \tag{2.55}$$

As a Consequence, these $V_{ij}^{a,\mu}$ and $A_{ij}^{a,\mu}$ diquark fields are represented by the chiral vector diquark field as

$$V_{ij}^{a,\mu} = \frac{1}{\sqrt{2}}(d_{ij}^{a,\mu} - d_{ji}^{a,\mu}) \;,\; A_{ij}^{a,\mu} = \frac{1}{\sqrt{2}}(d_{ij}^{a,\mu} + d_{ji}^{a,\mu}). \tag{2.56}$$

With refer to these vector diquark fields, we construct the chiral effective Lagrangian for vector and axial-vector diquarks. Using the chiral vector diquark field in Eq. (2.52) and the Σ meson field, the effective Lagrangian for these vector diquarks is formed as

$$\begin{aligned} \mathcal{L}_V =& -\frac{1}{2}\mathrm{Tr}[F^{\mu\nu}F_{\mu\nu}^{\dagger}] + m_{V0}^2\mathrm{Tr}[d^{\mu}d_{\mu}^{\dagger}] \\ &+ \frac{m_{V1}^2}{f_\pi^2}\mathrm{Tr}[\Sigma^{\dagger}d^{\mu}\Sigma^{T}d_{\mu}^{\dagger T}] + \frac{m_{V2}^2}{f_\pi^2}\left\{\mathrm{Tr}[\Sigma^{T}\Sigma^{\dagger T}d_{\mu}^{\dagger}d^{\mu}] + \mathrm{Tr}[\Sigma\Sigma^{\dagger}d^{\mu}d_{\mu}^{\dagger}]\right\}, \end{aligned} \tag{2.57}$$

where the superscript for colors is omitted. The mass-dimension of coefficients $m_{V0,V1,V2}$ are all one.

Same to Eq. (2.40), this Lagrangian is invariant under the chiral transformation, and also under the space inversion. Moreover, this Lagrangian is also invariant under the axial vector transformation, so that there are no chiral $U(1)_A$ anomaly effect. This $U(1)_A$ invariance is confirmed by Fig. 2.3, where the number of right/left handed quarks (R/L) are conserved through both of interaction vertices, m_{V1}^2 and m_{V2}^2.

For the first term of Eq. (2.57), $F^{\mu\nu} = \mathcal{D}^{\mu}d^{\nu} - \mathcal{D}^{\nu}d^{\mu}$ is the strength of chiral vector diquark fields, which denotes the kinetic term. The second term shows the mass term, and the others are the interaction terms with two Σ fields. Note that there are no interaction terms with only one Σ field which satisfy the chiral symmetry. For the others, We omit terms which includes $\mathrm{Tr}[\Sigma\Sigma^{\dagger}]$ as they do not affect to the difference of diquark masses. Also, we neglect terms including more than two Σ fields.

2.3.4 Mass formulae of vector diquarks

In the same way as the chiral effective Lagrangian for scalar diquarks, we derive the mass formulae of vector diquarks from chiral effective Lagrangian (2.57). Using the VEV of Σ field $\langle\Sigma\rangle_{SB}$ in Eq. (2.44), and classifying the chiral vector diquark field into the vector

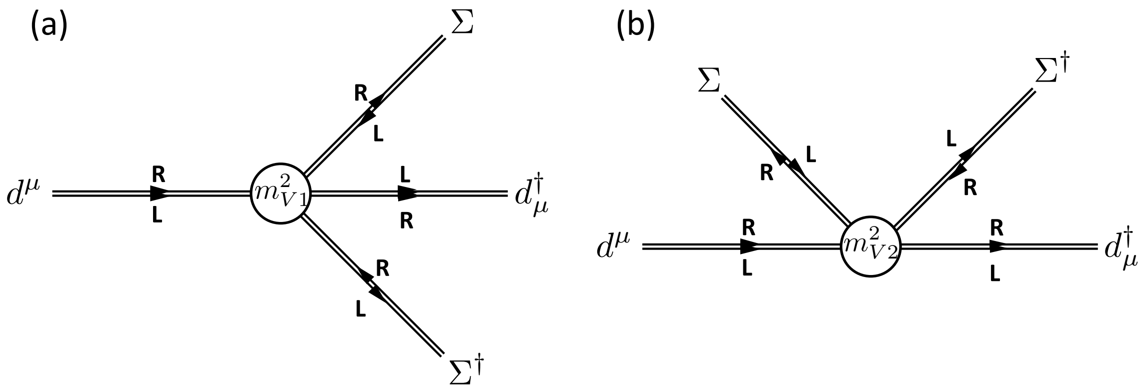

Figure2.3 Quark line representations for the effective Lagrangian $\mathcal{L}_V$ in Eq. (2.57), showing the interaction between vector diquarks and mesons. The left and right figure describe m^2_{V1} term and m^2_{V2} term, respectively.

and axial-vector diquark fields by Eq. (2.56), the mass term of this Lagrangian $\mathcal{L}_{Vmass}$ is given by

$$\begin{aligned}\mathcal{L}_V^{SB} &= -\frac{1}{2}\mathrm{Tr}[F^{\mu\nu}F^\dagger_{\mu\nu}] + \mathcal{L}_{Vmass},\\ \mathcal{L}_{Vmass} &= \frac{1}{2}m^2_{V0}\mathrm{Tr}[A^\mu A^\dagger_\mu] + \frac{1}{2}m^2_{V1}\mathrm{Tr}[XA^\mu XA^\dagger_\mu] + m^2_{V2}\mathrm{Tr}[X^2A^\mu A^\dagger_\mu]\\ &= \frac{1}{2}m^2_{V0}\mathrm{Tr}[V^\mu V^\dagger_\mu] - \frac{1}{2}m^2_{V1}\mathrm{Tr}[XV^\mu XV^\dagger_\mu] + m^2_{V2}\mathrm{Tr}[X^2V^\mu V^\dagger_\mu],\end{aligned} \tag{2.58}$$

where $X \equiv \mathrm{diag}\{1, 1, \check{\mathcal{A}}_s\}$. Therefore, the mass formulae of axial-vector diquarks and vector diquarks are given as

$$M^2_{nn}(1^+) = m^2_{V0} + m^2_{V1} + 2m^2_{V2}, \tag{2.59}$$
$$M^2_{ns}(1^+) = m^2_{V0} + \check{\mathcal{A}}_s m^2_{V1} + (1+\check{\mathcal{A}}_s^2)m^2_{V2}, \tag{2.60}$$
$$M^2_{ss}(1^+) = m^2_{V0} + \check{\mathcal{A}}_s^2 m^2_{V1} + 2\check{\mathcal{A}}_s^2 m^2_{V2}, \tag{2.61}$$
$$M^2_{ud}(1^-) = m^2_{V0} - m^2_{V1} + 2m^2_{V2}, \tag{2.62}$$
$$M^2_{ns}(1^-) = m^2_{V0} - \check{\mathcal{A}}_s m^2_{V1} + (1+\check{\mathcal{A}}_s^2)m^2_{V2}, \tag{2.63}$$

where n in the subscript of M denotes u, d quarks while s shows the strange quark, and $(1^\pm)$ shows the spin-parity states of diquarks.

For the parameter $\check{\mathcal{A}}_s$ in Eqs. (2.59) – (2.63), we newly define the parameter $\epsilon \equiv \check{\mathcal{A}}_s - 1 (= 2/3)$, and approximate the square of $\check{\mathcal{A}}_s$ as $\check{\mathcal{A}}_s^2 \simeq 1 + 2\epsilon$. Then these mass formulae is expressed with this new parameter ϵ as

$$M^2_{nn}(1^+) = m^2_{V0} + m^2_{V1} + 2m^2_{V2}, \tag{2.64}$$
$$M^2_{ns}(1^+) = m^2_{V0} + m^2_{V1} + 2m^2_{V2} + \epsilon(m^2_{V1} + 2m^2_{V2}), \tag{2.65}$$
$$M^2_{ss}(1^+) = m^2_{V0} + m^2_{V1} + 2m^2_{V2} + 2\epsilon(m^2_{V1} + 2m^2_{V2}), \tag{2.66}$$
$$M^2_{ud}(1^-) = m^2_{V0} - m^2_{V1} + 2m^2_{V2}, \tag{2.67}$$
$$M^2_{ns}(1^-) = m^2_{V0} - m^2_{V1} + 2m^2_{V2} + \epsilon(-m^2_{V1} + 2m^2_{V2}). \tag{2.68}$$

From these mass formulae, we can tell about the axial-vector diquark masses in Eqs. (2.64) – (2.66) that the mass difference between non-strange and singly strange diquarks is equivalent to that between singly strange and doubly strange diquarks, written as

$$M_{ss}^2(1^+) - M_{ns}^2(1^+) = M_{ns}^2(1^+) - M_{nn}^2(1^+) = \epsilon(m_{V1}^2 + 2m_{V2}^2). \tag{2.69}$$

This relation for axial-vector diquarks corresponds to the generalized Gell-Mann–Okubo mass formula for diquark bosons [116, 117], which is also given by the flavor symmetry breaking. Moreover, the equation (2.69) is also shown as $2M_{ns}^2(1^+) = M_{nn}^2(1^+) + M_{ss}^2(1^+)$, which leads to

$$4M_{ns}^2(1^+) - \{M_{nn}(1^+) + M_{ss}(1^+)\}^2 = \{M_{nn}(1^+) - M_{ss}(1^+)\}^2 \geq 0. \tag{2.70}$$

As a consequence, this equation indicates the mass relation written as

$$M_{nn}(1^+) + M_{ss}(1^+) \leq 2M_{ns}(1^+). \tag{2.71}$$

Without considering the interaction between an axial-vector diquark and a charm quark, this inequality leads to the mass relation of Σ_c, Ξ_c', and Ω_c baryons, i.e., Eq. (2.71) naively expresses the mass relation of singly charmed baryons as

$$M(\Omega_c; 1/2^+, 3/2^+) + M(\Sigma_c; 1/2^+, 3/2^+) \leq 2M(\Xi_c'; 1/2^+, 3/2^+). \tag{2.72}$$

The symbol $M(Y_c; 1/2^+, 3/2^+)$ denotes the spin-averaged mass of singly charmed baryon Y_c in the ground states with spin-parity $J^P = 1/2^+, 3/2^+$. According to PDG [12], these three mass values are $M(\Sigma_c; 1/2^+, 3/2^+) = 2496.60$ MeV, $M(\Xi_c'; 1/2^+, 3/2^+) = 2623.52$ MeV, and $M(\Omega_c; 1/2^+, 3/2^+) = 2742.33$ MeV, which satisfies Eq. (2.72).

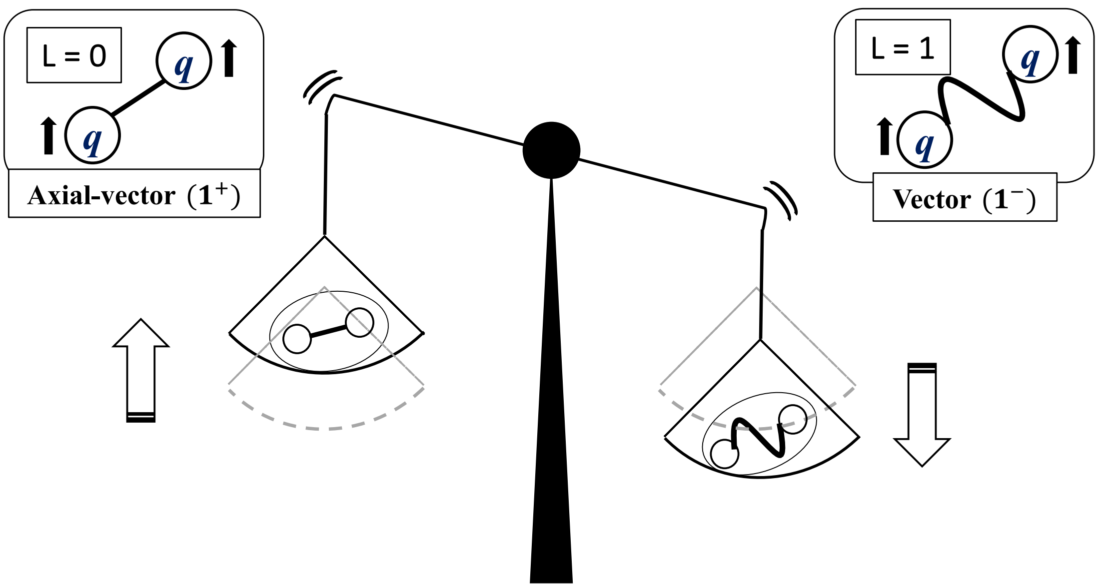

Figure2.4 Chiral partner structure by the vector and axial-vector diquarks. The masses of these diquarks are degenerate to m_{V0} in case that the chiral symmetry is satisfied in the chiral limit. When the chiral symmetry breaks, the axial-vector diquark becomes lighter than the vector diquark.

As the scalar and pseudoscalar diquarks, we next consider the mass relation of vector and axial-vector diquarks excluding the chiral symmetry breaking effect with the chiral limit. If the chiral symmetry is not broken with massless quarks, the VEV of scalar meson field becomes $\langle\tilde{\sigma}\rangle = 0$, and the parameters m_{V1}^2 and m_{V2}^2 in the mass formulae Eqs. (2.64) – (2.66) vanishes. Hence vector and axial-vector diquarks are all degenerate to the chiral invariant mass m_{V0}, meaning these diquarks with same spin 1 and opposite parity are the chiral partner.

From here, we note that we apply Eqs. (2.64) – (2.68) for the mass formulae of vector and axial-vector diquarks in usual, which lead to the generalized Gell-Mann–Okubo mass formula for axial-vector diquarks as in Eq. (2.69).

2.3.5 Chiral effective Lagrangian for scalar and vector diquarks

In the previous subsections, we created the fields which represent scalar and vector diquarks by using left and right handed quarks $q^a_{R/L,i}$, written as Eqs. (2.34) and (2.52). Using these fields, the chiral effective Lagrangians for scalar and vector diquarks are independently constructed as Eqs. (2.40) and (2.57), respectively. In this subsection, we explain the chiral effective Lagrangian with the mixture of diquark fields in Eqs. (2.34) and (2.52), which represents the interaction between scalar and vector diquarks. This type of Lagrangian is created with the partial derivative of Σ field, $\partial_\mu\Sigma$, and is written as

$$\begin{aligned}\mathcal{L}_{S-V} = & \, g_1\epsilon_{ijk}\left[d^\mu_{ni}(\partial_\mu\Sigma^\dagger)_{jn}d^\dagger_{R,k} + d^\mu_{in}(\partial_\mu\Sigma)_{jn}d^\dagger_{L,k}\right] \\ & + \frac{g_2}{f_\pi}\epsilon_{ijk}\Big[d^\mu_{in}\{\Sigma_{jn}(\partial_\mu\Sigma)_{km} - (\partial_\mu\Sigma)_{jn}\Sigma_{km}\}d^\dagger_{R,m} \\ & \qquad + d^\mu_{ni}\{\Sigma^\dagger_{jn}(\partial_\mu\Sigma^\dagger)_{km} - (\partial_\mu\Sigma^\dagger)_{jn}\Sigma^\dagger_{km}\}d^\dagger_{L,m}\Big], \end{aligned} \tag{2.73}$$

where the superscript for colors is omitted. The coefficients $g_{1,2}$ are the dimensionless coupling constant for terms including one and two Σ fields, respectively. The terms including more than two Σ fields are neglected.

Consequently, this Lagrangian is chiral invariant and also invariant under the parity transformation. However, under the axial vector transformation, only the g_2 term is $U(1)_A$ anomalous. We can confirm this chiral $U(1)_A$ anomaly effect from Fig. 2.5, where the number of right/left handed quarks (R/L) are not conserved only through the interaction vertex g_2.

To incorporate the explicit chiral symmetry breaking effect, we substitute $\langle\Sigma\rangle_{SB}$ in Eq. (2.44) for Σ fields in this interaction Lagrangian (2.73). Moreover, we use the parity eigenstates for diquark and meson fields, and truncate terms including the scalar meson field $\tilde{\sigma}$. As a result, The mean-field approximated Lagrangian with the interaction mediated by pseudoscalar mesons $\tilde{\pi}$ is expressed with

$$\mathcal{L}^{SB}_{S-V} = \mathcal{L}_{AS\pi} + \mathcal{L}_{VP\pi}, \tag{2.74}$$

where

$$\begin{aligned} i\mathcal{L}_{AS\pi} = & \,(g_1 + \check{A}_s g_2)\left[A^\mu_{1n}(\partial_\mu\tilde{\pi})_{2n}S^\dagger_3 - A^\mu_{2n}(\partial_\mu\tilde{\pi})_{1n}S^\dagger_3\right] \\ & + (g_1 + g_2)\Big[A^\mu_{2n}(\partial_\mu\tilde{\pi})_{3n}S^\dagger_1 - A^\mu_{3n}(\partial_\mu\tilde{\pi})_{2n}S^\dagger_1 \\ & \qquad + A^\mu_{3n}(\partial_\mu\tilde{\pi})_{1n}S^\dagger_2 - A^\mu_{1n}(\partial_\mu\tilde{\pi})_{3n}S^\dagger_2\Big], \end{aligned} \tag{2.75}$$

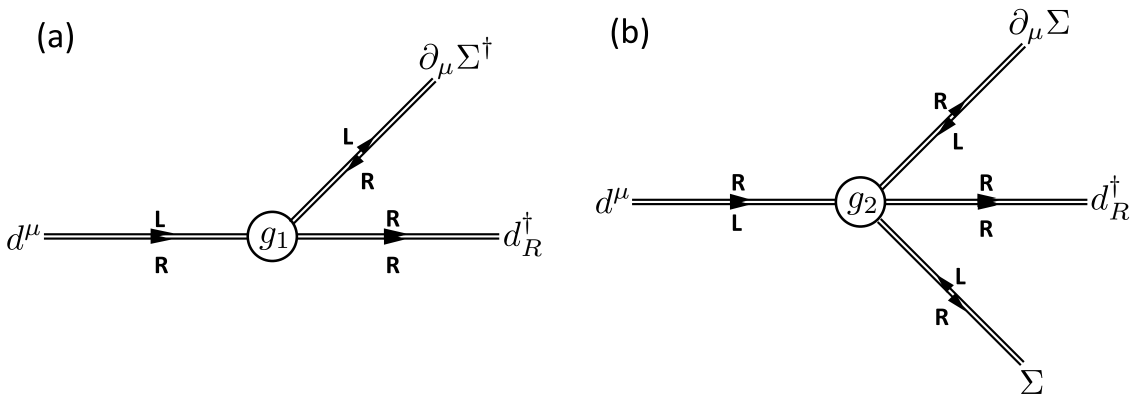

Figure2.5 Quark line representations for the effective Lagrangian $\mathcal{L}_{S-V}$ in Eq. (2.73), showing the interaction between scalar and vector diquarks meditated by mesons. The left and right figure describe g_1 term and g_2 term, respectively.

and

$$\begin{aligned}i\mathcal{L}_{VP\pi} = &-(g_1 - \check{\mathcal{A}}_{\rm s} g_2)\left[V^\mu_{1n}(\partial_\mu\tilde{\pi})_{2n}P_3^\dagger - V^\mu_{2n}(\partial_\mu\tilde{\pi})_{1n}P_3^\dagger\right]\\ &-(g_1 - g_2)\Big[V^\mu_{2n}(\partial_\mu\tilde{\pi})_{3n}P_1^\dagger - V^\mu_{3n}(\partial_\mu\tilde{\pi})_{2n}P_1^\dagger\\ &\qquad + V^\mu_{3n}(\partial_\mu\tilde{\pi})_{1n}P_2^\dagger - V^\mu_{1n}(\partial_\mu\tilde{\pi})_{3n}P_2^\dagger\Big]\\ &-(1+\check{\mathcal{A}}_{\rm s})g_2\left[V^\mu_{23}(\partial_\mu\tilde{\pi})_{1n}P_n^\dagger + V^\mu_{31}(\partial_\mu\tilde{\pi})_{2n}P_n^\dagger\right] - 2g_2\left[V^\mu_{12}(\partial_\mu\tilde{\pi})_{3n}P_n^\dagger\right].\end{aligned} \tag{2.76}$$

Each expression indicates that the interaction of two diquarks mediated by the pseudoscalar mesons must have the same parity: Diquarks with positive parity as the axial-vector and scalar diquarks interact through the $\tilde{\pi}$ meson field as Eq. (2.75). As the same, the negative-parity pair with vector and pseudoscalar diquarks interact with $\tilde{\pi}$ meson as Eq. (2.76).

Furthermore, the pseudoscalar meson field can be decomposed into the flavor singlet and octet parts as

$$\tilde{\pi}_{ij} = \sqrt{\frac{2}{3}}\eta_1\delta_{ij} + \sqrt{2}\begin{pmatrix} \frac{\pi^0}{\sqrt{2}} + \frac{\eta_8}{\sqrt{6}} & \pi^+ & K^+ \\ \pi^- & -\frac{\pi^0}{\sqrt{2}} + \frac{\eta_8}{\sqrt{6}} & K^0 \\ K^- & \bar{K}^0 & -\frac{2\eta_8}{\sqrt{6}} \end{pmatrix} \equiv \sqrt{\frac{2}{3}}\pi^{(1)}\delta_{ij} + \pi^{(8)}_{ij}. \tag{2.77}$$

By substituting Eq. (2.77) into Eqs. (2.75) and (2.76), the flavor structure becomes more transparent. In particular, the interaction between scalar and axial-vector diquarks is expressed as

$$\begin{aligned}i\mathcal{L}_{AS\pi} = &(g_1 + \check{\mathcal{A}}_{\rm s} g_2)\left[A^\mu_{1n}(\partial_\mu\pi^{(8)})_{2n}S_3^\dagger - A^\mu_{2n}(\partial_\mu\pi^{(8)})_{1n}S_3^\dagger\right]\\ &+(g_1 + g_2)\Big[A^\mu_{2n}(\partial_\mu\pi^{(8)})_{3n}S_1^\dagger - A^\mu_{3n}(\partial_\mu\pi^{(8)})_{2n}S_1^\dagger\\ &\qquad + A^\mu_{3n}(\partial_\mu\pi^{(8)})_{1n}S_2^\dagger - A^\mu_{1n}(\partial_\mu\pi^{(8)})_{3n}S_2^\dagger\Big],\end{aligned} \tag{2.78}$$

where the flavor singlet pseudoscalar meson $\pi^{(1)}$ is not associated to this interaction. This reason is that the flavor structure of axial-vector and scalar diquarks are different with each other as **6** and $\bar{\mathbf{3}}$, respectively. Therefore, only the flavor octet pseudoscalar meson $\pi^{(8)}$ can intermediate these diquarks with different flavors as $\bar{3}\otimes 8 = \bar{3}\oplus 6\oplus 15$ or as $6\otimes 8 = \bar{3}\oplus 6\oplus 15\oplus 24$. On the other hand, the vector diquark and pseudoscalar diquark are both flavor $\bar{\mathbf{3}}$, so that they can also interact with the flavor singlet pseudoscalar meson as

$$\begin{aligned}
i\mathcal{L}_{VP\pi} =& 2\sqrt{\frac{2}{3}}\{(\check{\mathcal{A}}_{\rm s}-1)g_2-g_1\}\left[V_{12}^{\mu}(\partial_\mu\pi^{(1)})P_3^\dagger\right] \\
&+\sqrt{\frac{2}{3}}\{(1-\check{\mathcal{A}}_{\rm s})g_2-2g_1\}\left[V_{23}^{\mu}(\partial_\mu\pi^{(1)})P_1^\dagger+V_{31}^{\mu}(\partial_\mu\pi^{(1)})P_2^\dagger\right] \\
&+\{g_1-(1+2\check{\mathcal{A}}_{\rm s})g_2\}\left[V_{23}^{\mu}(\partial_\mu\pi^{(8)})_{13}P_3^\dagger+V_{31}^{\mu}(\partial_\mu\pi^{(8)})_{23}P_3^\dagger\right] \\
&+\{g_1-(2+\check{\mathcal{A}}_{\rm s})g_2\}\left[V_{31}^{\mu}(\partial_\mu\pi^{(8)})_{21}P_1^\dagger+V_{23}^{\mu}(\partial_\mu\pi^{(8)})_{12}P_2^\dagger\right] \\
&+(g_1-3g_2)\left[V_{12}^{\mu}(\partial_\mu\pi^{(8)})_{31}P_1^\dagger+V_{12}^{\mu}(\partial_\mu\pi^{(8)})_{32}P_2^\dagger\right] \\
&+\{g_1-(2+\check{\mathcal{A}}_{\rm s})g_2\}\left[V_{12}^{\mu}(\partial_\mu\pi^{(8)})_{33}P_3^\dagger\right. \\
&\left.+V_{23}^{\mu}(\partial_\mu\pi^{(8)})_{11}P_1^\dagger+V_{31}^{\mu}(\partial_\mu\pi^{(8)})_{22}P_2^\dagger\right]. \qquad (2.79)
\end{aligned}$$

Hence it becomes more complicated than Eq. (2.78).

Chapter 3

Calculation method of diquark–heavy-quark few body systems

In the previous chapter, we constructed the chiral effective model for scalar and vector diquarks with color $\bar{\mathbf{3}}$. With the mean field approximation by the VEV of Σ meson field, we constructed the formulae of diquark mass relations. They are expressed as Eq. (2.49) showing the reversed mass relation of pseudoscalar diquarks, and Eqs. (2.64) – (2.68) leading to the generalized Gell-Mann–Okubo mass formula of axial-vector diquarks as in Eq. (2.69). Inputting some diquark masses into these equations, the other remained diquark masses can be derived.

If the interaction between a heavy quark and a diquark is given in the form of potential model, the masses of singly heavy baryons including a diquark substructure can be computed. Moreover, in the opposite way, the diquark–heavy-quark potential model enables us to give values of diquark masses from the well-known singly heavy baryon masses. In this chapter, we show the pictures of hadrons including diquarks as those building blocks, and explain the calculation method to solve properties of heavy hadrons with constituent diquarks.

3.1 Diquark–heavy-quark two body system

Singly heavy baryons are the conventional hadrons that are expected to form a diquark substructure with two constituent light quarks. Regarding a diquark as an element of singly heavy baryons, they can be treated as two body systems composed of a diquark and a heavy quark, where the Hamiltonian is expressed as

$$H = \frac{\boldsymbol{p}^2}{2\mu} + M_Q + M_{\mathcal{D}} + V(r). \tag{3.1}$$

Here $\mu = \frac{M_Q M_{\mathcal{D}}}{M_Q + M_{\mathcal{D}}}$ and $\boldsymbol{p} = \mu(\dot{\boldsymbol{r}}_{\mathcal{D}} - \dot{\boldsymbol{r}}_Q)$ are the reduced mass and the relative momentum between the heavy quark Q and the diquark $\mathcal{D}$, expressed with those velocities $\dot{\boldsymbol{r}}_{Q,\mathcal{D}}$ and masses $M_{Q,\mathcal{D}}$, respectively. $V(r)$ denotes the relative potential given in terms of the relative coordinate $r = |\boldsymbol{r}_{\mathcal{D}} - \boldsymbol{r}_Q|$.

Since quarks acquire more than about 300 MeV of masses by the chiral symmetry breaking, the effective mass of diquarks is predicted to be heavier than 600 MeV. Also, charm and bottom quarks as heavy quarks are about 1500 MeV and 4000 MeV, respectively. Therefore, both diquarks and heavy quarks have enough masses to treat in the non-relativistic physical dynamics. Hence, solving the Schrödinger equation with the Hamiltonian in Eq. (3.1), we can earn properties of singly heavy baryons such as those masses and relative wave functions between a heavy quark and a diquark substructure.

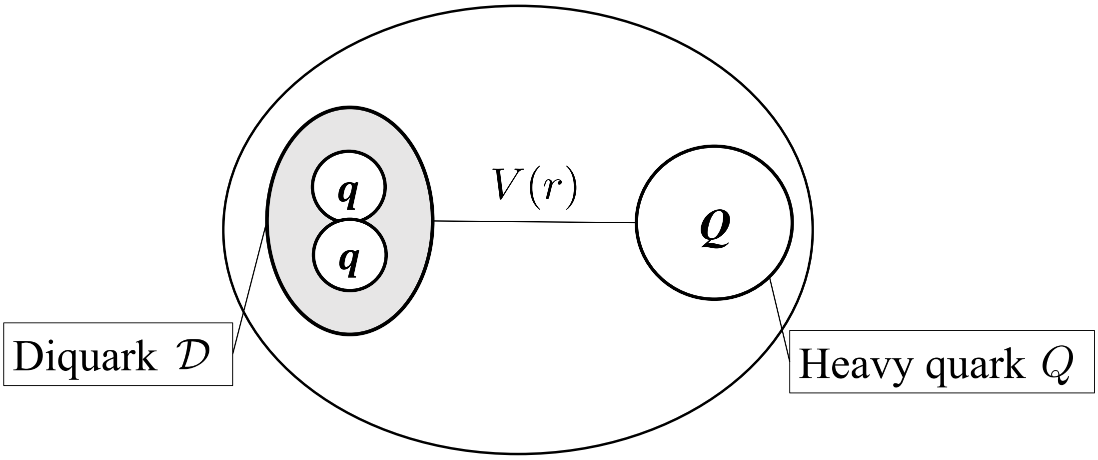

Figure3.1 The structure of diquark–heavy-quark two body system for singly heavy baryons. $V(r)$ denotes the diquark–heavy-quark potential, in which the Hamiltonian with this potential term leads to the solution of baryon masses.

3.2 Rayleigh–Ritz method

At first, we consider the Schrödinger equation expressed with Hamiltonian H, energy E, and wave function Ψ, written as

$$H|\Psi\rangle = E|\Psi\rangle. \tag{3.2}$$

Here if the energy E is the functional of the wave function Ψ as $E[\Psi]$, its variation

$$\delta E[\Psi] = \delta\left[\frac{\langle\Psi|H|\Psi\rangle}{\langle\Psi|\Psi\rangle}\right] = 0, \tag{3.3}$$

is identically equal to the Schrödinger equation (3.2). Eq. (3.3) comes from the variational principle, showing that the energy E does not change with the infinitesimal variation of the wave function Ψ.

Next, we expand the wave function Ψ with N pieces of basic functions ϕ_n as

$$|\Psi\rangle = \sum_{n=1}^{N} C_n|\phi_n\rangle. \tag{3.4}$$

Substituting this into Eq. (3.3), the variation of energy $E[\Psi]$ becomes as

$$\begin{aligned}\delta E[\Psi] &= \delta\left[\frac{\langle\Psi|H|\Psi\rangle}{\langle\Psi|\Psi\rangle}\right]\\ &= \delta\left[\frac{\sum_{n=1}^{N}\sum_{n'=1}^{N} C_n^* C_{n'}\langle\phi_n|H|\phi_{n'}\rangle}{\sum_{n=1}^{N}\sum_{n'=1}^{N} C_n^* C_{n'}\langle\phi_n|\phi_{n'}\rangle}\right]\\ &\equiv \delta\left[\frac{\sum_{n=1}^{N}\sum_{n'=1}^{N} C_n^* C_{n'} H_{nn'}}{\sum_{n=1}^{N}\sum_{n'=1}^{N} C_n^* C_{n'} N_{nn'}}\right] = 0,\end{aligned} \tag{3.5}$$

where we defined two matrices as $H_{kn} \equiv \langle\phi_k|H|\phi_n\rangle$ and $N_{kn} \equiv \langle\phi_k|\phi_n\rangle$. From Eq. (3.5), the wave function Ψ can be changed by the variation of parameters $C_n^{(*)}$. Thus, considering $E[\Psi]$ which does not change by the variation of Ψ, this energy is an extreme value with respect to variables C_n^*. This is expressed with the partial differential equation as

$$\begin{aligned}\frac{\partial E}{\partial C_n^*} &= \frac{\partial}{\partial C_n^*}\left[\frac{\sum_{n'=1}^{N}\sum_{n''=1}^{N} C_{n'}^* C_{n''} H_{n'n''}}{\sum_{n'=1}^{N}\sum_{n''=1}^{N} C_{n'}^* C_{n''} N_{n'n''}}\right]\\ &= \frac{\sum_{n''=1}^{N} C_{n''} H_{nn''}}{\sum_{n'=1}^{N}\sum_{n''=1}^{N} C_{n'}^* C_{n''} N_{n'n''}} - \frac{(\sum_{n'=1}^{N}\sum_{n''=1}^{N} C_{n'}^* C_{n''} H_{n'n''})(\sum_{n''=1}^{N} C_{n''} N_{nn''})}{(\sum_{n'=1}^{N}\sum_{n''=1}^{N} C_{n'}^* C_{n''} N_{n'n''})^2}\\ &= \frac{\sum_{n'=1}^{N} C_{n'}(H_{nn'} - EN_{nn'})}{\sum_{n'=1}^{N}\sum_{n''=1}^{N} C_{n'}^* C_{n''} N_{n'n''}} = 0,\end{aligned} \tag{3.6}$$

so that it needs to satisfy the equation expressed as below.

$$\sum_{n'=1}^{N} H_{nn'} C_{n'} = E \sum_{n'=1}^{N} N_{nn'} C_{n'}. \tag{3.7}$$

This is the same as the generalized eigenvalue problem with the eigenvalue E and the eigenvector $C_{n'}$. As in this way, the method which makes the Schrödinger equation into the generalized eigenvalue problem by the expansion of wave function Ψ, is called "Rayleigh–Ritz method".

Using the Rayleigh–Ritz method, the given energy $E[\Psi]$ becomes larger than the real energy value of the ground state E_0. For this proof, we define the Schrödinger equation (3.2) with the eigen-wave functions and energies expressed as ψ_i and E_i with $i = 0, 1, ...,$ satisfying

$$H|\psi_i\rangle = E_i|\psi_i\rangle\ ,\ E_0 \le E_1 \le E_2 \le \ldots\ . \tag{3.8}$$

At this time, the wave function Ψ is expressed with the linear combination of these orthogonal eigen-wave functions as

$$|\Psi\rangle = \sum_{i=0} c_i|\psi_i\rangle\ ,\ \langle\psi_i|\psi_j\rangle = \delta_{ij}. \tag{3.9}$$

Therefore, the energy $E[\Psi]$ satisfies the rule $E[\Psi] \ge E_0$ as below.

$$E[\Psi] = \frac{\langle\Psi|H|\Psi\rangle}{\langle\Psi|\Psi\rangle} = \frac{\sum_{i=0} E_i|c_i|^2}{\sum_{i=0}|c_i|^2} \ge \frac{E_0\sum_{i=0}|c_i|^2}{\sum_{i=0}|c_i|^2} = E_0. \tag{3.10}$$

3.3 Gaussian expansion method

One of the method to numerically solve the Schrödinger equation of few body system is "Gaussian expansion method (GEM)" [118, 119]. This method is the application of the Rayleigh–Ritz method, in which the basis functions of the expanded wave function ϕ_n are taken as the Gaussian functions for the radial component r. Some main reasons and advantages to use the Gaussian basis functions are written as below.

1. It is easy to read their geometric formation and physical conditions.
2. They can express various wave functions in the range of strong interaction.
3. Their non-orthogonality is not much large.

About the GEM, the wave function $\Psi(\boldsymbol{r})$ is classified into the radial component $\Phi(r)$ and the spherical functions $Y_{lm}(\hat{\boldsymbol{r}})$. Moreover, the radial part $\Phi(r)$ is represented by the linear combination of N pieces of gaussian basis functions in the form of "$\exp(-\nu r^2) \times r^l$" as

$$\begin{aligned} \Psi(\boldsymbol{r}) &= \Phi(r)Y_{lm}(\hat{\boldsymbol{r}}) = \sum_{n=1}^{N} C_{nl}\phi_{nl}(r)Y_{lm}(\hat{\boldsymbol{r}}), \\ \phi_{nl}(r) &= N_{nl}r^l e^{-\nu_n r^2}\ ,\ N_{nl} = \left[\frac{2^{l+2}}{(2l+1)!!}\sqrt{\frac{(2\nu_n)^{2l+3}}{\pi}}\right]^{1/2}, \end{aligned} \tag{3.11}$$

where l denotes the orbital angular momentum, and N_{nl} are the normalization factors of the basis functions satisfying $\langle\phi_{nl}|\phi_{nl}\rangle = 1$. About the coefficients ν_n in the index number of $\phi_{nl}(r)$, for GEM, they are determined by the geometric progression $\{\tilde{r}_n\}$ as

$$\nu_n = 1/\tilde{r}_n^2, \quad \tilde{r}_n = \tilde{r}_1 a^{n-1}\ (1 \le n \le N). \tag{3.12}$$

From Eqs. (3.11) and (3.12), the GEM derives the correct eigenvalue E and eigenvector C_{nl} by the definition of appropriate number of Gaussian basis function N, and appropriate geometric progression $\{\tilde{r}_n\}$. In general, the increase of the number N makes approach to the correct answer. Also, from Eq. (3.10), the eigen-energy of the ground state given by GEM, E_0^{GEM}, is not less than the correct value E_0 as $E_0^{\mathrm{GEM}} \ge E_0$. Therefore, to find the appropriate Gaussian basis functions, we need to make the lowest eigen-energy approaching to the correct energy, $\min\{E_0^{\mathrm{GEM}}\} \simeq E_0$, by the appropriate choice of parameters N and $\{\tilde{r}_n\}$. From this adjustment, we can give the correct energy value, and also can draw the wave function $\psi(\boldsymbol{r})$ by the derived eigenvector C_{nl} and the basis function $\phi_{nl}(r)$ fixed by the proper $\{\tilde{r}_n\}$.

3.4 Gaussian expansion method for three body problem

The other hadron we discuss in the present research is the T_{QQ} tetraquarks consist of two heavy quarks and two light anti-quarks. As shown in Fig. 3.2, they are described with anti-diquark substructure as the three body systems composed of two heavy quarks and one anti-diquark. The Hamiltonian for this three body system is written as

$$H_T = \sum_{Q_1,Q_2,\bar{\mathcal{D}}}\left(M_k + \frac{\boldsymbol{p}_k^2}{2M_k}\right) - K_{\mathrm{c.m.}} + V_{Q_1\bar{\mathcal{D}}}(r_1) + V_{Q_2\bar{\mathcal{D}}}(r_2) + V_{Q_1Q_2}(r_3), \tag{3.13}$$

where $M_{Q_i/\bar{\mathcal{D}}}$ and $\boldsymbol{p}_{Q_i/\bar{\mathcal{D}}}$ are the mass and momentum of constituent heavy quarks/anti-diquarks, respectively, and $K_{\rm c.m.}$ is the kinetic energy of the center of mass which is subtracted. To solve the Schrödinger equation for this three-body Hamiltonian, the wave function Ψ_{JM} is expressed with the summation of three wave functions in each channel of Jacobi coordinates $c = 1, 2, 3$ as

$$\Psi_{JM} = \Phi^{(c=1)}_{JM}(\boldsymbol{r}_1, \boldsymbol{R}_1) + \Phi^{(c=2)}_{JM}(\boldsymbol{r}_2, \boldsymbol{R}_2) + \Phi^{(c=3)}_{JM}(\boldsymbol{r}_3, \boldsymbol{R}_3), \tag{3.14}$$

where the subscript of the wave function, J and M, denote the total spin and the magnetic quantum number, respectively.

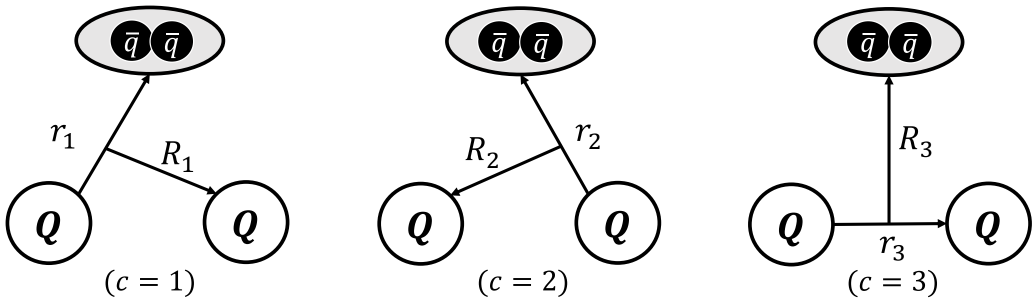

Figure3.2 Jacobi coordinates for the three body system of T_{QQ} tetraquarks composed of two heavy quarks Q and one anti-diquark $\bar{q}\bar{q}$.

In order to calculate the Schrödinger equation of three body system with use of GEM [118, 119], we expand the wave functions in each channel with the Gaussian basis functions of coordinates $\boldsymbol{r}_c$ and $\boldsymbol{R}_c$ as

$$\begin{aligned}
\Phi^{(c)}_{JM}(\boldsymbol{r}_c, \boldsymbol{R}_c) &= \sum_{n_c, l_c, N_c, L_c} C^{(c)}_{n_c, l_c, N_c, L_c} \left[\tilde{\phi}_{n_c, l_c}(\boldsymbol{r}_c)\tilde{\psi}_{N_c, L_c}(\boldsymbol{R}_c)\right]_{JM}, \\
\tilde{\phi}_{nlm}(\boldsymbol{r}) &= \tilde{\phi}_{nl}(r)Y_{lm}(\hat{\boldsymbol{r}}) = N_{nl} r^l e^{-\tilde{\nu}_n r^2} Y_{lm}(\hat{\boldsymbol{r}}), \\
\tilde{\psi}_{NLM'}(\boldsymbol{R}) &= \tilde{\psi}_{NL}(R)Y_{LM'}(\hat{\boldsymbol{R}}) = N_{NL} R^L e^{-\tilde{\lambda}_N R^2} Y_{LM'}(\hat{\boldsymbol{R}}).
\end{aligned} \tag{3.15}$$

The normalization factor $N_{nl(NL)}$ is expressed in Eq. (3.11), and the parameters $\tilde{\nu}_n$ and $\tilde{\lambda}_N$ are defined by the proper geometric progression similar to Eq. (3.12). From GEM, the eigenvalue E and eigenvector $C^{(c)}_{n_c, l_c, N_c, L_c}$ can be given correctly by the proper Gaussian basis functions.

Chapter 4

Masses of diquarks and spectrum of singly heavy baryons

In chapter 2, we created the chiral effective model of diquarks based on the $SU(3)$ linear sigma model, and derived the mass formulae as Eqs. (2.48) and (2.49) for scalar and pseudoscalar diquarks, and as Eqs. (2.64) – (2.68) for vector and axial-vector diquarks. In chapter 3, The GEM is explained for the numerical solution of Schrödinger equations for two and three body systems.

In this chapter, we use both these mass foumulae of diquarks and GEM for two body calculation, and derive numerical mass values of diquarks and singly heavy baryons. At first, we define the diquark–heavy-quark potential model and diquark masses. Then we show the numerical results of masses and energy spectra of singly heavy baryons, as well as diquarks for the substructures of those heavy baryons.

4.1 Diquark–heavy-quark potential model

In this section, we mainly construct the diquark–heavy-quark potential model and define diquark masses, so as to draw the energy spectra of singly heavy baryons in the next section.

4.1.1 Spin independent central potential

To solve the Schrödinger equation of diquark–heavy-quark two body system, where its Hamiltonian is written as Eq. (3.1), it is necessary to define the potential model between these two particles. Here we firstly construct its potential with only terms which are independent of the spins of diquarks, heavy quarks, and singly heavy baryons.

Since diquarks and heavy quarks inside singly heavy baryons have their own color as $\bar{\mathbf{3}}$ and $\mathbf{3}$, respectively, they have the attractive color-Coulomb interaction, and also the interaction by the color confinement. In the form of Corenell potential model [120], the potential based on these interactions are spin independent, and are expressed with the relative coordinate between a diquark and a heavy quark r as

$$V_0(r) = -\frac{\alpha}{r} + \lambda r + C. \tag{4.1}$$

Here α, λ, and C are coefficients of the Coulomb term, linear term, and constant shift term, respectively. We define these parameters on the basis of three types of potentials in Refs. [121–123], which are summarized in Table 4.1.

The name of these potentials in the leftmost column are taken from the initial of the

Potential	α	$\lambda(\text{GeV}^2)$	$C_c(\text{GeV})$	$C_b(\text{GeV})$	$M_c(\text{GeV})$	$M_b(\text{GeV})$
Y-pot. [121]	$0.06(\text{GeV})/\mu^*$	0.165^*	-0.831	-0.819	1.750^*	5.112^*
S-pot. [122]	0.5069 *	0.1653^*	-0.707	-0.696	1.836^*	5.227^*
B-pot. [123]	0.7281^*	0.1425^*	-0.191	-	1.4794^*	-

Table4.1 Parameters of spin independent potential terms and heavy quark masses, where the asterisk * denotes the quoted number from Refs. [121–123]. μ included in the parameter α of the Y-potential is the reduced mass of diquark and heavy quark.

first author of each reference [121–123] as Y (Yoshida et. al.), S (Silvestre-Brac), and B (Barnes et. al.). About these models, Y-potential is from the interaction of two quarks inside baryons. Also, the origins of S, B-potentials are the quarkonium $Q-\bar{Q}$ and the charmonium $c-\bar{c}$, respectively.

About the parameters in Table 4.1, α and λ are quoted from each reference. In particular, the parameter α of Y-potential depends on the reduced mass of constituent diquark and heavy quark, $\mu = \frac{M_{\mathcal{D}} M_Q}{M_{\mathcal{D}}+M_Q}$. On the other hand, about the constant $C_{c,b}$ where the subscript c, b denote the constituent charm and bottom quarks, respectively, those values are given by the two body calculation with GEM in this work. They are defined to be consistent with between the mass values of some singly heavy baryons and those constituent diquark. In concrete, C_c is derived from masses of Λ_c baryon in the ground state and its constituent ud scalar diquark. As the same, C_b is given by masses of Λ_b baryon in the ground state and its constituent ud scalar diquark. These mass values for parameter $C_{c,b}$ and those references are written as below.

1. The ud scalar diquark mass, $M_{ud}(0^+) = 725$ MeV, from lattice QCD calculation in Ref. [93].
2. The experimental Λ_c baryon mass in the ground state, $M(\Lambda_c, 1/2^+) = 2286.46$ MeV, in Ref. [12].
3. The experimental Λ_b baryon mass in the ground state, $M(\Lambda_b, 1/2^+) = 5619.60$ MeV, in Ref. [12].

Here $J^P = 1/2^+$ in second and third category shows the spin-parity state of Λ_Q baryons. For the other, the mass values of heavy quarks $M_{c,b}$ are also summarized in Table 4.1. These are quoted from each reference [121–123] as same as parameters α and λ.

About the B-potential, we note that the parameters related to the bottom quark, C_b and M_b, is not given in Table 4.1. This is because this potential model is originally used as for charmonium ($c\bar{c}$) in Ref. [123], so that there are no definition for bottom quark.

4.1.2 Masses of diquarks

In the previous subsection, we quoted the mass value of the non-strange ud scalar diquark from a result of lattice QCD simulation [93], so as to define the parameters of spin independent potential Eq. (4.1) as summarized in Table 4.1. From here, we derive the other diquark masses from diquark–heavy-quark potential models and masses of singly heavy baryons, and also from the mass formulae of diquarks in Eqs. (2.48), (2.49), and (2.64) – (2.68).

Before we give the diquark masses, we mainly introduce three types of structures for singly heavy baryons described in Fig. 4.1. The leftmost picture represents the ground state with only S-wave angular momenta, so that it is constructed by a scalar or an axial-vector diquark. In detail, from those diquark flavors in Tables 1.2 and 1.3, scalar diquarks

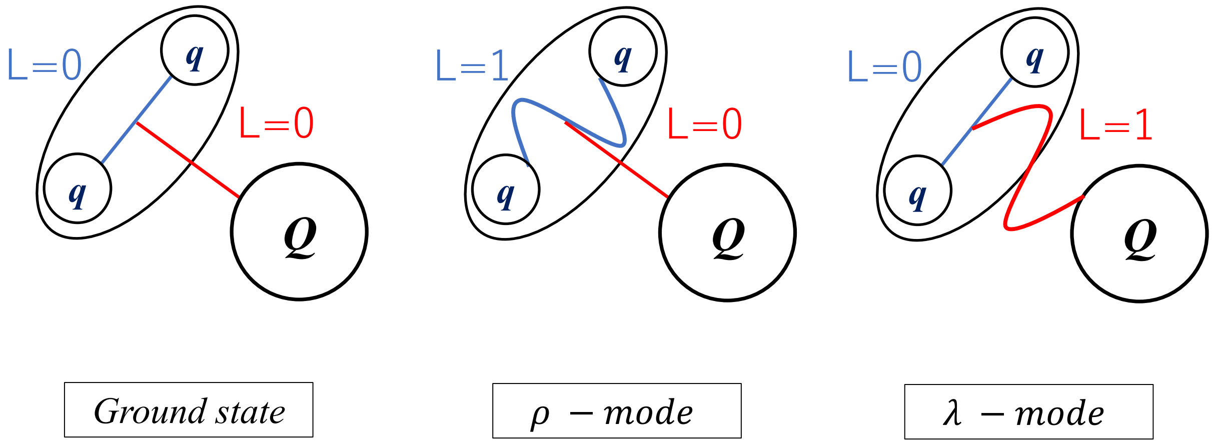

Figure4.1 Structures of singly heavy baryons, where the P-wave excitation states are classified into two kinds of orbital excitations: ρ-mode and λ-mode.

can be the component of Λ_Q and Ξ_Q baryons, while axial-vector diquarks can be that of Σ_Q, Ξ'_Q and Ω_Q baryons. The remained two states are the P-wave excited states: One in the center of Fig. 4.1 is called the ρ-mode, which has an orbital excitation between two light quarks inside a diquark, so that it is described by a pseudoscalar diquark or a vector diquark. On the other hand, the rightmost part of Fig. 4.1 is called the λ-mode, which has an orbital excitation between a heavy quark and a diquark, so that a scalar or an axial-vector diquark is the constituent of this state.

At first, we will derive the remained masses of scalar and pseudoscalar diquarks. Here we use two baryon mass values: One is the experimental mass of Ξ_c baryon in the ground state, $M(\Xi_c, 1/2^+) = 2469.42$ MeV, in Ref. [12]. This gives the mass of singly strange ns scalar diquark, where n denotes the u, d quarks. The other is the mass of Λ_c baryon estimated as the ρ-mode excited state, $M(\Lambda_c, 1/2^-) = 2890$ MeV, quoted from the 3 body calculation in Ref. [121]. We assume this baryon state giving the mass of non-strange ud pseudoscalar diquark. Giving these two diquark masses with applying the diquark–heavy-quark potential models, we earn three kinds of spin 0 diquark masses including the non-strange scalar diquark, $M_{ud}(0^+) = 725$ MeV. As a result, the remained mass of a singly strange pseudoscalar diquark can be derived by inputting these three masses into Eq. (2.49).

Next we will determine the masses of axial-vector and vector diquarks. Although there are some data by the lattice QCD simulations [93], we will give those spin 1 diquark masses mainly from the baryon masses and the diquark–heavy-quark potential models summarized in Eq. (4.1) and Table 4.1. However, since the form of potential models is spin independent, we will use the spin-averaged masses for some singly heavy baryons to give masses of those constituent diquarks. In concrete, we will give three diquark masses for each potential model from spin-averaged baryon masses quoted from Ref. [12], where those baryon mass values and corresponding diquarks are summarized as below.

1. The non-strange axial-vector diquark mass $M_{nn}(1^+)$ can be derived from $M(\Sigma_c; 1/2^+, 3/2^+) = 2496.60$ MeV representing the spin-averaged mass of two ground states of Σ_c baryon with $J^P = 1/2^+$ and $3/2^+$.
2. The singly strange axial-vector diquark mass $M_{ns}(1^+)$ can be derived from $M(\Xi_c'; 1/2^+, 3/2^+) = 2623.52$ MeV representing the spin-averaged mass of two ground states of Ξ_c' baryon with $J^P = 1/2^+$ and $3/2^+$.
3. Based on some assumptions, the mass of non-strange vector diquark $M_{ud}(1^-)$ can be derived from $M_\rho(\Lambda_c; 1/2^-, 3/2^-) = 2927.65$ MeV representing the spin-averaged mass of two ρ-mode states of Λ_c baryon with $J^P = 1/2^-$ and $3/2^-$.

Note that, however, the baryon mass $M_\rho(\Lambda_c; 1/2^-, 3/2^-) = 2927.65$ MeV in third category is given with the estimation written as below:

> About the experimental mass values of Λ_c baryons in Ref. [12], there are two data written as $M(\Lambda_c; 1/2^-) = 2592.25$ MeV and $M(\Lambda_c; 3/2^-) = 2628.11$ MeV. According to Ref. [121], they are expected to be the λ-mode excited states, in which the mass difference is 35.86 MeV. On the other hand, there is another mass information written as $M(\Lambda_c; 3/2^-) = 2939.60$ MeV, which can be assigned as the ρ-mode excited state. With the assumption that the mass splitting between $J^P = 1/2^-$ and $3/2^-$ P-wave states are the same for both λ-mode and ρ-mode, we can predict the mass of Λ_c baryon in the ρ-mode state with $J^P = 1/2^-$ as $M_\rho(\Lambda_c; 1/2^-) = 2939.60 - 35.86 = 2903.74$ MeV. As a result, we can give the spin-averaged mass of Λ_c baryon in the ρ-mode state as $M_\rho(\Lambda_c; 1/2^-, 3/2^-) = 2927.65$ MeV from $M_\rho(\Lambda_c; 1/2^-) = 2903.74$ MeV and $M_\rho(\Lambda_c; 3/2^-) = 2939.60$ MeV.

From these three spin-averaged mass values of singly heavy baryons, we can derive three diquark masses, $M_{nn}(1^+)$, $M_{ns}(1^+)$, and $M_{nn}(1^-)$. The remained diquark masses, $M_{ss}(1^+)$ and $M_{ns}(1^-)$, are given from Eqs. (2.64) – (2.68) with the parameter $\epsilon = 2/3$ [87, 109, 110].

When all of diquark masses are derived in each potential model, we can also calculate the parameters of chiral effective Lagrangian, meaning m_{S0}^2, m_{S1}^2, and m_{S2}^2 in Eq. (2.40), and the m_{V0}^2, m_{V1}^2, and m_{V2}^2 in Eq. (2.57). All values of diquark masses and parameters in chiral effective Lagrangians, Eqs. (2.40) and (2.57), are summarized in Table 4.2.

From here, we express four kinds of diquarks by those initials as "S" for "scalar", "P" for "pseudoscalar", "A" for "axial-vector", and "V" for "vector" diquarks, respectively.

For all of each potential model in Table 4.2, the mass of non-strange S diquark, $M_{ud}(0^+)$, is about 250 MeV lighter than that of singly strange S diquark, $M_{ns}(0^+)$, which obeys to the inequality (2.50). Conversely, the mass of non-strange P diquark , $M_{ud}(0^-)$, is about 150 MeV "heavier" than that of singly strange P diquark, , $M_{ns}(0^-)$, which obeys to the inequality (2.51). This reversed mass relation of P diquarks is the most characteristic point obtained from the chiral effective model of scalar diquarks, which is numerically shown in this table.

About the A diquarks, the mass difference between non-strange and singly strange types, $M_{nn}(1^+)$ and $M_{ns}(1^+)$, is about 150 MeV, which is almost the same as that between singly strange and doubly strange types, $M_{ns}(1^+)$ and $M_{ss}(1^+)$. This mass relation is numerically derived for all potential models in Table 4.2, which is associated to the generalized Gell-Mann–Okubo mass formula given in Eq. (2.69). Moreover, these results of A diquarks also satisfy the inequality (2.71).

On the other hand, the V diquarks have bigger mass difference between non-strange and singly strange types than that of A diquarks. In detail, the difference between $M_{ud}(1^-)$ and $M_{ns}(1^-)$ is more than 300 MeV for all potential models, while the difference between

	Potential model		
	Y-pot. [121]	S-pot. [122]	B-pot. [123]
Masses of S, P diquarks (MeV)			
$M_{ud}(0^+)$	725*	725*	725*
$M_{ns}(0^+)$	942	977	983
$M_{ud}(0^-)$	1406	1484	1496
$M_{ns}(0^-)$	1271	1331	1341
Masses of A, V diquarks (MeV)			
$M_{nn}(1^+)$	973	1013	1019
$M_{ns}(1^+)$	1116	1170	1179
$M_{ss}(1^+)$	1242	1309	1320
$M_{ud}(1^-)$	1447	1527	1540
$M_{ns}(1^-)$	1776	1883	1901
Parameters in $\mathcal{L}_S$ (MeV^2)			
m_{S0}^2	$(1119)^2$	$(1168)^2$	$(1176)^2$
m_{S1}^2	$(690)^2$	$(746)^2$	$(754)^2$
m_{S2}^2	$-(258)^2$	$-(298)^2$	$-(303)^2$
Parameters in $\mathcal{L}_V$ (MeV^2)			
m_{V0}^2	$(708)^2$	$(714)^2$	$(714)^2$
m_{V1}^2	$-(757)^2$	$-(808)^2$	$-(816)^2$
m_{V2}^2	$(714)^2$	$(765)^2$	$(773)^2$

Table4.2 Diquark masses and parameters of the chiral effective Lagrangians, $\mathcal{L}_S$ and $\mathcal{L}_V$, determined with each potential model. The asterisk in mass values of ud diquarks show for the quoted numbers from Ref. [93].

$M_{nn}(1^+)$ and $M_{ns}(1^+)$ is about 150 MeV. This is because the square mass difference between these vector diquarks is derived from Eqs. (2.67) and (2.68) as

$$[M_{qs}(1^-)]^2 - [M_{qq}(1^-)]^2 = \epsilon(-m_{V1}^2 + 2m_{V2}^2), \tag{4.2}$$

and is bigger than that of A diquark in Eq. (2.69) by the negativity of parameter $m_{V1}^2 < 0$. The reason why the parameter m_{V1}^2 is negative can be estimated by the stability of A diquarks compared with V diquarks, where the squared mass of non-strange A diquark in Eq. (2.64) becomes lighter than that of V diquark in Eq. (2.67). For the other, this mass difference of V diquarks with different flavors is also bigger than that of S and P diquarks in conclusion.

Comparing the data with each potential model, the Y-potential have smaller diquark masses than the other two potential models. This behavior comes from the difference of color-Coulomb interaction, especially the coefficient α in Eq. (4.1). For Y-potential, the strength of color-Coulomb interaction α is about $\alpha \simeq 0.1$ since the reduced mass of diquark and charm quark is about $\mu \simeq 600$ MeV, so that it is much weaker than that of the other models shown in Table 4.1. Therefore, the small binding energy by the small value of α requires the light diquark masses for the adjustment to the corresponding baryon masses.

4.1.3 Spin dependent potential

With only the spin independent potential terms as in Eq. (4.1), we cannot separate some degenerate states with those spin-averaged masses. To derive the baryon masses for each spin-parity state, we will consider the mass splitting caused by the spin-dependent interactions. In concrete, we add the spin dependent potential terms to the expression of diquark–heavy-quark potential model as

$$V(r) = -\frac{\alpha}{r} + \lambda r + C + V_{ss}(r) + V_{so}(r) + V_{ten}(r), \tag{4.3}$$

where the additional terms expressed as $V_{ss}(r), V_{so}(r)$, and $V_{ten}(r)$ are the spin-spin potential, the spin-orbit potential, and the tensor potential, respectively.

For the spin-spin potential V_{ss}, we take this term from Refs. [121–123] for each potential model, which is originally given in each previous work. However, the form of this term is different between the Y-, S-potentials in Refs. [121, 122] and the B-potential in Ref. [123]. In detail, the Y- and S-potentials have the Yukawa form as

$$V_{ss}(r) = (\boldsymbol{s}_{\mathcal{D}} \cdot \boldsymbol{s}_Q)\frac{\kappa_Q}{M_{\mathcal{D}} M_Q}\frac{\Lambda^2}{r}\exp(-\Lambda r), \tag{4.4}$$

and, on the other hand, the B-potential is expressed with a Gaussian function as

$$V_{ss}(r) = (\boldsymbol{s}_{\mathcal{D}} \cdot \boldsymbol{s}_Q)\frac{\kappa_Q}{M_{\mathcal{D}} M_Q}\left(\frac{\Lambda}{\sqrt{\pi}}\right)^3\exp(-\Lambda^2 r^2). \tag{4.5}$$

The common feature of these functions is that they are proportional to the inner product $(\boldsymbol{s}_{\mathcal{D}} \cdot \boldsymbol{s}_Q)$, where $\boldsymbol{s}_{\mathcal{D}}$ and $\boldsymbol{s}_Q$ are the spin of constituent diquark and heavy quark, respectively. Also, they are inversely proportional to the mass of both diquark and heavy quark, $M_{\mathcal{D}}$ and M_Q. About factors in these potentials, Λ is a cutoff parameter, in which we use the quoted values from Refs. [121–123]. On the other hand, we determine the coefficient κ_Q for the charm and bottom sectors $(Q = c, b)$ separately, so as to satisfy the mass splitting of Σ_Q baryons in the ground state. In detail, we determine κ_c from the experimental mass values of two Σ_c baryon ground states in Ref. [12],

- $M(\Sigma_c; 1/2^+) = 2453.54$ MeV,
- $M(\Sigma_c; 3/2^+) = 2518.13$ MeV,

in which κ_c fulfills the mass difference of these singly charmed baryons 64.59 MeV. In the same way, we determine κ_b from the experimental mass values of two Σ_b baryon ground states in Ref. [12],

- $M(\Sigma_b; 1/2^+) = 5813.10$ MeV,
- $M(\Sigma_b; 3/2^+) = 5832.53$ MeV,

in which κ_b fulfills the mass difference of these singly bottom baryons 19.43 MeV.

Next we explain the spin-orbit potential V_{so}. Because this term is originally included only in the work of Y-potential [121], we apply the same form also for the S- and B-potentials. According to Ref. [121], the spin-orbit potential is written as

$$V_{so}(r) = \eta\,\frac{(1-e^{-\Lambda r})^2}{r^3}\left\{\left(\frac{1}{M_{\mathcal{D}}^2} + \frac{1}{M_Q^2} + \frac{4}{M_{\mathcal{D}} M_Q}\right)(\boldsymbol{L}\cdot\boldsymbol{S}^+) + \left(\frac{1}{M_{\mathcal{D}}^2} - \frac{1}{M_Q^2}\right)(\boldsymbol{L}\cdot\boldsymbol{S}^-)\right\}. \tag{4.6}$$

For the inner product, $\boldsymbol{L}$ shows the orbital angular momentum between a diquark and a heavy quark, and $\boldsymbol{S}^{\pm}$ is the vector expressed with the spin of diquark and heavy quark as $\boldsymbol{S}^{\pm} \equiv \boldsymbol{s}_{\mathcal{D}} \pm \boldsymbol{s}_Q$. The cutoff parameter Λ is the same as that in the spin-spin potential $V_{ss}(r)$. For the coefficient η, we assume that this is independent of the flavor of heavy quark $Q = c, b$, and determine from the λ-mode excited Λ_c baryons as below.

The Λ_c baryons can be described as the two body system consist of a non-strange ud scalar diquark and a charm quark. Since the spin of scalar diquark is $\boldsymbol{s}_{\mathcal{D}} = 0$, the spin-orbit potential for Λ_c baryons becomes

$$V_{so}(r) = \eta \, \frac{(1 - e^{-\Lambda r})^2}{r^3} \left(\frac{2}{M_Q^2} + \frac{4}{M_{\mathcal{D}} M_Q} \right) (\boldsymbol{L} \cdot \boldsymbol{s}_Q) \quad (\text{if} \quad \boldsymbol{s}_{\mathcal{D}} = 0). \tag{4.7}$$

Using Eq. (4.7) for the λ-mode excited Λ_c baryons, we determine the parameter η so as to reproduce the mass difference between $M(\Lambda_c; 1/2^-) = 2592.25$ MeV and $M(\Lambda_c; 3/2^-) = 2628.11$ MeV from Ref. [12], in which the mass difference of these excited Λ_c baryons is 35.86 MeV.

As a result, the parameter η is given to be $\eta = 0.2494$.

Lastly, we explain the tensor potential V_{ten}, which is only defined in the work of Y-potential [121]. Thus, as the spin-orbit potential V_{so}, we apply the same form of V_{ten} also for the other S- and B-potentials. This tensor potential term in Ref. [121] is expressed as

$$V_{ten}(r) = 2\eta \, \frac{(1 - e^{-\Lambda r})^2}{M_{\mathcal{D}} M_Q r^3} \left[\frac{3(\boldsymbol{s}_{\mathcal{D}} \cdot \boldsymbol{r})(\boldsymbol{s}_Q \cdot \boldsymbol{r})}{r^2} - \boldsymbol{s}_{\mathcal{D}} \cdot \boldsymbol{s}_Q \right], \tag{4.8}$$

where the parameters Λ, η match to those in V_{ss} and V_{so}.

Potential	Λ (GeV)	κ_c	κ_b	η
Y-pot. [121]	0.691*	0.8586	0.6635	0.2494
S-pot. [122]	0.434*	1.1570	0.8145	0.2494
B-pot. [123]	1.0946*	2.7258	-	0.2494

Table4.3 Parameters of spin dependent potential terms, where the asterisk * denotes the quoted number from Refs. [121–123]. The parameter κ_b is not determined for the B-potential since this potential model is originally used as for charmonium $c\bar{c}$ and is not defined for bottom quarks.

The numerical results of parameters in V_{ss}, V_{so}, and V_{ten} potentials are summarized in Table 4.3. Most of the terms in spin dependent potentials, V_{ss}, V_{so}, and V_{ten}, are inversely proportional to the mass of heavy quark m_Q, so that the effect of these potentials become smaller in the heavy quark limit ($M_Q \to \infty$). In concrete, the surviving term by the heavy quark limit exists in spin-orbit potential and is expressed as

$$\lim_{M_Q \to \infty} V_{so}(r) = \eta \, \frac{(1 - e^{-\Lambda r})^2}{r^3} \frac{2}{M_{\mathcal{D}}^2} (\boldsymbol{L} \cdot \boldsymbol{s}_{\mathcal{D}}), \tag{4.9}$$

which is independent of the heavy quark spin $\boldsymbol{s}_Q$. This limit indicates the characteristic structures of hadron mass spectra associated to the "heavy-quark spin symmetry": This symmetry implies the conservation of heavy-quark spin when the mass of heavy quark is enough heavy [100–106], i.e.,

$$\lim_{M_Q \to \infty} [H(M_Q), \boldsymbol{s}_Q] = 0. \tag{4.10}$$

4.2 Energy spectrum of singly heavy baryons

The diquark masses and the diquark–heavy-quark potential models are formalized in the previous section. In this section, we propose the masses of singly heavy baryons calculated by the diquark–heavy-quark two body calculation. The numerical results of these baryon masses are described as the figures of energy spectra, which is applied for the discussion and comparison with other data.

4.2.1 Spectrum of singly heavy baryons

In this subsection, we show the numerical mass results and energy spectra of singly heavy baryons with looking into three types of state described in Fig. 4.1, meaning the lowest ground state and two P-wave states named the ρ-mode and the λ-mode. The mass values are summarized in Tables 4.4 – 4.6, which is classified by these three states. The experimental data from PDG [12] are also summarized in the rightmost column of each table, in which some values are the isospin averaged masses.

Baryon (J^P)	Diquark (J^P)	**Baryon masses in the ground state (MeV)**			
		Potential model			
		Y-pot. [121]	S-pot. [122]	B-pot. [123]	(exp.) [12]
Λ_c $(1/2^+)$	S (0^+)	2286*	2286*	2286*	2286.46
Σ_c $(1/2^+)$	A (1^+)	2452	2453	2441	2453.54
Σ_c $(3/2^+)$	A (1^+)	2516	2517	2521	2518.13
Ξ_c $(1/2^+)$	S (0^+)	2469*	2469*	2469*	2469.42
Ξ'_c $(1/2^+)$	A (1^+)	2583	2583	2571	2578.80
Ξ'_c $(3/2^+)$	A (1^+)	2642	2643	2647	2645.88
Ω_c $(1/2^+)$	A (1^+)	2700	2710	2689	2695.20
Ω_c $(3/2^+)$	A (1^+)	2755	2758	2762	2765.90
Λ_b $(1/2^+)$	S (0^+)	5620*	5620*	...	5619.60
Σ_b $(1/2^+)$	A (1^+)	5810	5797	...	5813.10
Σ_b $(3/2^+)$	A (1^+)	5829	5816	...	5832.53
Ξ_b $(1/2^+)$	S (0^+)	5796	5785	...	5794.45
Ξ'_b $(1/2^+)$	A (1^+)	5934	5914	...	5935.02
Ξ'_b $(3/2^+)$	A (1^+)	5952	5933	...	5953.82
Ω_b $(1/2^+)$	A (1^+)	6047	6022	...	6046.10
Ω_b $(3/2^+)$	A (1^+)	6064	6040	...	...

Table4.4 Masses of the ground-state singly heavy baryons with the S and A diquark from each diquark–heavy-quark potential model. The values with asterisk * denote the input values from PDG [12].

Repeatedly speaking, the values with the asterisk in Tables 4.4 – 4.5 are the quoted number from experimental data [12] or from three body calculation [121], which are used to determine the constant shift $C_{c,b}$ in the potential model and some masses of S and P diquarks. Also, though values have changed by the recalculation, the observed mass differences between $\Sigma_{c(b)}(1/2^+)$ and $\Sigma_{c(b)}(3/2^+)$ in Table 4.4 are the experimental data for the determination of potential parameters $\kappa_{c(b)}$. Moreover, the experimental mass differences between the λ-modes of the $\Lambda_c(1/2^-)$ and $\Lambda_c(3/2^-)$, summarized in Table 4.6, are applied to determine the potential parameter η. This mass difference is also used for

Baryon (J^P)	Diquark (J^P)	**Baryon masses in the ρ-mode state (MeV)**			
		Potential model			
		Y-pot. [121]	S-pot. [122]	B-pot. [123]	(exp.) [12]
Λ_c $(1/2^-)$	P (0^-)	2890*	2890*	2890*	...
Λ_c $(1/2^-)$	V (1^-)	2894	2892	2881	...
Λ_c $(3/2^-)$	V (1^-)	2943	2944	2949	(2939.60)
Ξ_c $(1/2^-)$	P (0^-)	2765	2758	2758	(2793.25)
Ξ_c $(1/2^-)$	V (1^-)	3209	3215	3205	...
Ξ_c $(3/2^-)$	V (1^-)	3252	3261	3267	...
Λ_b $(1/2^-)$	P (0^-)	6207	6174	...	...
Λ_b $(1/2^-)$	V (1^-)	6233	6197	...	...
Λ_b $(3/2^-)$	V (1^-)	6249	6214	...	...
Ξ_b $(1/2^-)$	P (0^-)	6084	6051	...	...
Ξ_b $(1/2^-)$	V (1^-)	6540	6497	...	...
Ξ_b $(3/2^-)$	V (1^-)	6554	6513	...	...

Table4.5 Masses of the ρ-mode excited-state singly heavy baryons with the P and V diquark from each diquark–heavy-quark potential model. The values with asterisk * denote the input values from Ref. [121].

the mass of non-strange V diquark with the observed mass value of $\Lambda_c(3/2^-)$ in Table 4.5. Furthermore, masses of singly bottom baryons are not given by the B-potential because the parameters related to the bottom quark is not defined in this potential model.

At first, we choose the potential model whose mass results matches to the experimental data [12] the best. Consequently, we can see that the values from Y-potential fit to the experimental data better than the other two potentials. For example, about the singly bottom baryons in Table 4.4, the mass differences between the results from Y-potential and those corresponding observed masses are only a few MeV. On the other hand, however, the masses from S-potential are mostly about 20 MeV lighter than corresponding experimental data. Therefore, from the viewpoints of ground state, the mass results from Y-potential satisfy the experimental data better than from S-potential.

The mass relation of singly bottom baryons in the ρ-mode state is similar to that in the ground state. In Table 4.5, the results from Y-potential are about 30 MeV lighter than those from S-potential. This difference of singly bottom baryon masses between Y- and S-potentials comes from the color-Coulomb interaction with parameter α, in which the parameter for the Y-potential is inversely proportional to the reduced mass μ. Hence, for Y-potential, the value α for singly bottom baryons becomes much smaller than that for charmed baryons, and the weak color-Coulomb interaction by the small α makes the singly bottom baryons heavier.

Baryon (J^P)	Diquark (J^P)	**Baryon masses in the λ-mode state (MeV)**			
		Potential model			
		Y-pot. [121]	S-pot. [122]	B-pot. [123]	(exp.) [12]
Λ_c ($1/2^-$)	S (0^+)	2589	2676	2700	(2592.25)
Λ_c ($3/2^-$)	S (0^+)	2625	2716	2749	(2628.11)
Σ_c ($1/2^-$)	A (1^+)	2717	2807	2830	...
Σ_c ($1/2^-$)	A (1^+)	2751	2847	2897	...
Σ_c ($3/2^-$)	A (1^+)	2781	2881	2919	...
Σ_c ($3/2^-$)	A (1^+)	2811	2916	2964	...
Σ_c ($5/2^-$)	A (1^+)	2844	2953	2994	...
Ξ_c ($1/2^-$)	S (0^+)	2754	2852	2887	(2793.25)
Ξ_c ($3/2^-$)	S (0^+)	2787	2890	2933	(2818.50)
Ξ'_c ($1/2^-$)	A (1^+)	2845	2942	2971	...
Ξ'_c ($1/2^-$)	A (1^+)	2876	2979	3033	...
Ξ'_c ($3/2^-$)	A (1^+)	2902	3010	3052	...
Ξ'_c ($3/2^-$)	A (1^+)	2926	3037	3090	...
Ξ'_c ($5/2^-$)	A (1^+)	2958	3073	3120	...
Ω_c ($1/2^-$)	A (1^+)	2960	3064	3098	...
Ω_c ($1/2^-$)	A (1^+)	2989	3100	3156	...
Ω_c ($3/2^-$)	A (1^+)	3013	3127	3173	...
Ω_c ($3/2^-$)	A (1^+)	3033	3150	3206	...
Ω_c ($5/2^-$)	A (1^+)	3063	3185	3235	...
Λ_b ($1/2^-$)	S (0^+)	5914	6018	...	(5912.20)
Λ_b ($3/2^-$)	S (0^+)	5927	6033	...	(5919.92)
Σ_b ($1/2^-$)	A (1^+)	6043	6143	...	...
Σ_b ($1/2^-$)	A (1^+)	6065	6171	...	...
Σ_b ($3/2^-$)	A (1^+)	6079	6187	...	...
Σ_b ($3/2^-$)	A (1^+)	6117	6234	...	...
Σ_b ($5/2^-$)	A (1^+)	6129	6247	...	...
Ξ_b ($1/2^-$)	S (0^+)	6069	6178	...	...
Ξ_b ($3/2^-$)	S (0^+)	6080	6192	...	...
Ξ'_b ($1/2^-$)	A (1^+)	6164	6269	...	...
Ξ'_b ($1/2^-$)	A (1^+)	6183	6293	...	...
Ξ'_b ($3/2^-$)	A (1^+)	6195	6307	...	...
Ξ'_b ($3/2^-$)	A (1^+)	6227	6346	...	...
Ξ'_b ($5/2^-$)	A (1^+)	6238	6359	...	...
Ω_b ($1/2^-$)	A (1^+)	6273	6383	...	...
Ω_b ($1/2^-$)	A (1^+)	6290	6404	...	...
Ω_b ($3/2^-$)	A (1^+)	6301	6418	...	...
Ω_b ($3/2^-$)	A (1^+)	6329	6452	...	...
Ω_b ($5/2^-$)	A (1^+)	6339	6464	...	...

Table4.6 Masses of the λ-mode excited-state singly heavy baryons with the S and A diquark from each diquark–heavy-quark potential model.

For the other, in Tables 4.6, the masses from Y-potential are about 100 – 200 MeV lighter than those from the other potential models. In other words, the excitation energy from the ground state to the λ-mode is approximately 200 – 300 MeV for the Y-potential and 300 – 400 MeV for the S- and B-potentials. This difference of the λ-mode states is also due to the color-Coulomb interaction, where its strength parameter α for Y-potential is much smaller than the others. About the Schrödinger equation of diquark–heavy-quark two body system, the Hamiltonian for the radial part is given by

$$H = M_Q + M_{\mathcal{D}} - \frac{1}{2\mu}\left(\frac{d^2}{dr^2} + \frac{2}{r}\frac{d}{dr}\right) + \frac{l(l+1)}{2\mu r^2} + V(r). \tag{4.11}$$

Here if the parameter α is small, it reduces the attraction between a diquark and a heavy quark at short distances, and it pushes the wave function $\Phi(r)$ to the large amount of radius r. As a result, for the λ-mode state, the effect of centrifugal repulsion term $l(l+1)/2\mu r^2$ is suppressed with small value of α, so that the energy value also decreases.

Although the color-Coulomb interaction of Y-potential is much weaker than the others, the data from Y-potential are much more consistent with the experimental data compared with the other two. This consistency of the small value of parameter α is also implied from the viewpoints of lattice QCD simulation in Refs. [94, 95]. These references propose that the magnitude of color-Coulomb interaction between a diquark and a charm quark is smaller than that between a charm and an anti-charm quarks inside the charmonium.

Now we concluded that the numerical results from Y-potential satisfies the experimental data better than the others, we then explain the mass splitting between ρ-mode and λ-mode states. Comparing Tables 4.5 and 4.6, we find that the excitation energy of ρ-mode states is bigger than the λ-mode states. The mass splitting of these orbital excited states comes from the suppression of the kinetic energy by heavy quarks and diquarks. Since the kinetic energy is inversely proportional to the reduced mass of two interacting particles, the excitation energy of λ-mode state becomes smaller than that of ρ-mode, i.e., the big masses of two interacting diquark and heavy quark lessens the kinetic energy of λ-mode state more than in the case of two light quarks in the ρ-mode state. Moreover, this weak kinetic energy makes the wave function between two particles $\Phi(r)$ concentrate in the short distance r. Therefore, the excitation energy by the color confinement effect also becomes smaller for the λ-mode state. As a result, the λ-mode states become dominant for low-lying excited states rather than the ρ-mode. For example, in the case of a harmonic oscillator potential, the ratio of ρ-mode excitation energy $\omega_\rho^{\mathrm{har}}$ to that of λ-mode $\omega_\lambda^{\mathrm{har}}$ is given by

$$\omega_\rho^{\mathrm{har}}/\omega_\lambda^{\mathrm{har}} = \sqrt{\frac{3M_Q}{2M_q + M_Q}} > 1, \tag{4.12}$$

according to Refs. [98, 121]. We can see that this ratio is bigger than 1, and it approaches the finite value $\sqrt{3}$ in the heavy quark limit ($M_Q \to \infty$). This relation of excitation energy between ρ and λ-mode is a general feature for non-relativistic potential models with a heavy quark, expect for the case when the color-Coulomb interaction dominates the binding.

Now we find that the mass results from Y-potential match to the experimental data better than the other two potentials from Tables 4.4 – 4.6, we then describe the energy spectra of singly heavy baryons given by the Y-potential. They are shown in Figs. 4.2 and 4.3 for baryons with a charm quark and a bottom quark, respectively. Four colors of spectrum lines and subscripts of baryons indicate the constituent diquark inside those singly heavy baryons as

Cyan, S : S (scalar) diquark,
Purple, P : P (pseudoscalar) diquark,
Magenta, V : V (vector) diquark,
Green, A : A (axial-vector) diquark.

Because S, P, and V diquarks have flavor $\bar{\mathbf{3}}$ representations, the Λ_Q and Ξ_Q baryons include these three types of diquarks as a component. On the other hand, the Σ_Q, Ξ'_Q, and Ω_Q baryons are described only by an A diquark with flavor $\mathbf{6}$ representation, so that there are no ρ-mode state for these three baryons [*1].

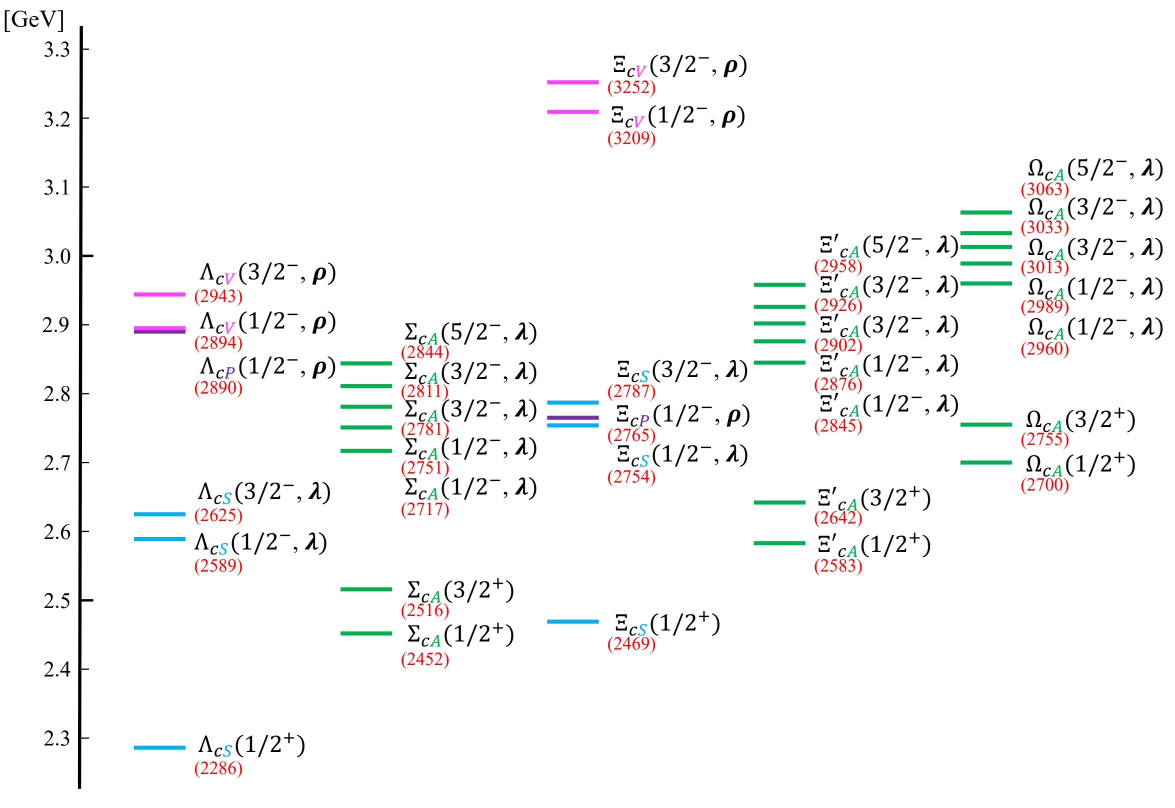

Figure4.2 The energy spectra of singly charmed baryons given by the Y-potential. The symbols $\boldsymbol{\rho}$ and $\boldsymbol{\lambda}$ for the negative parity states show the ρ-mode and λ-mode states, respectively.

In these figures, there are many features influenced by the chiral effective model of diquarks. One of them is the reversed mass relation of P diquarks expressed as in Eq. (2.51). From this effect, two purple lines in each figure show that the non-strange Λ_Q baryon is heavier than the singly strange Ξ_Q baryon for the ρ-mode excited states with P diquarks. As a result, two λ-mode states and one ρ-mode state of Ξ_Q baryons have

[*1] To calculate the ρ-mode state of Σ_Q, Ξ'_Q, and Ω_Q baryons with a chiral diquark model, we need to consider about the tensor diquark in Table 1.2, which is difficult to determine those numerical masses and parameters in Lagrangians because of the lack of experimental data.

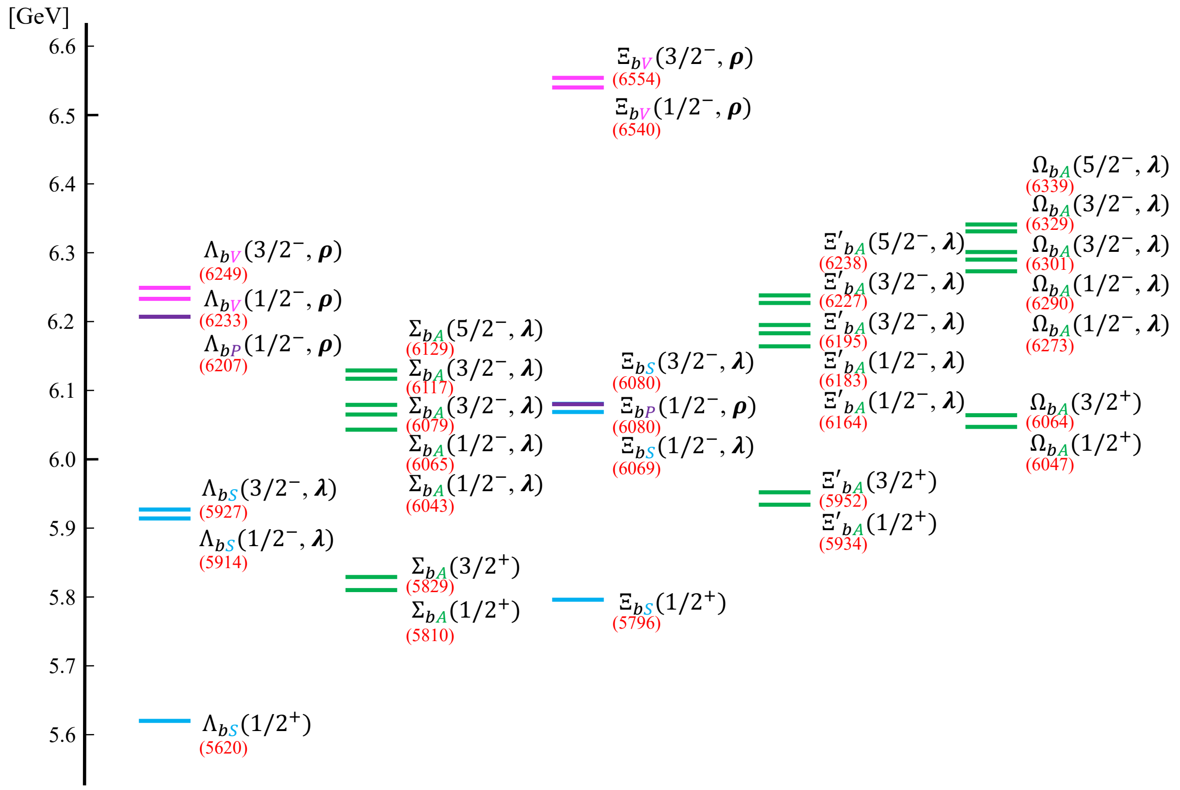

Figure4.3 The energy spectra of singly bottom baryons given by the Y-potential. The symbols $\boldsymbol{\rho}$ and $\boldsymbol{\lambda}$ for the negative parity states show the ρ-mode and λ-mode states, respectively.

almost the same mass value. Another characteristic is the V diquark in Λ_Q and Ξ_Q baryons, which makes the heaviest energy spectrum with the ρ-mode state. In detail, the mass of a singly strange V diquark is approximately 300 MeV larger than that of a non-strange one, so that the heaviest state appears in the spectrum of Ξ_Q baryons. As a summary about the ρ-mode state, the spectrum lines of Λ_Q baryons with a P diquark and a V diquark are near each other, but those of Ξ_Q baryons are much separated with about the mass difference 500 MeV. On the other hand, about the ground states and λ-mode states of Λ_Q and Ξ_Q including a S diquark, they generally become heavier with the increase of the number of constituent s quarks.

Next we see the energy spectra of the other baryons with a constituent A diquarks, such as Σ_Q, Ξ'_Q, and Ω_Q. From Figs. 4.2 and 4.3, the mass differences between Σ_Q and Ξ'_Q baryons in the same spin-parity states are about 130 MeV, and those between Ξ'_Q and Ω_Q baryons are about 120 MeV. This behavior comes from the generalized Gell-Mann–Okubo mass formula for A diquarks in Eq. (2.69), which satisfies the inequality in Eqs. (2.71) and (2.72).

Also, from our model, the masses of these baryons become heavier as the total spin increases. For instance, about the λ-mode states of Σ_c baryons, five states with two $J^P = 1/2^-$, two $3/2^-$, and one $5/2^-$ are in order. In detail, according to Fig. 4.4, these five states are degenerate when the spin dependent potential is not considered. In this figure, the spin-spin potential splits these states into two parts, and after, the symmetric term of spin-orbit potential splits these five states completely with in order of $1/2^- < 1/2^- < 3/2^- < 3/2^- < 5/2^-$. Finally, the antisymmetric term of spin-orbit potential and tensor potential mixes the same spin-parity states.

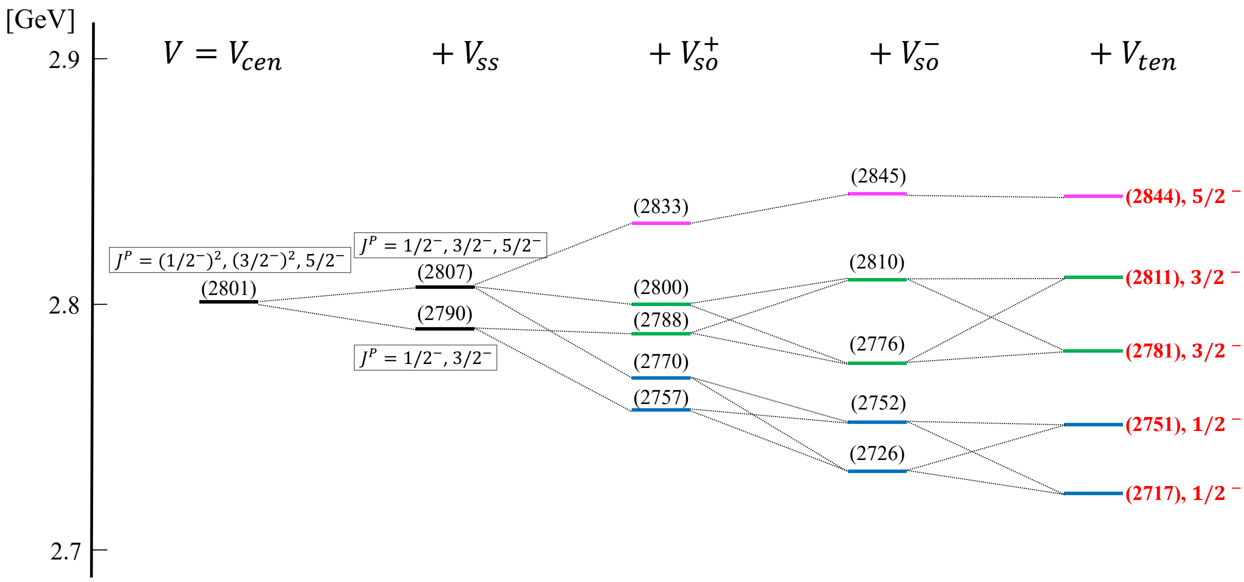

Figure4.4 The energy splitting and mixing of Σ_c baryons in the λ-mode states contributed to the spin dependent terms of the Y-potential.

From the viewpoints of the effect of diquark masses and the order of spectrum lines, Figs. 4.2 and 4.3 are similar to each other. However, there are the feature which depends on the difference of charm and bottom quark masses. As in Eqs. (4.9) and (4.10), the effect of spin dependent interaction decreases with the increase of heavy quark mass M_Q, which is caused by the heavy-quark spin symmetry [100–106]. Therefore, the energy splitting range of singly bottom baryons becomes smaller than that of charmed baryons. For example, masses of two ground states of Σ_b baryon with spin-parity $J^P = 1/2^+, 3/2^+$ are approaching more than those of Σ_c: The mass difference of these two states is about 60 MeV for charmed Σ_c baryons, and is shrinking to about 20 MeV for bottom Σ_b baryons. This feature is also seen in two ground states of Ξ'_Q and Ω_Q baryons, and these kinds of two states whose mass difference becomes smaller with the heavy quark limit ($M_Q \to \infty$) are called "heavy-quark spin (HQS) doublet". In general, the total spins of the pair of HQS doublet is expressed as $J = j \pm 1/2$, where j is from the diquark spins and orbital angular momentum and $1/2 = s_Q$ is the heavy quark spin. This is because, when the total spin J is conserved, the partial angular momentum j can be also conserved from $j = J \pm s_Q$ and Eq. (4.10) in the heavy quark limit. As a consequence, two states with $J = j \pm 1/2$ will be almost degenerate when M_Q is enough large. For the other examples of HQS doublets, they are summarized as below.

(i) The λ-modes of Λ_Q and Ξ_Q with $J^P = 1/2^-$ and $3/2^-$, containing S diquarks.
(ii) The ρ-modes of Λ_Q and Ξ_Q with $J^P = 1/2^-$ and $3/2^-$, containing V diquarks.
(iii) The λ-modes of Σ_Q, Ξ'_Q, and Ω_Q with $J^P = 1/2^-$ and $3/2^-$, containing A diquarks.
(iv) The λ-modes of Σ_Q, Ξ'_Q, and Ω_Q with $J^P = 3/2^-$ and $5/2^-$, containing A diquarks.

On the other hand, if $j = 0$, there are no pair which are degenerate by the heavy quark limit. This single state is called "HQS singlet", in which the total spin is only $J = 1/2$ due to the quantum number $j = 0$ from the cancellation of the diquark spin and orbital angular momentum.

4.2.2 Addition of excited states with positive parity

In the previous subsection, we discussed the energy spectra of singly heavy baryons related to the chiral effective model of diquarks. Those energy spectra in Figs. 4.2 and 4.3 are composed of ground states and two types of negative-parity excited states called the ρ-mode and the λ-mode. In this subsection, we study two types of excited states with the positive parity: One is the radial excited states, where the node takes $n = 1$ [*2] and the orbital angular momentum between a diquark and a heavy quark is $l = 0$. The other one is the excited state where the orbital angular momentum between a diquark and a heavy quark is in D-wave as $l = 2$, but without the radial excitation ($n = 0$). These positive parity states are described with S or A diquark, and the mass values of these states given by the Y-potential are summarized in Table 4.7. The experimental values from PDG [12] is also written in this table, however, only Λ_Q baryons are observed about these excited states. (About these comparison, see the next subsection.)

The energy spectra of Λ_Q and Σ_Q baryons from the data in Tables 4.4, 4.5, 4.6, and 4.7 are described as Figs. 4.5 and 4.6. Here the energy spectra with the positive parity are expressed with blue lines, whereas the negative parity states are with red lines. Comparing these different colors (parities), the λ-mode states are lying in between the ground states and positive-parity excited states, and the ρ-mode states of Λ_Q baryons are slightly heavier than the positive-parity excited states.

Giving attention to only the positive-parity excited states, we find that the radially excited states are lighter than those corresponding D-wave excited states, though the mass differences between these states are not so much large. Moreover, for each excited state with positive parity, the mass becomes heavier as the total spin becomes larger, which is the same as the λ-mode state. Furthermore, comparing Figs. 4.5 and 4.6, we can see one pair of HQS doublet in the D-wave excitation of Λ_Q baryons, and also see four pairs of HQS doublet in both radial and D-wave excitations of Σ_b baryons. The only remained radially excited Λ_Q baryons are the HQS singlet. Similar orders and combinations can be seen for the other spectra of $\Xi_Q^{(\prime)}$ and Ω_Q baryons, according to Table 4.7.

[*2] In other words, the principal quantum number is 2.

Baryon (J^P)	(n, l)	Mass	(exp.) [12]	Baryon (J^P)	(n, l)	Mass	(exp.) [12]
$\Lambda_c(1/2^+)$	$(1, 0)$	2825	(2765)	$\Lambda_b(1/2^+)$	$(1, 0)$	6121	6072.30
$\Lambda_c(3/2^+)$	$(0, 2)$	2869	2856.10	$\Lambda_b(3/2^+)$	$(0, 2)$	6172	6146.20
$\Lambda_c(5/2^+)$	$(0, 2)$	2897	2881.63	$\Lambda_b(5/2^+)$	$(0, 2)$	6178	6152.50
$\Sigma_c(1/2^+)$	$(1, 0)$	2974	...	$\Sigma_b(1/2^+)$	$(1, 0)$	6274	...
$\Sigma_c(1/2^+)$	$(0, 2)$	3016	...	$\Sigma_b(1/2^+)$	$(0, 2)$	6304	...
$\Sigma_c(3/2^+)$	$(1, 0)$	3013	...	$\Sigma_b(3/2^+)$	$(1, 0)$	6286	...
$\Sigma_c(3/2^+)$	$(0, 2)$	3043	...	$\Sigma_b(3/2^+)$	$(0, 2)$	6316	...
$\Sigma_c(3/2^+)$	$(0, 2)$	3053	...	$\Sigma_b(3/2^+)$	$(0, 2)$	6330	...
$\Sigma_c(5/2^+)$	$(0, 2)$	3076	...	$\Sigma_b(5/2^+)$	$(0, 2)$	6341	...
$\Sigma_c(5/2^+)$	$(0, 2)$	3094	...	$\Sigma_b(5/2^+)$	$(0, 2)$	6365	...
$\Sigma_c(7/2^+)$	$(0, 2)$	3115	...	$\Sigma_b(7/2^+)$	$(0, 2)$	6373	...
$\Xi_c(1/2^+)$	$(1, 0)$	2976	...	$\Xi_b(1/2^+)$	$(1, 0)$	6260	...
$\Xi_c(3/2^+)$	$(0, 2)$	3017	...	$\Xi_b(3/2^+)$	$(0, 2)$	6307	...
$\Xi_c(5/2^+)$	$(0, 2)$	3043	...	$\Xi_b(5/2^+)$	$(0, 2)$	6313	...
$\Xi'_c(1/2^+)$	$(1, 0)$	3088	...	$\Xi'_b(1/2^+)$	$(1, 0)$	6381	...
$\Xi'_c(1/2^+)$	$(0, 2)$	3131	...	$\Xi'_b(1/2^+)$	$(0, 2)$	6411	...
$\Xi'_c(3/2^+)$	$(1, 0)$	3124	...	$\Xi'_b(3/2^+)$	$(1, 0)$	6392	...
$\Xi'_c(3/2^+)$	$(0, 2)$	3155	...	$\Xi'_b(3/2^+)$	$(0, 2)$	6423	...
$\Xi'_c(3/2^+)$	$(0, 2)$	3164	...	$\Xi'_b(3/2^+)$	$(0, 2)$	6434	...
$\Xi'_c(5/2^+)$	$(0, 2)$	3186	...	$\Xi'_b(5/2^+)$	$(0, 2)$	6444	...
$\Xi'_c(5/2^+)$	$(0, 2)$	3200	...	$\Xi'_b(5/2^+)$	$(0, 2)$	6465	...
$\Xi'_c(7/2^+)$	$(0, 2)$	3221	...	$\Xi'_b(7/2^+)$	$(0, 2)$	6472	...
$\Omega_c(1/2^+)$	$(1, 0)$	3194	...	$\Omega_b(1/2^+)$	$(1, 0)$	6480	...
$\Omega_c(1/2^+)$	$(0, 2)$	3236	...	$\Omega_b(1/2^+)$	$(0, 2)$	6511	...
$\Omega_c(3/2^+)$	$(1, 0)$	3227	...	$\Omega_b(3/2^+)$	$(1, 0)$	6491	...
$\Omega_c(3/2^+)$	$(0, 2)$	3259	...	$\Omega_b(3/2^+)$	$(0, 2)$	6522	...
$\Omega_c(3/2^+)$	$(0, 2)$	3268	...	$\Omega_b(3/2^+)$	$(0, 2)$	6532	...
$\Omega_c(5/2^+)$	$(0, 2)$	3288	...	$\Omega_b(5/2^+)$	$(0, 2)$	6541	...
$\Omega_c(5/2^+)$	$(0, 2)$	3300	...	$\Omega_b(5/2^+)$	$(0, 2)$	6559	...
$\Omega_c(7/2^+)$	$(0, 2)$	3320	...	$\Omega_b(7/2^+)$	$(0, 2)$	6567	...

Table4.7 Masses of singly heavy baryons in the radially excited state with the node being $n = 1$ and the D-wave excited state with the orbital angular momentum between a diquark and a heavy quark being $l = 2$, which is in the units of MeV. Y-potential is used for this calculation.

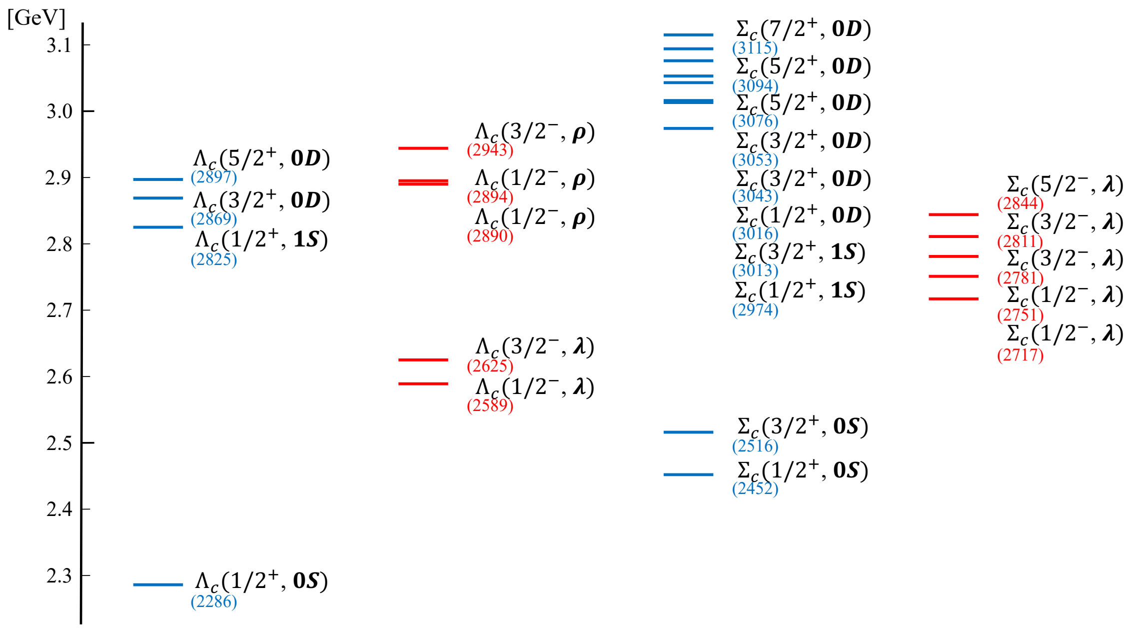

Figure4.5 The energy spectra of Λ_c and Σ_c baryons from Tables 4.4, 4.5, 4.6, and 4.7, given by the Y-potential. The colors of lines show the parities as blue for positive parity and red for negative parity. For the blue spectra, they are classified by the node number $n = 0, 1$, and the orbital angular momentum with S- or D-wave, expressed as $\boldsymbol{nl} = \mathbf{0}S, \mathbf{1}S$, and $\mathbf{0}D$.

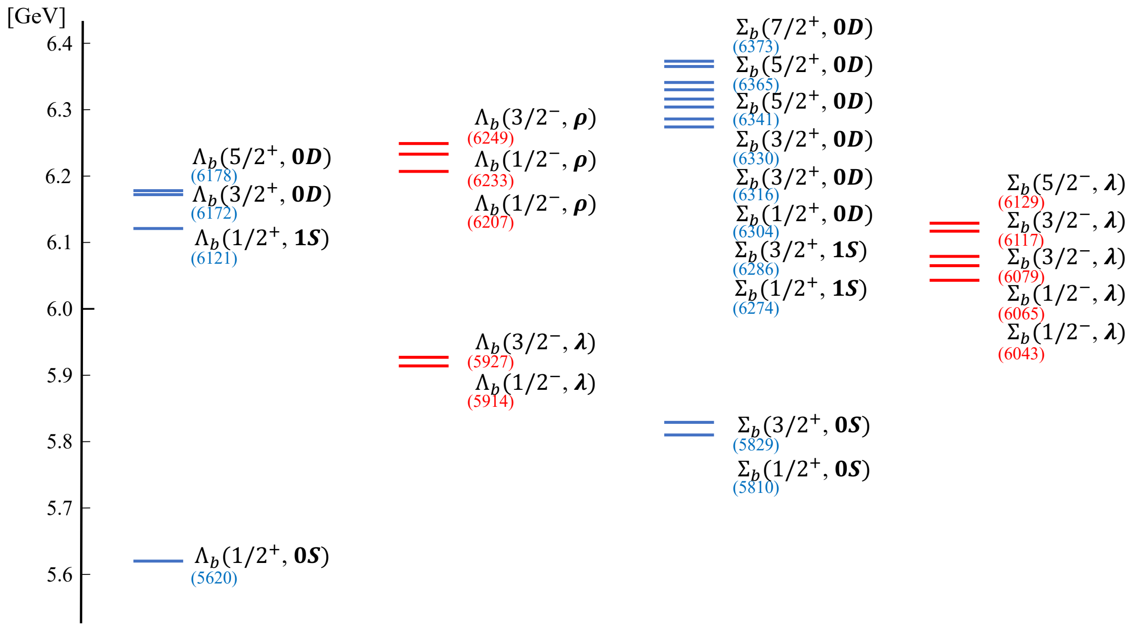

Figure4.6 The energy spectra of Λ_b and Σ_b baryons from Tables 4.4, 4.5, 4.6, and 4.7, given by the Y-potential. The colors of lines show the parities as blue for positive parity and red for negative parity. For the blue spectra, they are classified by the node number $n = 0, 1$, and the orbital angular momentum with S- or D-wave, expressed as $\boldsymbol{nl} = \mathbf{0}S, \mathbf{1}S$, and $\mathbf{0}D$.

4.2.3 Comparison with experimental data

As we calculated the energy spectra of singly heavy baryons with five types of states, we now compare these theoretical results with the experimental data from PDG [12]. The energy spectra containing both our results and observed data are shown in Figs. 4.7 and 4.8. In these figures, the dotted lines show the results from our calculation with using Y-potential, and the color blue or red shows the positive or negative parity states, respectively. The remained black solid lines denote the observed data, in which informations about spin-parity are also written beside those mass values. Note that the spectra of Ξ_Q and Ξ'_Q baryons are described in the same place.

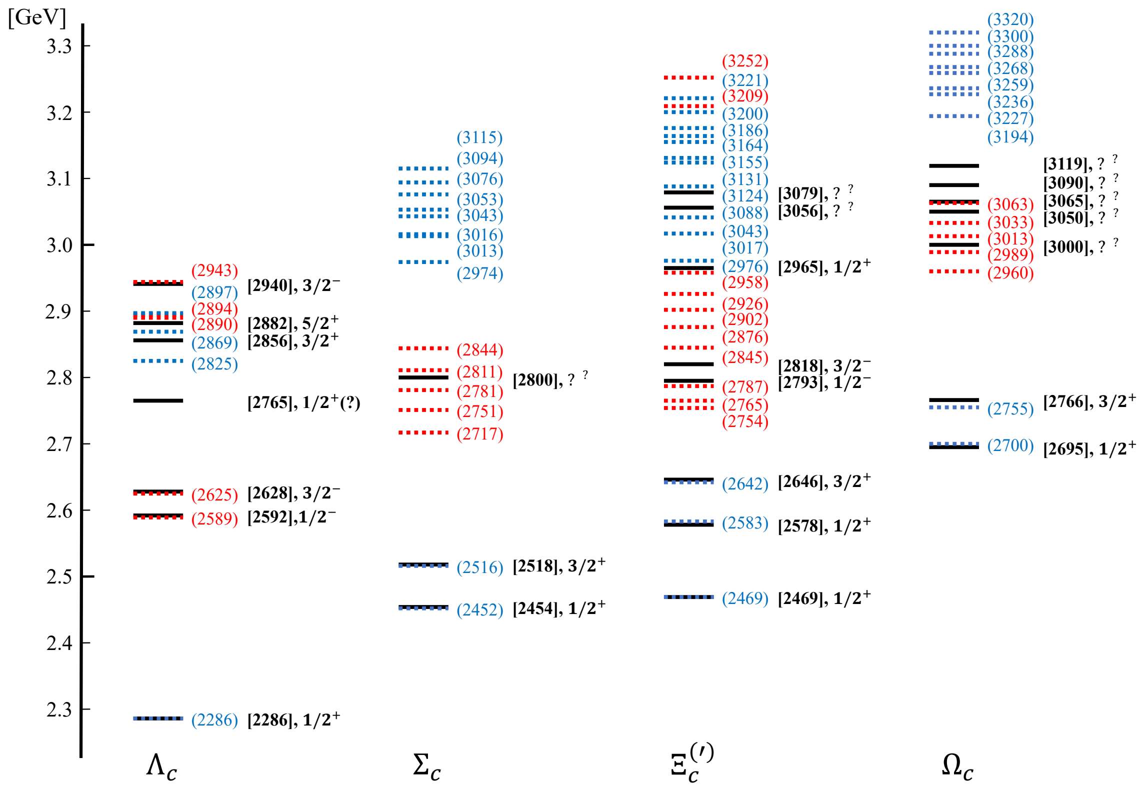

Figure4.7 Energy spectra of singly charmed baryons from our model with the Y-potential (blue or red dotted lines), and from the experimental data in PDG [12] (black solid lines). Here we put the spectra of Ξ_c and Ξ'_c together.

In these figures, the Λ_Q and Ξ_c baryons in the ground states are the input values, so that they are completely matched to the experimental data. Also, as the mass difference between two ground states of Σ_Q baryons and between two λ-mode states of Λ_c baryons are the inputs, their results are similar to the observed masses. Moreover, two ground states of Ξ'_c baryons and the highest Λ_c baryon are well corresponded to the experimental data, since these are used for the determination of A and V diquark masses. Hence, the pure outputs from our model is $\Xi_b^{(\prime)}$ and Ω_Q baryons. Looking into the spectra of $\Xi_b^{(\prime)}$ and Ω_Q in the ground states, and also the spectrum of Λ_b in the λ-mode states, those states are near those observed masses. This correspondence indicates the consistency of the relation of A diquark masses and the diquark–heavy-quark potential model. On the other

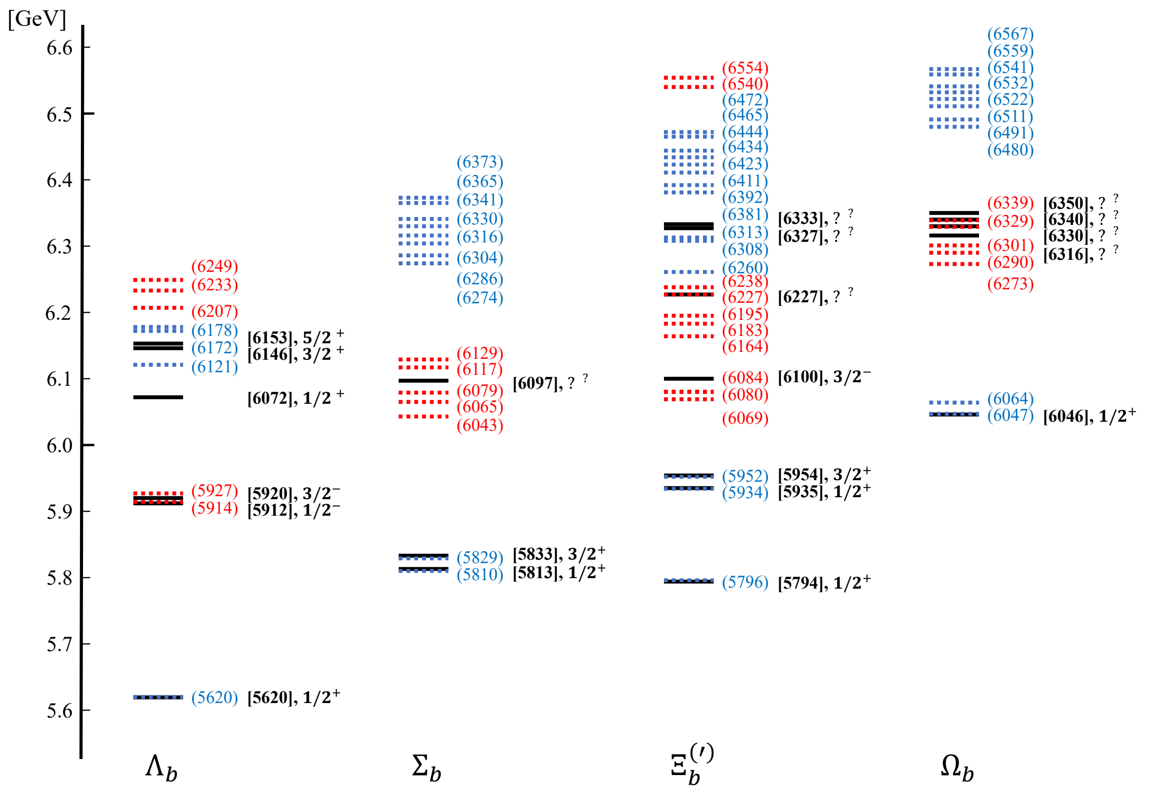

Figure4.8 Energy spectra of singly bottom baryons from our model with the Y-potential (blue or red dotted lines), and from the experimental data in PDG [12] (black solid lines). Here we put the spectra of Ξ_c and Ξ_c' together.

hand, from the spectra of Ω_Q in the λ-mode states, the experimental value are heavier than our results. From this point of view, it seems that some potential terms or diquark masses are needed to be adjusted.

About the total spin and parity, some experimental values in the spectra of Σ_Q, $\Xi_Q^{(\prime)}$, and Ω_Q baryons are not correctly determined yet. Although their total spins are hard to define, we can roughly estimate those parities from our results at least. If our theoretical results are mostly correct, the observed Σ_Q and Ω_Q excited states can be predicted as the negative-parity states. Also, the observed $\Xi_Q^{(\prime)}$ in the higher range of their spectra would have the positive parity.

The remained observed data that we need to discuss is the positive-parity excited states of Λ_Q baryons, which could be applicable to the radially excited or D-wave excited states. About the Λ_Q with $J^P = 3/2^+$ and $5/2^+$, they are expected to be the D-wave excited states from our results. Although they are about 20 MeV lighter than our calculation, the mass splitting between these HQS doublets are mostly the same. On the other hand, About the Λ_Q with $J^P = 1/2^+$, they are about 50 MeV lighter than our results, so that their masses are much smaller than those from the diquark–heavy-quark picture. This is because these states are expected to be an analogy of the Roper-like resonance state in the nucleon spectrum, in which the theoretical mass result from the quark model becomes much larger than the observed mass. In detail, about $\Lambda_c(2765)$, this isospin is determined by the Belle Collaboration [124]. However, the total spin and parity of this is not given yet, but is assumed to be $J^P = 1/2^+$. Also, about $\Lambda_b(6072)$, this is observed by the LHCb

Collaboration [125, 126]. Both of them are proposed recently in 2020.

4.2.4 Comparison with three quark system

Next we compare our results by the diquark–heavy-quark picture with another theoretical result by the three-quark model in Ref. [121]. Since there are no information about $\Xi_Q^{(\prime)}$ baryons, we mainly compare the energy spectra of Λ_Q, Σ_Q, and Ω_Q baryons as described in Figs. 4.9, 4.10, and 4.11.

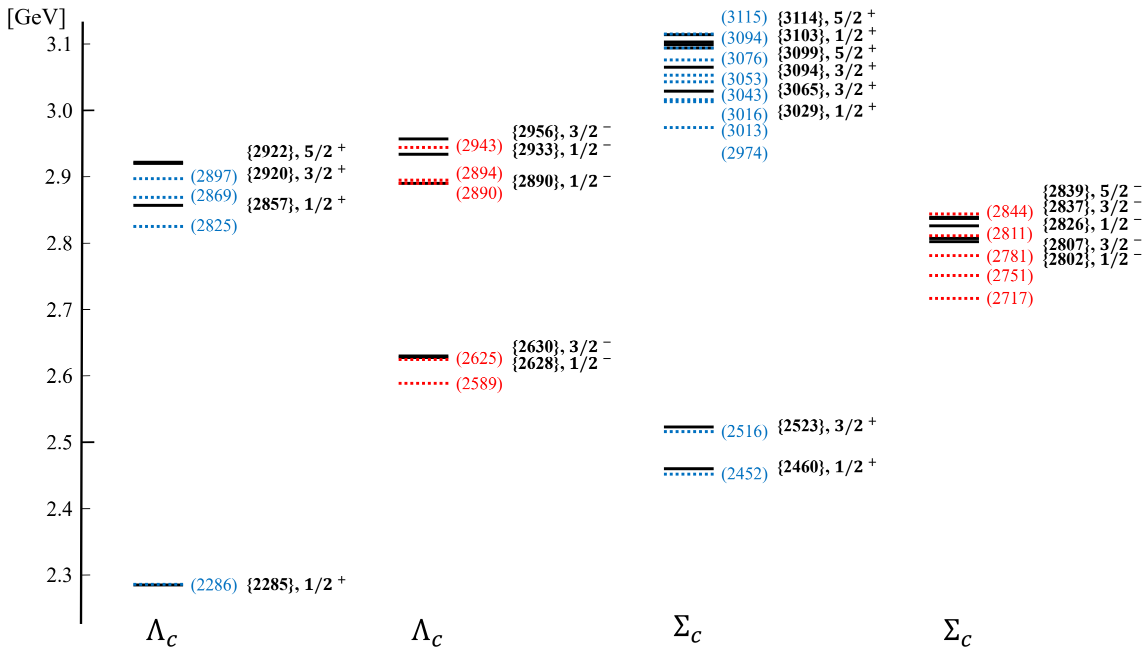

Figure4.9 Energy spectra of Λ_c and Σ_c from our model with Y-potential (blue or red dotted lines), and from the three-quark model in Ref. [121] (black solid lines).

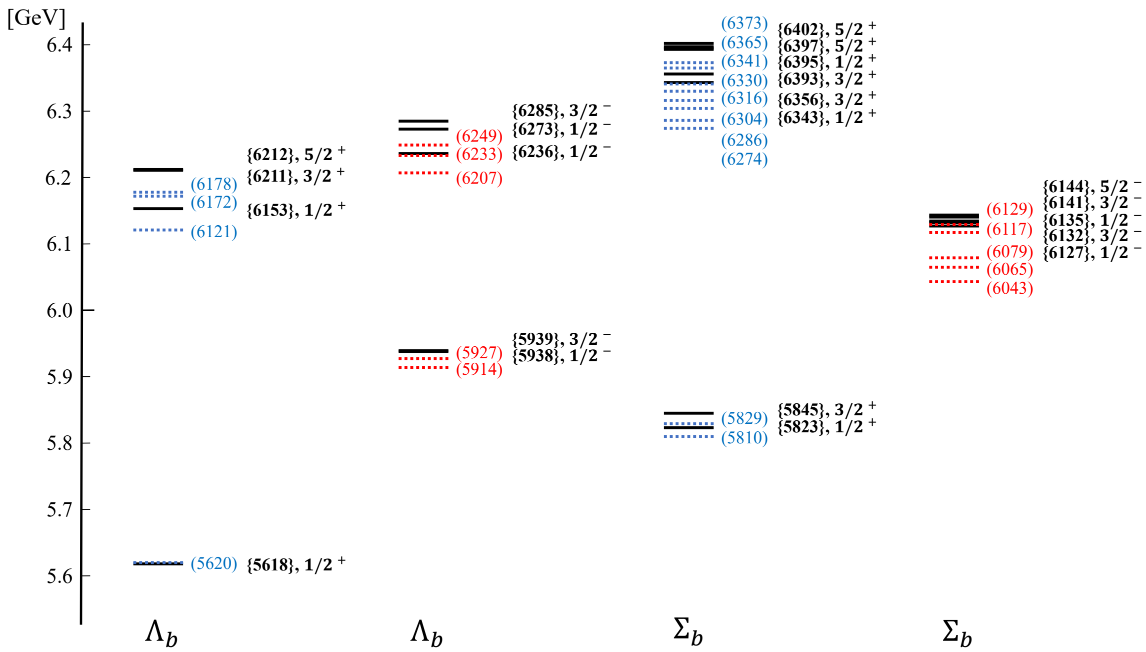

Figure4.10 Energy spectra of Λ_b and Σ_b from our model with Y-potential (blue or red dotted lines), and from the three-quark model in Ref. [121] (black solid lines).

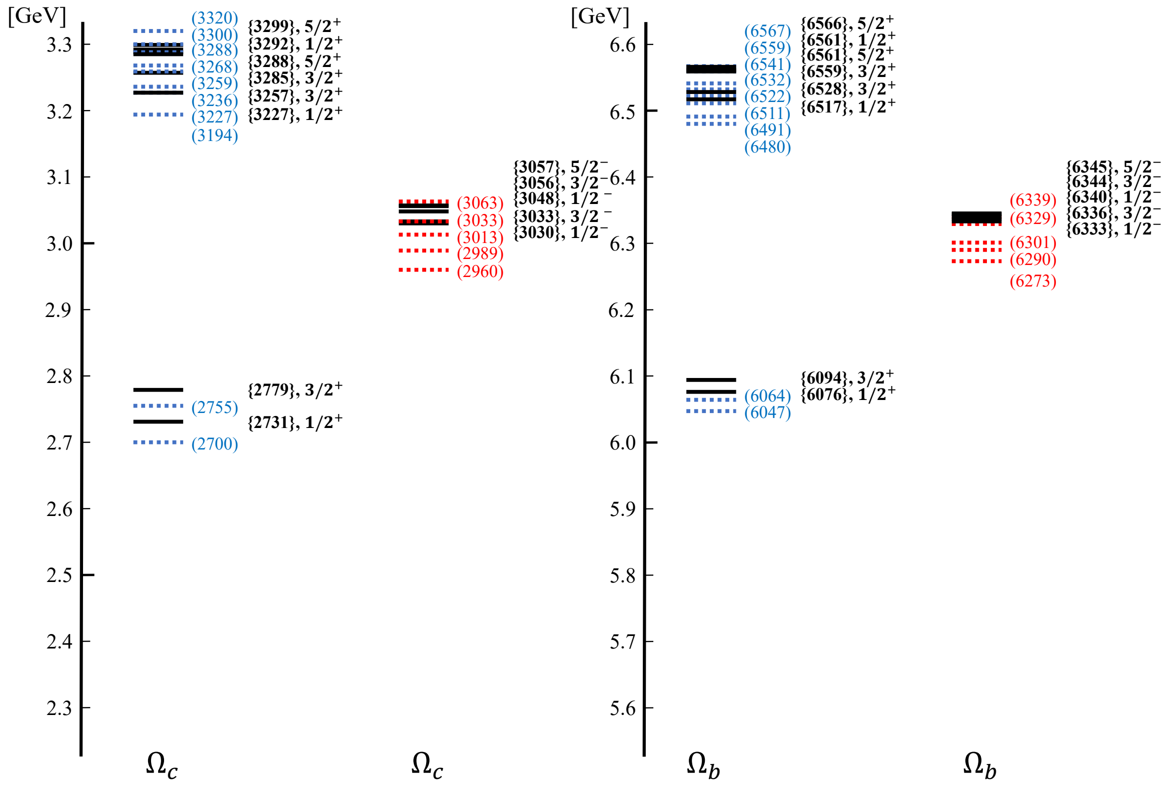

Figure4.11 Energy spectra of Ω_Q from our model with Y-potential (blue or red dotted lines), and from the three-quark model in Ref. [121] (black solid lines).

The form of energy spectra is similar to each calculation method. However, the masses in excited states given by the three-quark model are heavier than those by our diquark–heavy-quark picture. In addition, about the range of mass splitting in excited states, our results from diquark–heavy-quark picture is wider than those from the three-quark model. This difference of mass splitting comes from the coefficient η in the spin-orbit potential, where its value is defined as $\eta = 0.026$ in the three-quark model and it is much smaller than that we defined as $\eta = 0.2494$. This difference of factor η is due to the different strategy to choose its value: $\eta = 0.026$ from the three-quark model is determined by hyperons [*3], not by the singly heavy baryons as ours.

The small value of η in the three-quark model makes another difference from our diquark method, which is the order of total spin J along the energy spectrum. For example, the order of Σ_Q or Ω_Q baryons in the λ-mode states is given by $1/2^- < 1/2^- < 3/2^- < 3/2^- < 5/2^-$ from our work, which comes from the effect of spin-orbit potential term as in Fig. 4.4. On the other hand, about the three-quark model, the mass splitting by the spin-orbit potential is not so much large because of the small value of η. Thus the order of those Σ_Q becomes $1/2^- < 3/2^- < 1/2^- < 3/2^- < 5/2^-$ by this previous work, which is different from ours.

[*3] The baryons composed of three light quarks with at least one strange quark s.

Chapter 5

Strong decays of singly heavy baryons and chiral restoration

In chapter 4, we summarized the numerical results of singly heavy baryon masses given by the diquark mass formulae in chapter 2 and the calculation method for two body system in chapter 3. The results of these theoretical mass values are depicted as the figures of energy spectra, and they are discussed with our calculation methods. We also compared these results with the experimental data and other theoretical results.

In this chapter, we study the strong decays of singly heavy baryons from the viewpoints of diquarks. We firstly explain the calculation method to determine parameters in the chiral effective model of diquarks, and next we consider the chiral symmetry restoration and its contribution to those strong decays.

5.1 Strong decays of singly heavy baryons

In this section, we explain the calculation method to derive the decay width about strong decays of singly heavy baryon. The main reaction we focus on is the one pion decay which is expressed as

$$\text{“}\Sigma_Q \to \Lambda_Q \pi\text{”}, \text{ or } \text{“}\Xi'_Q \to \Xi_Q \pi\text{”}.$$

These reactions start from the ground states of Σ_Q or Ξ'_Q baryon, and each of them decays to the ground state of Λ_Q or Ξ_Q baryon with the emission of one pion π. The decay width of these reactions with a charged pion $\pi^{\pm}$ are mostly observed, and those experimental data from PDG [12] are summarized in Table. 5.1.

For these decay reactions, at first, we formulate the expression of decay width with the use of chiral effective model of diquarks. Then, using the constructed decay width formula, we determine the parameters $g_{1,2}$ in the effective Lagrangian Eq. (2.73) so as to realize the experimental data of decay width in Table 5.1.

5.1.1 Theoretical framework for strong decay width

The $\Sigma_Q \to \Lambda_Q \pi$ and $\Xi'_Q \to \Xi_Q \pi$ decays are one pion emission decays, where all the singly heavy baryons associated to these reactions are in the ground state. Using diquarks as elements, these baryons are composed of a diquark and a heavy quark with the interaction of these two constituent particles. In detail, Λ_Q and Ξ_Q in the final states includes a non-strange and a singly strange S diquark, while Σ_Q and Ξ'_Q in the initial states consist of a non-strange and a singly strange A diquark. Therefore, the constituent heavy quark Q is steady along these strong decays, whereas a constituent diquark changes from A to S and

Baryon	J^P	Mass (MeV)	Full width (MeV)	Decay mode
Λ_c	$1/2^+$	2286.46 ± 0.14	(No strong decay)	
$\Sigma_c^{++}(2455)$	$1/2^+$	2453.97 ± 0.14	$1.89^{+0.09}_{-0.18}$	$\Sigma_c^{++} \to \Lambda_c\pi^+$
$\Sigma_c^{+}(2455)$	$1/2^+$	2452.9 ± 0.4	(< 4.6)	$\Sigma_c^{+} \to \Lambda_c\pi^0$
$\Sigma_c^{0}(2455)$	$1/2^+$	2453.75 ± 0.14	$1.83^{+0.11}_{-0.19}$	$\Sigma_c^{0} \to \Lambda_c\pi^-$
$\Sigma_c^{++}(2520)$	$3/2^+$	$2518.41^{+0.21}_{-0.19}$	$14.78^{+0.30}_{-0.40}$	$\Sigma_c^{*++} \to \Lambda_c\pi^+$
$\Sigma_c^{+}(2520)$	$3/2^+$	2517.5 ± 2.3	(< 17)	$\Sigma_c^{*+} \to \Lambda_c\pi^0$
$\Sigma_c^{0}(2520)$	$3/2^+$	2518.48 ± 0.20	$15.3^{+0.4}_{-0.5}$	$\Sigma_c^{*0} \to \Lambda_c\pi^-$
Ξ_c^+	$1/2^+$	2467.71 ± 0.23	(No strong decay)	
Ξ_c^0	$1/2^+$	2470.44 ± 0.28	(No strong decay)	
$\Xi_c^{\prime +}$	$1/2^+$	2578.2 ± 0.5	(No strong decay)	
$\Xi_c^{\prime 0}$	$1/2^+$	2578.7 ± 0.5	(No strong decay)	
$\Xi_c^{+}(2645)$	$3/2^+$	2645.10 ± 0.30	2.14 ± 0.19	$\Xi_c^{\prime *+} \to \Xi_c^{0(+)}\pi^{+(0)}$
$\Xi_c^{0}(2645)$	$3/2^+$	2646.16 ± 0.25	2.35 ± 0.22	$\Xi_c^{\prime *0} \to \Xi_c^{+(0)}\pi^{-(0)}$
Ω_c	$1/2^+$	2695.2 ± 1.7	(No strong decay)	
$\Omega_c(2770)$	$3/2^+$	2765.9 ± 2.0	(No strong decay)	
Λ_b	$1/2^+$	5619.60 ± 0.17	(No strong decay)	
Σ_b^+	$1/2^+$	5810.56 ± 0.25	5.0 ± 0.5	$\Sigma_b^+ \to \Lambda_b\pi^+$
Σ_b^0	$1/2^+$	$\cdots$	$\cdots$	$\cdots$
Σ_b^-	$1/2^+$	5815.64 ± 0.27	5.3 ± 0.5	$\Sigma_b^- \to \Lambda_b\pi^-$
Σ_b^{*+}	$3/2^+$	5830.32 ± 0.27	9.4 ± 0.5	$\Sigma_b^{*+} \to \Lambda_b\pi^+$
Σ_b^{*0}	$3/2^+$	$\cdots$	$\cdots$	$\cdots$
Σ_b^{*-}	$3/2^+$	5834.74 ± 0.30	10.4 ± 0.8	$\Sigma_b^{*-} \to \Lambda_b\pi^-$
Ξ_b^0	$1/2^+$	5791.9 ± 0.5	(No strong decay)	
Ξ_b^-	$1/2^+$	5797.0 ± 0.6	(No strong decay)	
$\Xi_b^{\prime 0}$	$1/2^+$	$\cdots$	$\cdots$	$\cdots$
$\Xi_b^{\prime -}(5935)$	$1/2^+$	5935.02 ± 0.05	(< 0.08)	$\Xi_b^{\prime -} \to \Xi_b^{0(-)}\pi^{-(0)}$
$\Xi_b^{0}(5945)$	$3/2^+$	5952.3 ± 0.6	0.90 ± 0.18	$\Xi_b^{\prime *0} \to \Xi_b^{-(0)}\pi^{+(0)}$
$\Xi_b^{-}(5955)$	$3/2^+$	5955.33 ± 0.13	1.65 ± 0.33	$\Xi_b^{\prime *-} \to \Xi_b^{0(-)}\pi^{-(0)}$
Ω_b	$1/2^+$	6046.1 ± 1.7	$\cdots$	$\cdots$
Ω_b^*	$3/2^+$	$\cdots$	$\cdots$	$\cdots$

Table5.1 Experimental values of masses and decay widths of singly heavy baryons in the ground state from PDG [12].

it is the remarkable variation under these reactions. Moreover, the interaction between a diquark and a heavy quark also changes due to the change of a diquark. In this work, we express this diquark–heavy-quark interaction with the wave function $\phi_{\mathcal{D},J}$, where the subscript $\mathcal{D} = A, S$ and $J = 1/2, 3/2$ denote the constituent diquark and the total spin of singly heavy baryons, respectively. About the total spin of baryons in the initial state, Σ_Q and Ξ'_Q, there are two types as $J = 1/2, 3/2$ due to the A diquark with spin 1. On the other hand, the total spin of baryons in the final state, Λ_Q and Ξ_Q, are fixed to $J = 1/2$ because of the S diquark with spin 0. From here, we define symbols for baryons in the initial state as $A_Q (= \Sigma_Q, \Xi'_Q)$, and also in the final state as $S_Q (= \Lambda_Q, \Xi_Q)$, where the symbol A and S are from a diquark inside those baryons. The diagram for these decays is described in Fig. 5.1.

Now we found that $\Sigma_Q \to \Lambda_Q\pi$ and $\Xi'_Q \to \Xi_Q\pi$ decays, totally expressed as $A_Q \to$

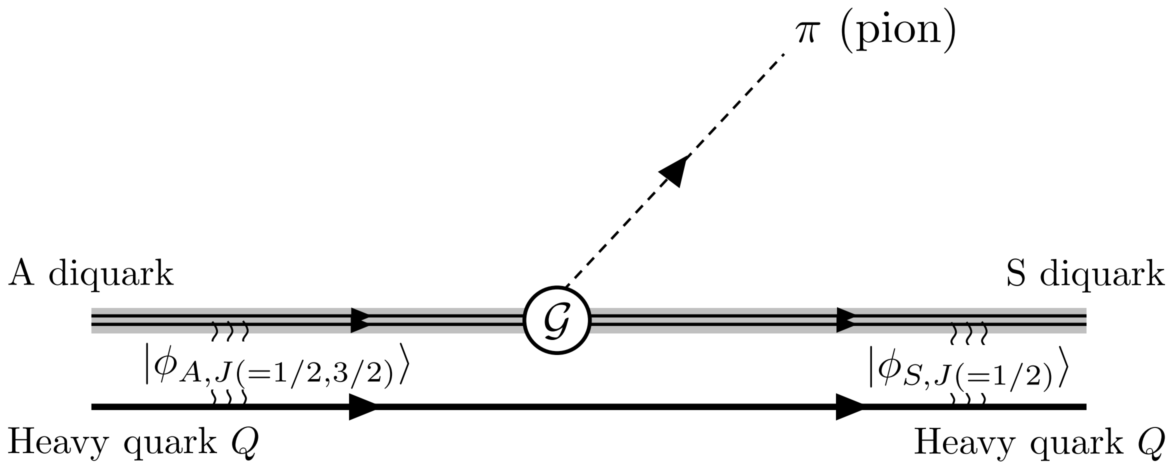

Figure5.1 The diagram for the one pion decay of a singly heavy baryon from the perspective of a diquark, including the wave function $|\phi_{\mathcal{D},J}\rangle$ in between a diquark and a heavy quark. $\mathcal{G}$ is the coupling constant for diquarks and a pion.

$S_Q\pi$, are generally represented by the one pion decay of diquarks changing from A to S. Therefore, we need to consider the couplings between S and A diquarks mediated by a pion. According to Eqs. (2.75) and (2.78), The Lagrangian for this interaction is given by

$$\begin{aligned}\mathcal{L}_{A\to S\pi} = -\sqrt{2}iG_1 &\left[A^{\mu}_{\{uu\}}(\partial_\mu\pi^-)S^\dagger_{[ud]} - A^{\mu}_{\{ud\}}(\partial_\mu\pi^0)S^\dagger_{[ud]} - A^{\mu}_{\{dd\}}(\partial_\mu\pi^+)S^\dagger_{[ud]}\right] \\ &- iG_2\left[A^{\mu}_{\{ds\}}(\partial_\mu\pi^+)S^\dagger_{[su]} - A^{\mu}_{\{us\}}(\partial_\mu\pi^-)S^\dagger_{[ds]}\right] \\ &+ \frac{i}{\sqrt{2}}G_2\left[A^{\mu}_{\{us\}}(\partial_\mu\pi^0)S^\dagger_{[su]} + A^{\mu}_{\{ds\}}(\partial_\mu\pi^0)S^\dagger_{[ds]}\right],\end{aligned} \tag{5.1}$$

where only the pion components in the pseudoscalar meson field $\tilde{\pi}$ are extracted by Eq. (2.77). For diquark fields in this Lagrangian, we have rewritten the representation of supscripts from numbers to flavors as

$$A^{\mu}_{ij} = \frac{1}{\sqrt{2}}\begin{pmatrix}\sqrt{2}A^{\mu}_{\{uu\}} & A^{\mu}_{\{ud\}} & A^{\mu}_{\{us\}} \\ A^{\mu}_{\{ud\}} & \sqrt{2}A^{\mu}_{\{dd\}} & A^{\mu}_{\{ds\}} \\ A^{\mu}_{\{us\}} & A^{\mu}_{\{ds\}} & \sqrt{2}A^{\mu}_{\{ss\}}\end{pmatrix},\ S_i = \begin{pmatrix}S_{[ds]} \\ S_{[su]} \\ S_{[ud]}\end{pmatrix}. \tag{5.2}$$

For the other, $G_{1,2}$ are the new coupling constants represented by the linear combination of parameters $g_{1,2}$ in the interaction Lagrangian Eq. (2.73) as

$$G_1 = g_1 + \check{\mathcal{A}}_s g_2,\quad G_2 = g_1 + g_2. \tag{5.3}$$

About G_1, the coefficient $\check{\mathcal{A}}_s$ beside g_2 is the third components of the effective quark mass matrix in Eq. (2.43). Repeatedly speaking, this constant $\check{\mathcal{A}}_s$ is used for the VEV of Σ field with considering the explicit chiral symmetry breaking as in Eq. (2.44), and it represents the flavor $SU(3)$ symmetry breaking due to the heavier s quark mass than the other u, d quarks. From Eq. (5.1), we can find that G_1 and G_2 are the coupling constants for $\Sigma_Q \to \Lambda_Q\pi$ decay and $\Xi'_Q \to \Xi_Q\pi$ decay, respectively. For the convenience, we express the absolute value of those coupling constants as $|\mathcal{G}|$ synthetically, meaning

$$|\mathcal{G}| = \begin{cases} \sqrt{2}G_1 & (\Sigma_Q \to \Lambda_Q\pi^{\pm,0}) \\ G_2 & (\Xi'_Q \to \Xi_Q\pi^{\pm}) \\ G_2/\sqrt{2} & (\Xi'_Q \to \Xi_Q\pi^{0}) \end{cases} . \tag{5.4}$$

The dynamics of these one pion decays of singly heavy baryons can be described by the Lagrangian Eq. (5.1) from the perspective of diquarks. However, not only a constituent diquark but also a constituent heavy quark and a diquark–heavy-quark interaction give features of singly heavy baryons. With the diquark–heavy-quark picture, the state of singly heavy baryon $|\mathcal{D}_Q\rangle$ with its momentum $\vec{P}_{\mathcal{D}_Q}$ and energy $E_{\mathcal{D}_Q}$ is represented as the product of a diquark state $|\mathcal{D}\rangle$ with $\vec{p}_{\mathcal{D}}$ and $E_{\mathcal{D}}$, and a heavy-quark state $|Q\rangle$ with $\vec{p}_Q$ and E_Q, superposed by the relative wave function $\phi_{\mathcal{D},J}$, written as

$$|\mathcal{D}_Q(P_{\mathcal{D}_Q}, J)\rangle = \sqrt{2E_{\mathcal{D}_Q}} \int \frac{d^3p}{(2\pi)^3}\phi_{\mathcal{D},J}(\vec{p}) \times \frac{1}{\sqrt{2E_{\mathcal{D}}}}\frac{1}{\sqrt{2E_Q}}|\mathcal{D}(p_{\mathcal{D}}, s_{\mathcal{D}})\rangle|Q(p_Q, s_Q)\rangle. \tag{5.5}$$

In this expression, there are the integral with respect to $\vec{p}$ which shows the relative momentum of two constituent particles. Using the mass of diquark and heavy quark, $M_{\mathcal{D}}$ and M_Q, the momentum of constituent diquark and heavy quark are expressed with this relative momentum $\vec{p}$ and the baryon's momentum $\vec{P}_{\mathcal{D}_Q}$ as

$$\vec{p}_{\mathcal{D}} = \frac{M_{\mathcal{D}}}{M_{\mathcal{D}} + M_Q}\vec{P}_{\mathcal{D}_Q} + \vec{p}, \quad \vec{p}_Q = \frac{M_Q}{M_{\mathcal{D}} + M_Q}\vec{P}_{\mathcal{D}_Q} - \vec{p}, \tag{5.6}$$

so that both diquark and heavy-quark states depend on $\vec{p}$ with keeping the momentum conservation rule as $\vec{p}_{\mathcal{D}} + \vec{p}_Q = \vec{P}_{\mathcal{D}_Q}$. Those momenta are also represented in Fig. 5.2. For the other symbols, $s_{\mathcal{D}}$ and s_Q in diquark and heavy-quark state kets stand for the spins of diquark and heavy quark, respectively.

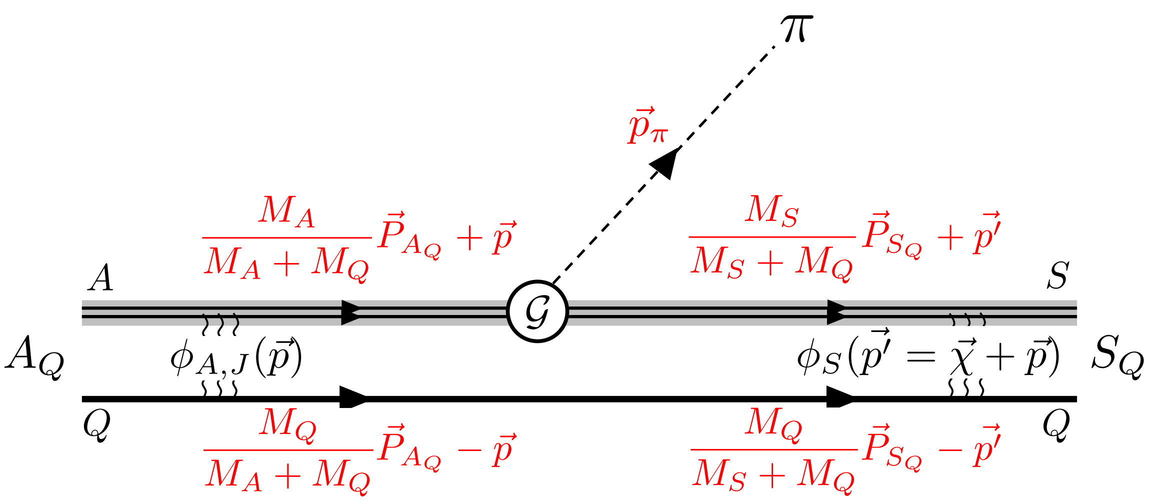

Figure5.2 Kinematics of $A_Q \to S_Q\pi$ decays as in Fig. 5.1, including the momenta of particles expressed with the momentum of baryons $\vec{P}_{\mathcal{D}_Q}$ and the relative momentum $\vec{p}$ and $\vec{p'}$. $\vec{p}_\pi$ denotes the pion momentum.

About the energies of diquark and heavy quark, they are expressed in the relativistic way as $E_{\mathcal{D}} = \sqrt{|\vec{p}_{\mathcal{D}}|^2 + M_{\mathcal{D}}^2}$ and $E_Q = \sqrt{|\vec{p}_Q|^2 + M_Q^2}$, respectively. Since the momenta $\vec{p}_{\mathcal{D}}$ and $\vec{p}_Q$ depend on the relative momentum, we can say that these energies also depend on the relative momentum $\vec{p}$. On the other hand, the energy of baryon written as $E_{\mathcal{D}_Q} = \sqrt{|\vec{P}_{\mathcal{D}_Q}|^2 + M_{\mathcal{D}_Q}^2}$ with the mass of baryon $M_{\mathcal{D}_Q}^2$ is independent of $\vec{p}$ while the momentum obeys to the conservation rule as $\vec{P}_{A_Q} = \vec{P}_{S_Q} + \vec{p}_\pi$. Also, the normalization of states of singly heavy baryon and its constituent diquark and heavy quark are also defined in the relativistic way as

$$\begin{aligned}
&\langle \mathcal{D}'_Q(P'_{\mathcal{D}_Q}, J'_{\mathcal{D}_Q})|\mathcal{D}_Q(P_{\mathcal{D}_Q}, J_{\mathcal{D}_Q})\rangle = 2E_{\mathcal{D}_Q}(2\pi)^3\delta(\vec{P'}_{\mathcal{D}_Q} - \vec{P}_{\mathcal{D}_Q})\delta_{J'_{\mathcal{D}_Q}J_{\mathcal{D}_Q}}, \\
&\langle \mathcal{D}'(p'_{\mathcal{D}}, s'_{\mathcal{D}})|\mathcal{D}(p_{\mathcal{D}}, s_{\mathcal{D}})\rangle = 2E_{\mathcal{D}}(2\pi)^3\delta(\vec{p'}_{\mathcal{D}} - \vec{p}_{\mathcal{D}})\delta_{s'_{\mathcal{D}}s_{\mathcal{D}}}, \\
&\langle Q'(p'_Q, s'_Q)|Q(p_Q, s_Q)\rangle = 2E_Q(2\pi)^3\delta(\vec{p'}_Q - \vec{p}_Q)\delta_{s'_Q s_Q},
\end{aligned} \tag{5.7}$$

so that the factors such as $\sqrt{2E_{\mathcal{D}_Q}}$, $\sqrt{2E_{\mathcal{D}}}$, and $\sqrt{2E_Q}$ are included in Eq. (5.5). On the other hand, the normalization of wave functions is given as

$$\int \frac{d^3p}{(2\pi)^3}|\phi_{A,J}(\vec{p})|^2 = 1, \quad \int \frac{d^3p'}{(2\pi)^3}|\phi_S(\vec{p'})|^2 = 1, \tag{5.8}$$

for both initial and final states. Here the symbol of the total spin J is omitted from ϕ_S since it takes only $J = 1/2$. About the relative momentum in these wave functions, $\vec{p}$ and $\vec{p'}$, they are different from each state but are connected with the recoil momentum $\vec{\chi}$ as $\vec{\chi} = \vec{p'} - \vec{p}$, which is also shown in Fig. 5.2. In particular, when the A_Q baryon is at the rest frame as $\vec{P}_{A_Q} = \vec{0}$, we can define it as

$$\vec{\chi} = \frac{M_Q}{M_S + M_Q}\vec{P}_{S_Q} = -\frac{M_Q}{M_S + M_Q}\vec{p}_\pi, \tag{5.9}$$

with confirming the momentum conservation rule, $\vec{P}_{S_Q} + \vec{p}_\pi = \vec{P}_{A_Q} = \vec{0}$. Also, in this system, the magnitude of the pion's momentum $\vec{p}_\pi$ can be derived from the energy conservation rule as

$$\begin{aligned}
M_{A_Q} &= \sqrt{M_{S_Q}^2 + |\vec{p}_\pi|^2} + \sqrt{M_{S_Q}^2 + |\vec{p}_\pi|^2} \\
\Longleftrightarrow \quad |\vec{p}_\pi| &= \frac{\sqrt{\left[M_{A_Q}^2 - (M_{S_Q} + M_\pi)^2\right]\left[M_{A_Q}^2 - (M_{S_Q} - M_\pi)^2\right]}}{2M_{A_Q}},
\end{aligned} \tag{5.10}$$

which is described only by the masses of baryons and pion, $M_{\mathcal{D}_Q}$ and M_π.

Keeping above in mind, we then calculate the decay amplitude $\mathcal{M}$ which appears in the elements of S-matrix for a scattering or decay process. The S-matrix for the $A_Q \to S_Q\pi$ decay is expressed with the interaction Lagrangian in Eq. (5.1) as

$$\int d^4x \langle S_Q(P_{S_Q}, J_{S_Q})\pi(p_\pi)|i\mathcal{L}_{A\to S\pi}|A_Q(P_{A_Q}, J_{A_Q})\rangle, \tag{5.11}$$

by the first order perturbation. According to Eq. (5.1), all of the terms in this Lagrangian are expressed as $\mathcal{G}A^\mu_{\{qq\}}(\partial_\mu\pi)S^\dagger_{[qq]}$, and they are represented with diquarks and pion state kets by

$$\langle S(p_S,s_S)\pi(p_\pi)|i\mathcal{G}A^\mu_{\{qq\}}(x)\{\partial_\mu\pi(x)\}S^\dagger_{[qq]}(x)|A(p_A,s_A)\rangle$$
$$= -\mathcal{G}(p_\pi)_\mu\epsilon^\mu_A(p_A,s_A)e^{i(p_S+p_\pi-p_A)x}, \quad (5.12)$$

in the form of plane wave. Here $\epsilon^\mu_A(p_A,s_A)$ denotes the polarization vector from the spinor sector of A diquark. Therefore, each term of Eq. (5.11) are calculated from Eqs. (5.5) and (5.12), and those decay amplitude is given by

$$\int d^4x\langle S_Q(P_{S_Q},J_S)\pi(p_\pi)|i\mathcal{G}A^\mu_{\{qq\}}(x)\{\partial_\mu\pi(x)\}S^\dagger_{[qq]}(x)|A_Q(P_{A_Q},J_A)\rangle$$
$$= -\frac{\mathcal{G}\sqrt{E_{A_Q}E_{S_Q}}}{3}\int\frac{d^3p}{(2\pi)^3}\phi^*_S(\vec{\chi}+\vec{p})\phi_{A,J}(\vec{p})$$
$$\times\frac{1}{\sqrt{E_AE_S}}(p_\pi)_\mu\epsilon^\mu_A(p_A,s_A)\times(2\pi)^4\delta^{(4)}(p_S+p_\pi-p_A),$$
$$\therefore\ \mathcal{M} = i\frac{\mathcal{G}}{3}\frac{\sqrt{E_{A_Q}E_{S_Q}}}{\sqrt{E_AE_S}}\int\frac{d^3p}{(2\pi)^3}\phi^*_S(\vec{\chi}+\vec{p})\phi_{A,J}(\vec{p})(p_\pi)_\mu\epsilon^\mu_A(p_A,s_A). \quad (5.13)$$

As a consequence, the decay width of $A_Q\to S_Q\pi$ two body decay is given with the amplitude in Eq. (5.13) as

$$\Gamma[A_Q\to S_Q\pi] = \frac{|\vec{p}_\pi|}{32\pi^2M^2_{A_Q}}\times\int d\Omega\left[\frac{1}{3}\sum_{s_A=-1}^{+1}|\mathcal{M}|^2\right], \quad (5.14)$$

with taking the spin average for A diquark.

About the decay amplitude $\mathcal{M}$, if the momentum $\vec{p}_A$ is fixed to some value and does not relate to the relative momentum $\vec{p}$, the integral in Eq. (5.13) only involves to the wave functions $\phi^*_S(\vec{\chi}+\vec{p})$ and $\phi_{A,J}(\vec{p})$. At this time, the decay width in Eq. (5.14) is expressed as

$$\Gamma[A_Q\to S_Q\pi] = \frac{|\mathcal{G}|^2|\vec{p}_\pi|E_{S_Q}}{864\pi^2M_{A_Q}E_AE_S}|\langle\phi_S|\phi_{A,J}\rangle|^2$$
$$\times\int d\Omega\ \left[(p_\pi)_\mu\left(-g^{\mu\nu}+\frac{p^\mu_Ap^\nu_A}{M^2_A}\right)(p_\pi)_\nu\right], \quad (5.15)$$

where we defined the inner product $\langle\phi_S|\phi_{A,J}\rangle\equiv\int\frac{d^3p}{(2\pi)^3}\phi^*_{S_Q}(\vec{\chi}+\vec{p})\phi_{A_Q}(\vec{p})$ for wave functions, and used the summation of the polarization vector expressed as

$$\sum_{s=-1}^{1}\epsilon^{*\mu}_A(p_A,s_A)\epsilon^\nu_A(p_A,s_A) = -g^{\mu\nu}+\frac{p^\mu_Ap^\nu_A}{M^2_A}. \quad (5.16)$$

To give the decay width from Eq. (5.15), we define the expectation values of the relative momentum $\vec{p}$ and its square, which are the same as those of $\vec{p}_A$ at the rest frame of A_Q baryon. Therefore, in the present work, these expectation values can be calculated by the wave function of A_Q baryon as

$$\langle\vec{p}\rangle\equiv\int\frac{d^3p}{(2\pi)^3}\vec{p}\ |\phi_{A,J}(\vec{p})|^2 = 0,\quad \langle p^2\rangle\equiv\int\frac{d^3p}{(2\pi)^3}|\vec{p}|^2|\phi_{A,J}(\vec{p})|^2. \quad (5.17)$$

In this way, the squared momentum of the S diquark is evaluated as $|\vec{p}_S|^2 = \langle p^2 \rangle + |\vec{p}_\pi|^2$ from the momentum conservation rule, $\vec{p}_S + \vec{p}_\pi = \vec{p}_A = \vec{p}$. Therefore, the energies of diquarks are represented by

$$E_A = M_A\sqrt{1+v_A^2}, \quad E_S = M_S\sqrt{1+\frac{M_A^2}{M_S^2}v_A^2+\frac{|\vec{p}_\pi|^2}{M_S^2}}, \tag{5.18}$$

where the squared velocity v_A^2 is defined as $\langle p^2 \rangle \equiv M_A^2 v_A^2$. Moreover, this expectation value is also applied to the p_A appeared by Eq. (5.16), in which the integrand in Eq. (5.15) becomes as

$$\left[(p_\pi)_\mu\left(-g^{\mu\nu}+\frac{p_A^\mu p_A^\nu}{m_A^2}\right)(p_\pi)_\nu\right] = |\vec{p}_\pi|^2 + E_\pi^2 v_A^2 + |\vec{p}_\pi|^2 v_A^2\cos^2\theta, \tag{5.19}$$

with the energy of pion $E_\pi = \sqrt{M_\pi^2+|\vec{p}_\pi|^2}$. About Eq. (5.19), we note that the terms proportional to $\cos\theta$ are truncated because of $\int d\Omega\cos\theta = 0$, whereas $\int d\Omega\cos^2\theta = 4\pi/3$. Finally, by substituting Eqs. (5.18) and (5.19) into Eq. (5.15), we obtain the decay width formula with v_A^2:

$$\Gamma[A_Q \to S_Q\pi] = \frac{|\mathcal{G}|^2|\vec{p}_\pi|E_{S_Q}}{216\pi M_{A_Q}}\left\{\frac{|\vec{p}_\pi|^2(3+v_A^2)+3E_\pi^2 v_A^2}{3E_A E_S}\right\}|\langle\phi_S|\phi_{A,J}\rangle|^2. \tag{5.20}$$

At this time, the energy of S_Q baryon is expressed as $E_{S_Q} = \sqrt{|\vec{p}_\pi|^2+M_{S_Q}^2}$ with $|\vec{p}_\pi|$ in Eq. (5.10).

Now we can give values of coupling constant $\mathcal{G}$ from Eq. (5.20). For this calculation, we need the masses of pion and singly heavy baryons. The experimental data for those baryons are summarized in Table 5.1, and the observed pion masses are shown as $m_{\pi^\pm} = 139.57$ MeV and $m_{\pi^\pm} = 134.97$ MeV in PDG [12]. For the others, the diquark–heavy-quark potential model is requested as for the inputs of diquark and heavy-quark masses, and also for the diquark–heavy-quark wave functions used in the expectation value $\langle p^2 \rangle$ and the inner product $|\langle\phi_S|\phi_{A,J}\rangle|$. For these inputs, we use the Y-potential defined in chapter 4, where its potential parameters and masses of heavy quarks are summarized in Table 4.1. About the values of S and A diquark masses, they are already summarized in Table 4.2, where we use the values given by solving the Schrödinger equation with the Hamiltonian Eq. (3.1) including the Y-potential term. Also, the relative wave functions $\phi_S(\vec{p})$ and $\phi_{A,J}(\vec{p})$ can be obtained by this solution. From Eqs. (4.3) and (4.4), the detailed form of Y-potential in this work is expressed as

$$V(r) = -\frac{\alpha}{r} + \lambda r + C_Q + (\boldsymbol{s}_\mathcal{D}\cdot\boldsymbol{s}_Q)\frac{\kappa_Q}{M_\mathcal{D}M_Q}\frac{\Lambda^2}{r}e^{-\Lambda r}. \tag{5.21}$$

Here the spin-orbit and tensor potential terms are neglected, since we only consider about the ground state of singly heavy baryons and thus there are no effect by the S-wave orbital angular momentum. As a summary, the Y-potential parameters and particle masses for this strong decay calculation are summarized in Table. 5.2, which correspond to values in Tables 4.1, 4.2, and 4.3.

5.1.2 Numerical results of coupling constants

In this subsection, we determine the values of coupling constants $g_{1,2}$ in the effective interaction Lagrangian (2.73). These parameters are used for the absolute value of the

Y-pot. parameters		Masses (MeV)	
α	$0.06(\mathrm{GeV})/\mu$	$M_{ud}(0^+)$	725
$\lambda(\mathrm{GeV}^2)$	0.165	$M_{ns}(0^+)$	942
$C_c(\mathrm{GeV})$	-0.831	$M_{nn}(1^+)$	973
$C_b(\mathrm{GeV})$	-0.819	$M_{ns}(1^+)$	1116
$\Lambda(\mathrm{GeV})$	0.691	M_c	1750
κ_c	0.8586	M_b	5112
κ_b	0.6635		

Table5.2 Parameters of the Y-potential model and masses of diquarks and heavy quarks related to the decay width calculation of $A_Q \to S_Q\pi$ reaction. μ in the parameter α is the reduced mass of diquark–heavy-quark two-body system. (See chapter 4 for the determination of these values.)

coupling constant $|\mathcal{G}|$ in the formula (5.20), and these are represented by the coupling constants of strong decays, i.e., G_1 for $\Sigma_Q \to \Lambda_Q\pi$ decay and G_2 for $\Xi'_Q \to \Xi_Q\pi$ decay as in Eq. (5.4). According to Eq. (5.3), the parameter $g_{1,2}$ are expressed with $G_{1,2}$ as

$$g_1 = \frac{\check{\mathcal{A}}_\mathrm{s} G_2 - G_1}{\check{\mathcal{A}}_\mathrm{s} - 1}, \quad g_2 = \frac{G_1 - G_2}{\check{\mathcal{A}}_\mathrm{s} - 1}. \tag{5.22}$$

Hence, the parameters $g_{1,2}$ can be quantified by the translation of values of $G_{1,2}$, which can be given from the decay width formula (5.20).

To compute the values of $G_{1,2}$, we use the observed decay width and masses of singly heavy baryons in Table 5.1. Moreover, we use the Y-potential model for the masses of constituent diquark and heavy quark, and also for the wave functions between a diquark and a heavy quark, which are summarized in Table. 5.2. In concrete, each G_1 and G_2 is given as follows:

(i) The value of G_1 are determined by the experimental data of the $\pi^\pm$ emission decays of $\Sigma_Q^{(*)}$ baryons. About the π^0 emission decays, they only give the upper limit of the decay width, so that they are not considered.

(ii) The value of G_2 is determined by the experimental data of the $\pi^\pm$ and π^0 emission decays of Ξ'_Q baryons with the total spin $J = 3/2$. The decays of Ξ'_Q baryons with $J = 1/2$ are not considered, because there are no available data in PDG [12] [*1].

The numerical results of $G_{1,2}$ are summarized in Tables 5.3 and 5.4 with corresponding reactions and those decay widths, respectively. The main values of these parameters are evaluated from the averaged experimental data, and those errors are also estimated by the errors of experimental masses and decay widths of correlated baryons and pions. Neglecting the errors, we can find that both of these parameters are in the range between 20 and 30, which are about $21 < G_1 < 27$ and $24 < G_2 < 30$ in detail. The range of error is about 6 for both G_1 and G_2, and G_1 is rather smaller than G_2.

We then take the average of parameters $G_{1,2}$ from Tables 5.3 and 5.4 without considering

[*1] In particular, the Ξ'_c baryons with $J = 1/2$ are not heavy enough to decay to the ground state of Ξ_c baryons with one pion emission.

Baryon	J^P	Decay mode	Decay width (MeV)	G_1
$\Sigma_c^{++}(2455)$	$1/2^+$	$\Sigma_c^{++} \to \Lambda_c\pi^+$	$1.89^{+0.09}_{-0.18}$	$21.16^{+0.63}_{-1.15}$
$\Sigma_c^0(2455)$	$1/2^+$	$\Sigma_c^0 \to \Lambda_c\pi^-$	$1.83^{+0.11}_{-0.19}$	$20.92^{+0.75}_{-1.24}$
$\Sigma_c^{++}(2520)$	$3/2^+$	$\Sigma_c^{*++} \to \Lambda_c\pi^+$	$14.78^{+0.30}_{-0.40}$	$25.93^{+0.34}_{-0.43}$
$\Sigma_c^0(2520)$	$3/2^+$	$\Sigma_c^{*0} \to \Lambda_c\pi^-$	$15.3^{+0.4}_{-0.5}$	$26.37^{+0.42}_{-0.51}$
Σ_b^+	$1/2^+$	$\Sigma_b^+ \to \Lambda_b\pi^+$	5.0 ± 0.5	$21.93^{+1.21}_{-1.24}$
Σ_b^-	$1/2^+$	$\Sigma_b^- \to \Lambda_b\pi^-$	5.3 ± 0.5	$21.12^{+1.10}_{-1.13}$
Σ_b^{*+}	$3/2^+$	$\Sigma_b^{*+} \to \Lambda_b\pi^+$	9.4 ± 0.5	$23.77^{+0.73}_{-0.75}$
Σ_b^{*-}	$3/2^+$	$\Sigma_b^{*-} \to \Lambda_b\pi^-$	10.4 ± 0.8	$23.88^{+1.02}_{-1.05}$

Table5.3 The coupling constant G_1 determined from the decay widths of $\Sigma_Q \to \Lambda_Q\pi^\pm$ decays.

Baryon	J^P	Decay mode	Decay width (MeV)	G_2
$\Xi_c^+(2645)$	$3/2^+$	$\Xi_c^{'*+} \to \Xi_c\pi$	2.14 ± 0.19	$26.73^{+1.45}_{-1.47}$
		$\Xi_c^{'*+} \to \Xi_c^0\pi^+$	$1.32^{+0.12}_{-0.11}$*	
		$\Xi_c^{'*+} \to \Xi_c^+\pi^0$	$0.82^{+0.07}_{-0.08}$*	
$\Xi_c^0(2645)$	$3/2^+$	$\Xi_c^{'*0} \to \Xi_c\pi$	2.35 ± 0.22	$27.07^{+1.48}_{-1.52}$
		$\Xi_c^{'*0} \to \Xi_c^+\pi^-$	$1.56^{+0.14}_{-0.15}$*	
		$\Xi_c^{'*0} \to \Xi_c^0\pi^0$	$0.79^{+0.08}_{-0.07}$*	
$\Xi_b^0(5945)$	$3/2^+$	$\Xi_b^{'*0} \to \Xi_b\pi$	0.90 ± 0.18	$24.76^{+3.33}_{-3.35}$
		$\Xi_b^{'*0} \to \Xi_b^-\pi^+$	$0.50^{+0.09}_{-0.10}$*	
		$\Xi_b^{'*0} \to \Xi_b^0\pi^0$	$0.41^{+0.08}_{-0.09}$*	
$\Xi_b^-(5955)$	$3/2^+$	$\Xi_b^{'*-} \to \Xi_b\pi$	1.65 ± 0.33	$29.55^{+3.38}_{-3.55}$
		$\Xi_b^{'*-} \to \Xi_b^0\pi^-$	1.13 ± 0.23*	
		$\Xi_b^{'*-} \to \Xi_b^-\pi^0$	0.52 ± 0.10*	

Table5.4 The coupling constant G_2 determined from the decay widths of $\Xi_Q' \to \Xi\pi$ decays, where the spin-parity of Ξ_Q' are all $J^P = 3/2^+$. The values with the asterisk * are the partial decay widths predicted in this work.

those errors. For G_1, the isospin averages are given by

$$\begin{aligned}
G_1^{c(1/2)} &\equiv \frac{1}{2}\left(G_1|_{\Sigma_c^{++}(2455)} + G_1|_{\Sigma_c^0(2455)}\right) \simeq 21.04 \ , \\
G_1^{c(3/2)} &\equiv \frac{1}{2}\left(G_1|_{\Sigma_c^{++}(2520)} + G_1|_{\Sigma_c^0(2520)}\right) \simeq 26.15 \ , \\
G_1^{b(1/2)} &\equiv \frac{1}{2}\left(G_1|_{\Sigma_b^+} + G_1|_{\Sigma_b^-}\right) \simeq 21.53 \ , \\
G_1^{b(3/2)} &\equiv \frac{1}{2}\left(G_1|_{\Sigma_b^{*+}} + G_1|_{\Sigma_b^{*-}}\right) \simeq 23.82 \ ,
\end{aligned} \tag{5.23}$$

and the spin averages are given as

$$\begin{aligned}
G_1^c &\equiv \frac{1}{3}\left(\bar{G}_1^{c(1/2)} + 2\bar{G}_1^{c(3/2)}\right) \simeq 24.45 \ , \\
G_1^b &\equiv \frac{1}{3}\left(\bar{G}_1^{b(1/2)} + 2\bar{G}_1^{b(3/2)}\right) \simeq 23.06 \ ,
\end{aligned} \tag{5.24}$$

for charm and bottom sectors, respectively. As the same, we can take the isospin average for G_2 as

$$
\begin{aligned}
G_2^c &\equiv \frac{1}{2}\left(G_2|_{\Xi_c^+(2645)} + G_2|_{\Xi_c^0(2645)}\right) \simeq 26.90 \ , \\
G_2^b &\equiv \frac{1}{2}\left(G_2|_{\Xi_b^0(5945)} + G_2|_{\Xi_b^-(5955)}\right) \simeq 27.16 \ .
\end{aligned} \tag{5.25}
$$

Using these averaged values in Eqs. (5.24) and (5.25), and also $\check{\mathcal{A}}_{\mathrm{s}}$ approximated in Eq. (2.43), the parameters $g_{1,2}$ are evaluated by Eq. (5.22) as

$$
(g_1^c, g_2^c) = (30.56, -3.66), \quad (g_1^b, g_2^b) = (33.28, -6.12), \tag{5.26}
$$

for each heavy-quark sector. From these values, it is obvious that the magnitude of g_2 is much smaller than g_1, which comes from the little difference between G_1 and G_2. In concrete, the absolute value of the ratio of g_2 to g_1 is evaluated to be $|g_2^c/g_1^c| \simeq 0.12$ and $|g_2^b/g_1^b| \simeq 0.18$ for the charm and bottom sector, respectively. With this little effect of g_2 term, we can also make the conclusion that the chiral $U(1)_A$ anomaly induced by the interactions between scalar and vector diquarks meditated by two mesons are small [*2].

Baryon (J^P)	Mass (MeV)	G_1	Decay mode	Decay width (cal.) (MeV)	Decay width (exp.) (MeV)
$\Sigma_c^+(1/2^+)$	2452.9 ± 0.4	$21.04^{+0.69}_{-1.20}$	$\Sigma_c^+ \to \Lambda_c \pi^0$	$2.05^{+0.18}_{-0.27}$	(< 4.6)
$\Sigma_c^{*+}(3/2^+)$	2517.5 ± 2.3	$26.15^{+0.38}_{-0.47}$	$\Sigma_c^{*+} \to \Lambda_c \pi^0$	$15.42^{+1.10}_{-1.15}$	(< 17)
$\Sigma_b^0(1/2^+)$	5809.88*	$21.53^{+1.16}_{-1.19}$	$\Sigma_b^0 \to \Lambda_b \pi^0$	$5.10^{+0.59}_{-0.57}$	$\cdots$
$\Sigma_b^{*0}(3/2^+)$	5829.31*	$23.82^{+0.88}_{-0.90}$	$\Sigma_b^{*0} \to \Lambda_b \pi^0$	$9.75^{+0.77}_{-0.75}$	$\cdots$

Table5.5 Our predictions of π^0 emission decay widths of Σ_Q baryons. The mass with the asterisk * is the calculated value from Y-potential. For the decay width, (cal.) and (exp.) represent our predictions and experimental data [12], respectively.

Baryon (J^P)	Mass (MeV)	G_2	Decay mode	Decay width (cal.) (MeV)	Decay width (exp.) (MeV)
$\Xi_b'^0(1/2^+)$	5934.16*	$27.16^{+3.36}_{-3.45}$	$\Xi_b'^0 \to \Xi_b \pi$	0.14 ± 0.04	$\cdots$
			$\Xi_b'^0 \to \Xi_b^- \pi^+$	(No strong decay)	
			$\Xi_b'^0 \to \Xi_b^0 \pi^0$	0.14 ± 0.04	$\cdots$
$\Xi_b'^-(1/2^+)$	5935.02 ± 0.05	$27.16^{+3.36}_{-3.45}$	$\Xi_b'^- \to \Xi_b \pi$	$0.24^{+0.10}_{-0.08}$	(< 0.08)
			$\Xi_b'^- \to \Xi_b^0 \pi^-$	$0.17^{+0.07}_{-0.05}$	$\cdots$
			$\Xi_b'^- \to \Xi_b^- \pi^0$	$0.07^{+0.03}_{-0.02}$	$\cdots$

Table5.6 Our predictions of π emission decay widths of $\Xi_b'(1/2^+)$ baryons. The mass with the asterisk * is the calculated value from Y-potential. For the decay width, (cal.) and (exp.) represent our predictions and experimental data [12], respectively.

For the application of these coupling constants, we give the predictions for decay widths which is not explicitly known in experimental ways as in Table 5.1. Firstly, Table 5.5

[*2] The same conclusion is also obtained from the other chiral effective model based on the decay of singly heavy baryon itself [3, 127–129].

indicates the prediction of $\Sigma_Q \to \Lambda_Q \pi^0$ decay widths, where the isospin averaged values in Eq. (5.23) are used for G_1. For the non-observed masses of Σ_b baryons, we have used the values predicted by the diquark–heavy-quark two body calculation with Y-potential, whose values are round to two decimal places and are more detail than those in Table 4.4. As a result, since the predicted widths for Σ_c^+ and Σ_c^{*+} are below the experimental upper limits, our predictions are consistent with the experiments for the singly charmed baryons. Secondly, Table 5.6 are the prediction for the decays of Ξ_b' baryons with spin-parity $J^P = 1/2^+$. Here we used the isospin averaged value for the coupling constant G_2, and the non-observed $\Xi_b^{'0}$ mass is replaced to the theoretically predicted value from our diquark–heavy-quark two body calculation with Y-potential, whose value is round to two decimal places in more detail. However, about the $\Xi_b^{'-} \to \Xi_b \pi$ decay, the predicted width from our model, 0.24 MeV, is about three times larger than the experimental upper limit, 0.08 MeV. For this satisfaction, the coupling constant G_2 needs to be less than 15.61. If the same, the decay width of $\Xi_b^{'0} \to \Xi_b^{(0)} \pi^{(0)}$ may become smaller than our prediction 0.14 MeV, which would be less than 0.045 MeV by inputting $G_2 \leq 15.61$.

5.2 Chiral symmetry restoration

The spontaneous chiral symmetry breaking is the QCD effect from the chiral condensation. In the ordinary vacuum state, the VEV of scalar meson takes a finite value as $\langle \bar{q}q \rangle \neq 0$, so that the chiral symmetry breaking occurs and it brings about the effective masses for light quarks. However, at high temperature and/or high baryon density, the matters in the QCD scale is expected to move in the phase where the chiral symmetry is restored. In terms of the chiral condensate $\langle \bar{q}q \rangle$, this value approaches toward zero as $\langle \bar{q}q \rangle \to 0$ by the transition to the chiral symmetry restored phase.

Previously, we have made the chiral effective model of diquarks based on the $SU(3)$ linear sigma model, and applied to the mass spectrum and strong decays of singly heavy baryons. Here, the chiral condensate $\langle \bar{q}q \rangle$ is the same as the VEV of Σ field in the linear sigma model. It is of great interest and importance to study how diquarks change by the order of chiral symmetry breaking, because diquarks are expected to exist in the wide phase from low to high baryon density within the low temperature.

In this section, we consider the change of diquarks, especially the non-strange diquarks, from the variation of chiral condensation in the present chiral effective model. After this, we apply the relation between non-strange diquarks and chiral condensation to the $\Sigma_Q \to \Lambda_Q \pi^{\pm}$ decays. For this work, we define the parameter x multiplied to the VEV of Σ field in the vacuum state as

$$\langle \Sigma \rangle = x \langle \Sigma \rangle|_{\text{vac}} = x \times \text{diag}(f_\pi, f_\pi, f_s) \quad (0 \leq x \leq 1). \tag{5.27}$$

Changing the factor x restricted to $0 \leq x \leq 1$, we can express the phase transition as $x = 1$ corresponding to the ordinary vacuum state with the broken chiral symmetry, while $x = 0$ corresponding to the chiral symmetry restored phase with high temperature and/or high baryon density. In more detail, according to Ref. [130], the chiral condensate $\langle \bar{q}q \rangle$ starts to decrease rapidly at the cross-over temperature, and becomes $x \simeq 0.4$ at a temperature of 200 MeV. From the viewpoints of density, Refs. [28, 29, 130] show the reduction of chiral condensate $\langle \bar{q}q \rangle$ by the increase of density, where its value takes about $x \simeq 0.7$ for the nuclear density 0.17 fm^{-3}.

5.2.1 Diquark masses toward chiral restoration

At first, we discuss the mass formulae of diquarks as functions of x. From the multiplicated x to the VEV of Σ field, the non-strange diquark masses in Eqs. (2.48), (2.64) and (2.66) are given by

$$M_{ud}(0^+) = \sqrt{m_{S0}^2 - (x\frac{f_s}{f_\pi} + \frac{m_s}{g_s f_\pi})m_{S1}^2 - x^2 m_{S2}^2}, \tag{5.28}$$

$$M_{ud}(0^-) = \sqrt{m_{S0}^2 + (x\frac{f_s}{f_\pi} + \frac{m_s}{g_s f_\pi})m_{S1}^2 + x^2 m_{S2}^2}, \tag{5.29}$$

$$M_{nn}(1^+) = \sqrt{m_{V0}^2 + x^2(m_{V1}^2 + 2m_{V2}^2)}, \tag{5.30}$$

$$M_{ud}(1^-) = \sqrt{m_{V0}^2 + x^2(-m_{V1}^2 + 2m_{V2}^2)}, \tag{5.31}$$

where the parameters in Lagrangians (2.40) and (2.57) are already given as in Table 4.2. Here we use the values from Y-potential as follows in the units of MeV^2,

$$(m_{S0}^2, m_{S1}^2, m_{S2}^2) = ((1119)^2, (690)^2, -(258)^2)\ , \tag{5.32}$$

$$(m_{V0}^2, m_{V1}^2, m_{V2}^2) = ((708)^2, -(757)^2, (714)^2)\ . \tag{5.33}$$

Note that these are given from the spectrum of singly heavy baryons in the ordinary vacuum state ($x = 1$). In the present work, we assume that these parameters are independent of the chiral condensation parameter x. For the other physical numbers, we use the values $f_\pi = 92.1$ MeV, $f_s = 128.1$ MeV, $m_s = 93.1$ MeV, and $g_s = 2\pi/\sqrt{3}$ quoted from Refs. [12, 109, 110], which give the value $\check{\mathcal{A}}_s = 5/3$ defined in chapter 2.

According to Eqs. (5.32) and (5.33), the chiral invariant masses of non-strange diquarks in this work are given as $m_{S0} = 1119$ MeV and $m_{V0} = 708$ MeV for S/P and A/V diquarks, respectively. This indicates that the mass of non-strange S diquark could be about 400 MeV heavier than that of A diquark in the chiral symmetry restored phase. This is in the opposite situation compared with those diquark masses in the ordinary vacuum state, where the non-strange S diquark is about 200 MeV lighter than A diquark. Therefore, if these diquark masses change continuously by the phase transition parameter x, there may some crossing points in $0 \leq x \leq 1$ where the non-strange S and A diquark masses are equal.

Now we show the figure of non-strange diquark masses in the function of x, in which Eqs. (5.28) – (5.31) are illustrated as in Fig. 5.3. From the definition of x, the right-hand side near to $x = 1$ shows the ordinary vacuum state, while the left-hand side with approach to $x = 0$ indicates the chiral symmetry restored phase. With the change of x from 1 towards 0, we can see the increasing mass for S diquark, while the other masses are decreasing. This increase of S diquark mass at high temperature with chiral symmetry restored condition is also predicted in Ref. [131].

As we predicted from the chiral invariant mass, the masses of S and A diquarks are inversed when the chiral symmetry is restored, and its cross section is in between $0.6 \leq x \leq 0.7$. This behavior of the S and A diquark masses towards chiral restoration implies the significant change of the properties of singly heavy baryons with approach to the finite temperature and/or baryon density. It may also affect the appearance of color superconductivity in high density matter, where the A diquark becomes stabler than the S diquark from the viewpoints of each mass.

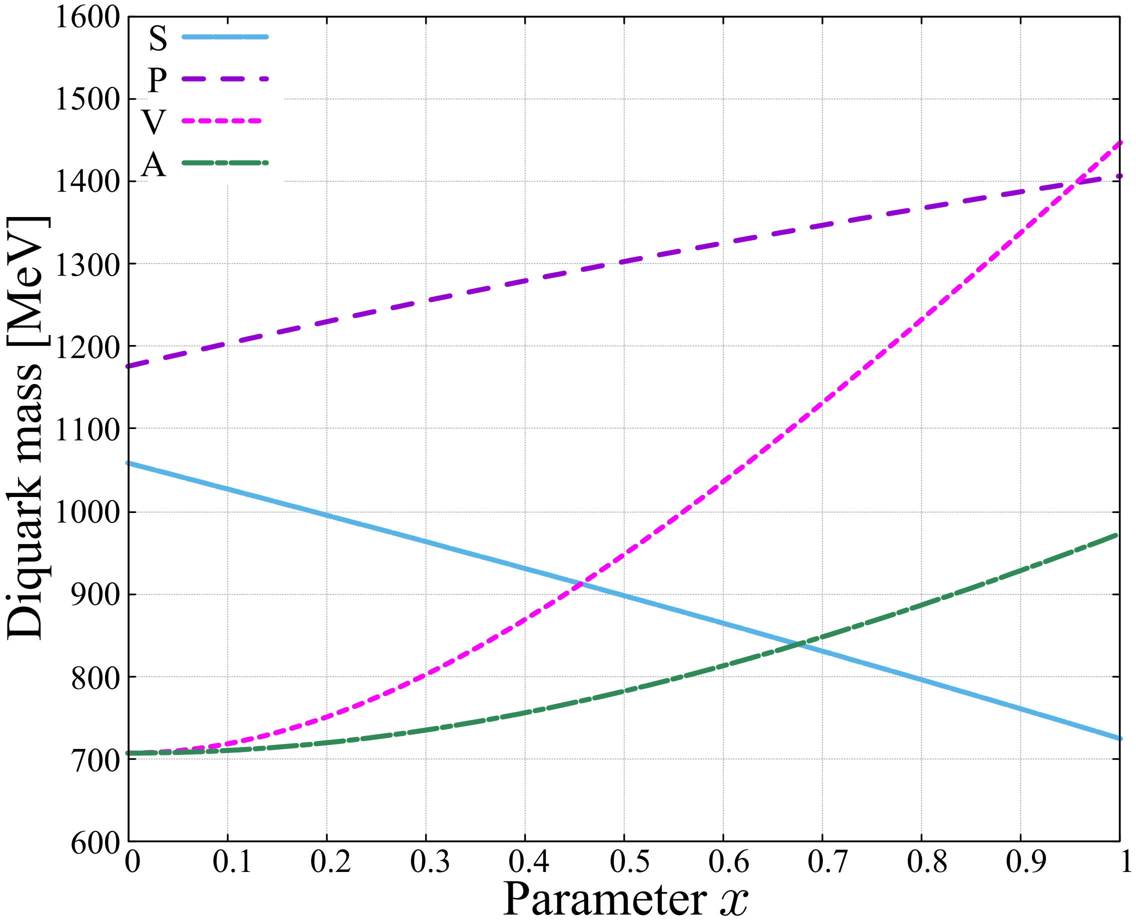

Figure5.3 Dependence of the non-strange diquark masses on the chiral condensation parameter x.

For another point of Fig. 5.3, the inversion of masses by the chiral symmetry restoration also occurs between S and V diquarks, because A and V are degenerate to the same mass with its value $m_{V0} = 708$ MeV at $x = 0$ phase. On the other hand, however, the S and P diquarks are not degenerate to $m_{S0} = 1119$ MeV at $x = 0$, and they have the mass difference with about 100 MeV. This is due to the contribution of the strange quark mass, confirmed by the m_{S1} term in Eqs. (5.28) and (5.29). In other words, the remaining $U(1)_A$ anomaly effect in the m_{S1} term disturbs its degeneration. Thus if the $U(1)_A$ symmetry also restores in $x = 0$ phase, these diquarks are degenerate with the chiral invariant mass $m_{S0} = 1119$ MeV. Note that, in this work, we assume to be intact about the $U(1)_A$ anomaly effect under the chiral symmetry restoration $x \to 0$.

5.2.2 Strong decays toward chiral restoration

Taking into account the relation between chiral condensation and non-strange diquark masses expressed as Eqs. (5.28) – (5.31), we then consider about the variation of $\Sigma_Q \to \Lambda_Q \pi$ decays under the chiral restoration. In this reaction, the masses of Λ_Q and Σ_Q baryons in the ground state change because of the constituent S and A diquarks. Besides, not only diquark masses but also the coupling constants $G_{1,2}$ are in functions of parameter

x as

$$G_1 = g_1 + (x\frac{f_s}{f_\pi} + \frac{m_s}{g_s f_\pi})g_2, \quad G_2 = g_1 + xg_2. \tag{5.34}$$

Here we use the value of $g_{1,2}$ in Eq. (5.26) for each heavy quark sector, so that the coupling constant G_1 for $\Sigma_Q \to \Lambda_Q\pi$ decays becomes the spin averaged value at $x = 1$ phase as in Eq. (5.24). About this coupling constant G_1, its value increases with the transition to chiral symmetry restored phase $x \to 0$, since the constant g_2 is given to be negative as in Eq. (5.26). Therefore, the $\Sigma_Q \to \Lambda_Q\pi$ decay width proportional to the squared G_1 would slightly increase with only considering this coupling constant.

With the masses of S and A diquarks and the coupling constant G_1 dependent on the chiral condensation parameter x, we compute the variation of $\Sigma_Q \to \Lambda_Q\pi^\pm$ decay width in the function of x. In Figs. 5.4 and 5.5, the x dependence of Λ_Q and $\Sigma_Q^{(*)}$ baryon masses and the decay width of $\Sigma_Q \to \Lambda_Q\pi^\pm$ reactions are depicted within the range of $0.80 \leq x \leq 1.00$. From these figures, we can see that the Λ_Q becomes heavier while the Σ_Q^* becomes lighter, whose behaviors are the same as S and A diquark masses inside them. As a consequence, the mass differences between Λ_Q and Σ_Q^* become smaller, and finally become insufficient to emit one pion. In accordance with the change of these baryon masses, the decay widths monotonically decreases and finally vanishes before the partial chiral restoration at $x = 0.80$. The threshold of x where the strong decay becomes to be prohibited is estimated to be about 0.96, 0.86, 0.92, and 0.89 for each initial Σ_c, Σ_c^*, Σ_b, and Σ_b^* baryon state, respectively.

In this calculation, we have neglected the variation of pion mass, which also depends on the change of chiral symmetry breaking. According to Refs. [132–136], the mass of pion is on the rise with approach to the finite temperature and/or density, since the NG boson nature declines from light pions when the magnitude of spontaneous chiral symmetry breaking is suppressed by $x \to 0$. In this situation, the threshold of x where the $\Sigma_Q \to \Lambda_Q\pi^\pm$ decay stops may move nearer to $x = 1$ side, because baryons in initial and final states, Σ_Q and Λ_Q, need those sufficient mass difference to emit this heavy pion. However, Refs. [132, 135, 136] insist that there are no big change of pion mass when a temperature is lower than 200 MeV and a density is lower than the nuclear density, which corresponds to $0.7 \leq x \leq 1.0$ from the viewpoints of chiral condensation according to Refs. [28, 29, 130]. Therefore, the increase of pion mass is almost negligible in the range of $0.80 \leq x \leq 1.00$, so that the change of $\Sigma_Q \to \Lambda_Q\pi^\pm$ decay widths in Figs. 5.4 and 5.5 are good approximations.

This suppression of $\Sigma_Q \to \Lambda_Q\pi^\pm$ decay by the partial chiral restoration is possible to examine in an experimental way, because recent particle accelerators can make the high temperature enough to achieve in the chiral symmetry restored environment. According to Refs. [130, 137], the cross-over temperature is about 160 MeV and the VEV of chiral condensate $\langle\bar{q}q\rangle$ starts to decline around here, while most experiments can realize higher temperature [138] [*3]. If this theoretical implication is confirmed to be correct experimentally, we can estimate that the masses of non-strange S and A diquarks inside those baryons are getting closer with the chiral symmetry restoration.

[*3] The highest recorded man-made temperature is about 5.5 trillion degrees Celsius (9.9 trillion degrees Fahrenheit), and is about 500 MeV. This temperature was achieved at CERN's Large Hadron Collider (LHC) in 2012.

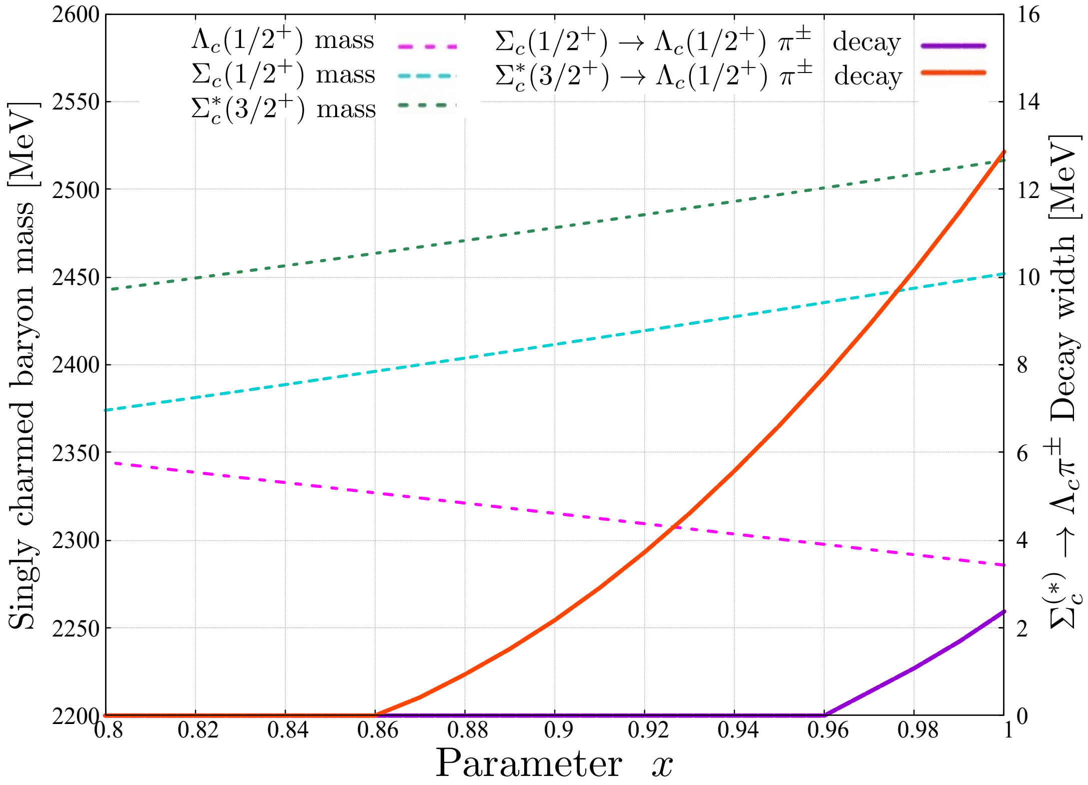

Figure5.4 Dependence of the singly charmed baryon masses and decay width of $\Sigma_c^{(*)} \to \Lambda_c\pi^\pm$ on the chiral condensation parameter x in the range of $0.80 \le x \le 1.00$.

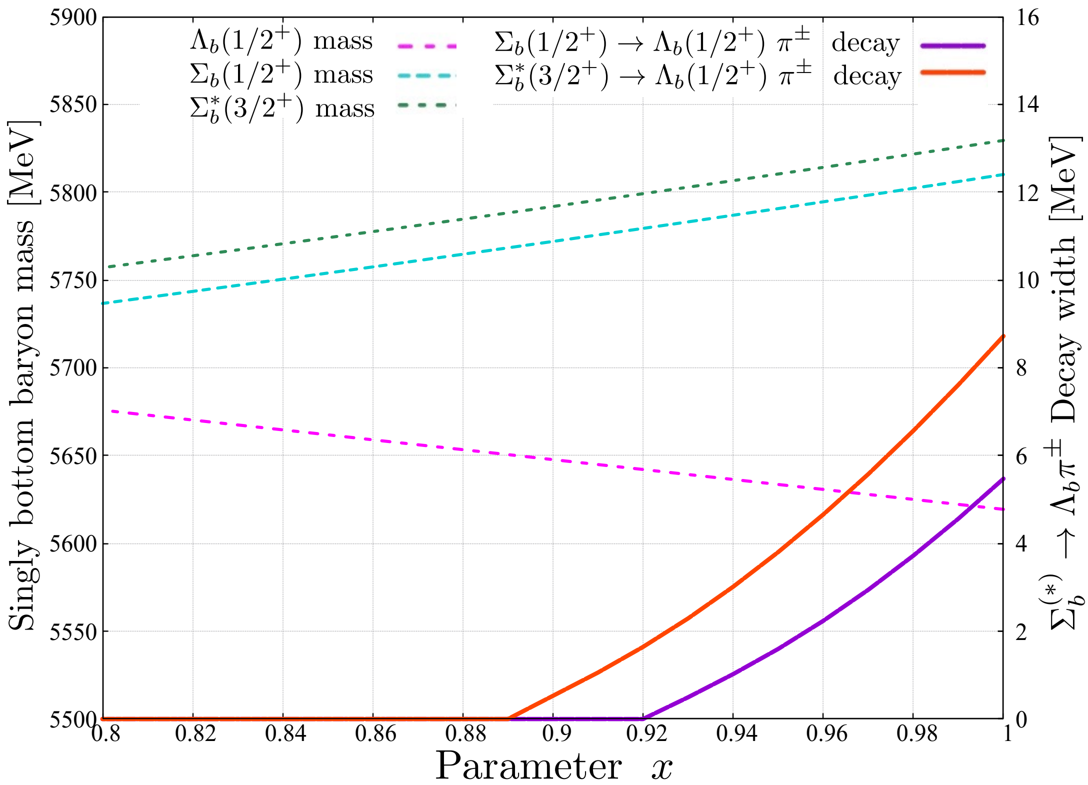

Figure5.5 Dependence of the singly bottom baryon masses and decay width of $\Sigma_b^{(*)} \to \Lambda_c\pi^\pm$ on the chiral condensation parameter x in the range of $0.80 \le x \le 1.00$.

Chapter 6

T_{QQ} tetraquarks with diquark picture

In this chapter, apart from the research of singly heavy baryons, we investigate about the T_{QQ} tetraquark bound states introduced in chapter 1 with employing diquarks and diquark–heavy-quark potentials established in previous chapters. As described in Fig. 1.9, T_{QQ} tetraquarks can be considered as the three body system including two heavy quarks and one anti-diquark. Therefore, we can compute those masses by GEM for three body calculation [118, 119] as explained in the last section of chapter 3.

Before the calculation, we start from the introduction of T_{QQ} tetraquarks with broadly speaking of the history of exotic hadrons. Since the quark model was established [7–9], QCD have been developed as the theory of strong interaction between quarks meditated by gluons. In ordinary, quarks and anti-quarks as building blocks of hadrons gather together with only the number of two or three. As in Fig. 1.1, these conventional hadrons are called as baryons with three-quark configuration and mesons with the quark-antiquark paired structure. However, QCD also allows some exotic color-singlet hadrons such as compact multiquark states, hadronic molecules, glueballs, and so on.

Tetraquarks are one of the group of exotic hadrons, which are composed of two quarks and two antiquarks as "$\bar{q}\bar{q}qq$". The candidates of tetraquarks are newly observed one after another from this century. In 2003, the first candidate of tetraquarks is observed by the Belle Collaboration [139], and is named as $X(3872)$. After this, another candidates of tetraquarks are also discovered as in Ref. [140, 141]. All of these tetraquarks are expected to have the "$c\bar{c}q\bar{q}$" composition, and are introduced such as the charmonium with resonance-like state and charged charmonium structure. Moreover, the LHCb collaboration have discovered many kinds of charmonium-like tetraquarks for the past decade [142], as described in Fig. 6.1. Starting from $X(3872)$, these $c\bar{c}q\bar{q}$ tetraquarks including the charmonium-like pair are also called "hidden-charmed tetraquark".

Recently, at the European Physical Society conference on High Energy Physics (EPS-HEP) in July 29, 2021, the LHCb Collaboration reported the discovery of new tetraquark called "T_{cc}^{+}" [143, 144]. About this tetraquark, values of the binding energy relative to $D^{*+}D^0$ two-meson threshold and the decay width were firstly determined as -273 ± 61 keV and 410 ± 165 keV with the Breit-Wigner profile [143], and are updated as -361 ± 40 keV and 47.8 ± 1.9 keV with the unitarized Breit-Wigner profile [144], respectively. For another, the quantum numbers of T_{cc}^{+} such as the isospin, total spin, and parity are assumed to be $I(J^P) = 0(1^+)$. The most characteristic point of this discovered T_{cc}^{+} tetraquark is that they are composed of two charm quarks and two light anti-quarks as "$cc\bar{q}\bar{q}$" composition, which is different from the hidden-charmed tetraquark as ever observed. Hence this is the first discovery of a doubly "open-charmed" tetraquark.

On the theoretical points of view related to the T_{cc}^{+}, the early studies of exotic hadrons including two heavy quarks as "$QQ\bar{q}\bar{q}$" have been started in the 1980s [145–150]. Af-

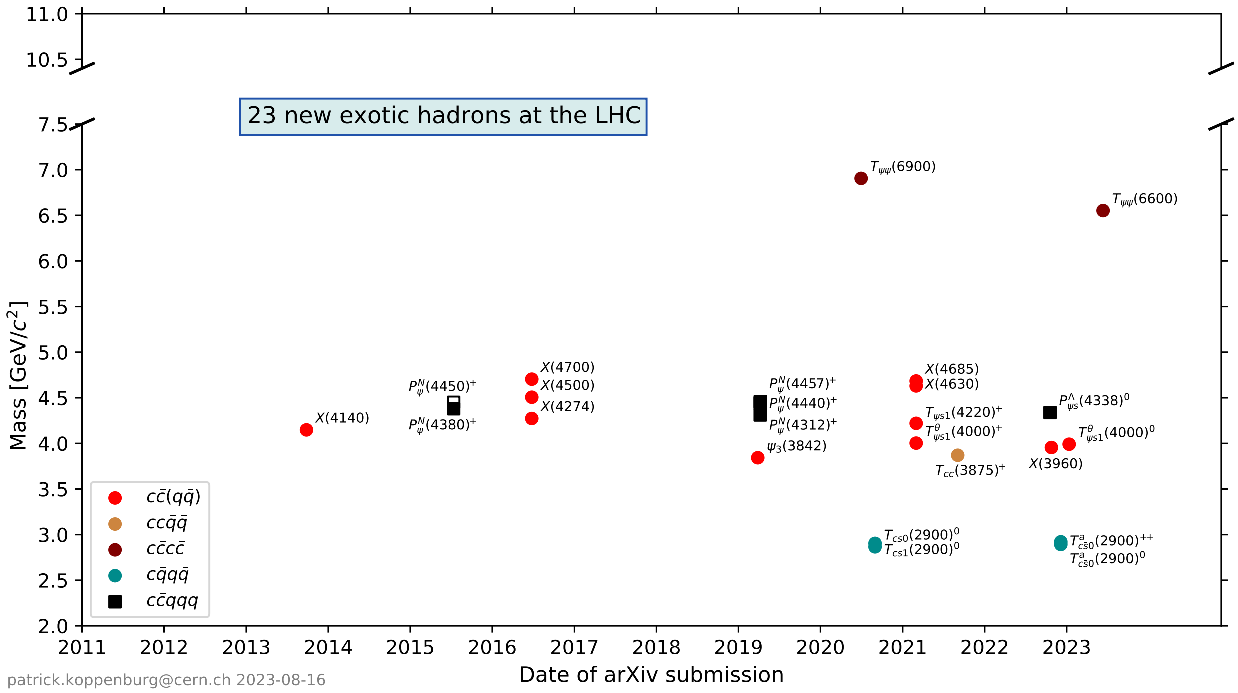

Figure6.1 Masses and discovery date of exotic hadrons observed at the LHC, quoted from Ref. [142].

ter these previous works, many researchers attempted to the study of doubly heavy T_{QQ} tetraquarks with many kinds of approaches, such as quark-level models [151–203], chromo-magnetic interaction models [204–213], QCD sum rules [214–233], lattice QCD simulations [234–253] and so on. To summarize conclusions of these theoretical researches, most of them predict the existence of the compact doubly bottom T_{bb} tetraquarks which do not bring about the strong decay reaction. This means that there are stable T_{bb} tetraquarks below the strong-decay threshold, such as the non-strange $T_{bb;\bar{u}\bar{d}}$ tetraquark below the BB^* two-meson threshold and the singly anti-strange $T_{bb;\bar{n}\bar{s}}$ tetraquark below the B_sB^* threshold. On the other hand, there are no doubly charmed T_{cc} tetraquarks with the compact structure which are predicted to be stable. For the bottom-charmed T_{cb} tetraquarks, those predictions are divided whether it is stable or not.

Exotic hadrons with multiquark configurations are often considered from the perspective of substructures such as mesons or diquarks. For the theoretical researches of T_{QQ} tetraquarks, there are two types of cluster: One is the system of hadronic molecule structure with two heavy-light mesons as "$(Q\bar{q}) - (Q\bar{q})$" [159, 163, 176, 191, 193, 236, 250]. The other type of system have diquarks as substructures, such as the interaction of a heavy-diquark and an anti-diquark as "$(QQ) - (\bar{q}\bar{q})$", or the three body system with a heavy-diquark cluster as "$(QQ) - \bar{q} - \bar{q}$" [167, 168, 175, 180, 199, 201, 205, 210, 250]. Although our method for T_{QQ} tetraquarks are similar to these diquark-like system, the unique point is that only two light anti-quarks are forming an anti-diquark substructure as "$Q - Q - (\bar{q}\bar{q})$".

To discuss these stable states of T_{QQ} tetraquarks, we only consider S or A anti-diquark as a component. This is because we only need to consider these tetraquarks in the lowest ground state. For the excited states of T_{QQ} tetraquarks with another constituent anti-diquark and/or quantum numbers, see Ref. [4]. Moreover, we neglect the color $\bar{\mathbf{6}}$ anti-diquarks which cannot define from our chiral diquark model in the present research.

6.1 Potential model

In order to calculate the mass of T_{QQ} tetraquarks including a color $\mathbf{3}$ anti-diquarks, we solve the Schrödinger equation for the Hamiltonian in Eq. (3.13), written as

$$H_T = \sum_{Q_1,Q_2,\bar{\mathcal{D}}} \left(M_k + \frac{\boldsymbol{p}_k^2}{2M_k} \right) - K_{\text{c.m.}} + V_{Q_1\bar{\mathcal{D}}}(r_1) + V_{Q_2\bar{\mathcal{D}}}(r_2) + V_{Q_1Q_2}(r_3).$$

Thus we need to define two types of potential models: One is about the interaction between two heavy quarks, $V_{Q_1Q_2}$, and the other one shows that between a heavy quark and a color $\mathbf{3}$ anti-diquark, $V_{Q_i\bar{\mathcal{D}}}$. For these potentials, we consider the strength of color-Coulomb interaction expressed as $(\boldsymbol{\lambda}_i \cdot \boldsymbol{\lambda}_j)$ by the Gell-Mann matrices. At first, about the $V_{Q_1Q_2}$ potential, two heavy quarks inside T_{QQ} tetraquarks takes the color $\bar{\mathbf{3}}$ representation in this work, so as to be color singlet with connection to a color $\mathbf{3}$ anti-diquark. At this time, the color strength with the color structure $\mathbf{3} \otimes \mathbf{3} = \bar{\mathbf{3}}$ is expressed as $(\boldsymbol{\lambda}_i^{(Q_1)} \cdot \boldsymbol{\lambda}_j^{(Q_2)}) = -8/3$. On the other hand, the mesons with quark–anti-quark pictures have the color structure $\mathbf{3} \otimes \mathbf{3} = \mathbf{1}$, so that its factor takes the value as $(\boldsymbol{\lambda}_i^{(Q_1)} \cdot \boldsymbol{\lambda}_j^{(\bar{Q}_2)}) = -16/3$. Therefore, these are summarized as

$$\begin{cases} (\boldsymbol{\lambda}_i^{(Q_1)} \cdot \boldsymbol{\lambda}_j^{(Q_2)}) = -8/3 & (Q - Q \text{ with color } \mathbf{3} \otimes \mathbf{3} = \bar{\mathbf{3}}) \\ (\boldsymbol{\lambda}_i^{(Q_1)} \cdot \boldsymbol{\lambda}_j^{(\bar{Q}_2)}) = -16/3 & (Q - \bar{Q} \text{ with color } \mathbf{3} \otimes \bar{\mathbf{3}} = \mathbf{1}) \end{cases}. \tag{6.1}$$

As the same, about the $V_{Q_i\bar{\mathcal{D}}}$ potential, the value of $(\boldsymbol{\lambda}_i \cdot \boldsymbol{\lambda}_j)$ for between a heavy quark and an color $\mathbf{3}$ anti-diquark takes $(\boldsymbol{\lambda}_i^{(Q_i)} \cdot \boldsymbol{\lambda}_j^{(\bar{\mathcal{D}})}) = -8/3$ with the total color $\bar{\mathbf{3}}$, while its factor for between a heavy quark and a diquark inside singly heavy baryons takes $(\boldsymbol{\lambda}_i^{(Q_i)} \cdot \boldsymbol{\lambda}_j^{(\mathcal{D})}) = -16/3$. Therefore, these are summarized as

$$\begin{cases} (\boldsymbol{\lambda}_i^{(Q_i)} \cdot \boldsymbol{\lambda}_j^{(\bar{\mathcal{D}})}) = -8/3 & (Q - \bar{\mathcal{D}} \text{ with color } \mathbf{3} \otimes \mathbf{3} = \bar{\mathbf{3}}) \\ (\boldsymbol{\lambda}_i^{(Q_i)} \cdot \boldsymbol{\lambda}_j^{(\mathcal{D})}) = -16/3 & (Q - \mathcal{D} \text{ with color } \mathbf{3} \otimes \bar{\mathbf{3}} = \mathbf{1}) \end{cases}. \tag{6.2}$$

From Eqs. (6.1) and (6.2), both the structure $\mathbf{3} \otimes \mathbf{3} = \bar{\mathbf{3}}$ and $\mathbf{3} \otimes \mathbf{3} = \mathbf{1}$ have attractive color-Coulomb interactions at the ratio $1 : 2$. As a consequence, if all potential terms such as the color-Coulomb potential and the color confinement potential are generalized to the form proportional to $(\boldsymbol{\lambda}_i \cdot \boldsymbol{\lambda}_j)$, we can define the relation of these potentials as

$$V_{Q_1Q_2}(r) = \frac{1}{2} V_{Q_1\bar{Q}_2}(r), \ \ V_{Q_i\bar{\mathcal{D}}}(r) = \frac{1}{2} V_{Q\mathcal{D}}(r). \tag{6.3}$$

Hence, we can make $V_{Q_1Q_2}$ and $V_{Q_i\bar{\mathcal{D}}}$ by halving the potential of heavy mesons with $Q\bar{Q}$ picture, $V_{Q_1\bar{Q}_2}$, and that of singly heavy baryons with diquark–heavy-quark picture, $V_{Q\mathcal{D}}$.

From Eq. (6.3), we then determine the potentials of heavy mesons and singly heavy baryons for potential terms in Eq. (3.13). About the diquark–heavy-quark potential for singly heavy baryons, we use the Y-potential which we have applied to calculate the energy spectrum and decay width of those baryons in previous chapters. However, since we only consider the ground states of T_{QQ} tetraquark, we neglect the spin-orbit term and tensor term as

$$V_{Q\mathcal{D}}(r) = -\frac{\alpha}{r} + \lambda r + C'_Q + (\boldsymbol{s}_{\mathcal{D}} \cdot \boldsymbol{s}_Q) \frac{\kappa_Q}{M_{\mathcal{D}} M_Q} \frac{\Lambda^2}{r} e^{-\Lambda r}. \tag{6.4}$$

Also, for the definition of potential $V_{Q_1\bar{Q}_2}$, we apply the model which is called "$AP1$" potential in Ref. [122]. This is expressed with the color-Coulomb term, confinement term, spin-spin term, and constant term as

$$V_{Q_1\bar{Q}_2}(r) = -\frac{\breve{\alpha}}{r} + \breve{\lambda} r^{2/3} + \breve{C} + (\boldsymbol{s}_{Q_1}\cdot\boldsymbol{s}_{\bar{Q}_2})\frac{8\breve{\kappa}}{3M_{Q_1}M_{\bar{Q}_2}\sqrt{\pi}}\frac{e^{-r^2/r_0^2}}{r_0^3} \left(r_0 = \breve{A}\left\{\frac{2M_{Q_1}M_{\bar{Q}_2}}{M_{Q_1}+M_{\bar{Q}_2}}\right\}^{-\breve{B}} \right). \tag{6.5}$$

The parameters in these potentials Eqs. (6.4) and (6.5) are summarized in the left side of Tables 6.1 and 6.2, respectively. For the masses of constituent quarks, we use those values from the $AP1$ potential in Ref. [122], which are summarized in Table 6.2. Therefore, about the Y-potential, we adjust the constant shift term to the new values $C'_{c,b}$ from $C_{c,b}$ in Tables 4.1 and 5.2, so as to apply the same heavy quark masses in $AP1$ potential. On the other hand, the right side of Tables 6.1 and 6.2 show the comparison of theoretical and experimental hadron masses. About Table 6.1, though the constant shift have changed from $C_{c,b}$ to $C'_{c,b}$, we can verify that the updated Y-potential for T_{QQ} tetraquarks also satisfies the baryon masses in the ground state. Moreover, the mass comparison in Table 6.2 indicates that the meson masses from $AP1$ potential are more accurate for doubly heavy mesons with $Q\bar{Q}$ configuration than the other singly heavy mesons with $Q\bar{q}$ picture. Therefore, this $AP1$ potential is proper to compute the interactions of two heavy quarks inside T_{QQ} tetraquarks.

As a summary, we can calculate the Schrödinger equation for the Hamiltonian Eq. (3.13) by the potentials in Eqs. (6.3), (6.4), and (6.5). Repeatedly speaking, We only use

Parameters (Y-pot.)		Masses (MeV)		
		Baryons	Y-pot.	(exp.) [12]
α	$60/\mu$	Λ_c $(1/2^+)$	2284	2286.46
λ (GeV^2)	0.165	Σ_c $(1/2^+)$	2451	2453.54
C'_c (GeV)	-0.900	Σ_c $(3/2^+)$	2513	2518.13
C'_b (GeV)	-0.913	Ξ_c $(1/2^+)$	2467	2469.42
κ_c	0.8586	Ξ'_c $(1/2^+)$	2581	2578.80
κ_b	0.6635	Ξ'_c $(3/2^+)$	2639	2645.88
Λ (GeV)	0.691	Ω_c $(1/2^+)$	2699	2695.20
		Ω_c $(3/2^+)$	2752	2765.90
		Λ_b $(1/2^+)$	5619	5619.60
		Σ_b $(1/2^+)$	5810	5813.10
		Σ_b $(3/2^+)$	5829	5832.53
		Ξ_b $(1/2^+)$	5796	5794.45
		Ξ'_b $(1/2^+)$	5934	5935.02
		Ξ'_b $(3/2^+)$	5952	5953.82
		Ω_b $(1/2^+)$	6046	6046.10
		Ω_b $(3/2^+)$	6063	...

Table6.1 Parameters of the Y-potential in Eq. (6.4), and the calculated masses of ground-state singly heavy baryons compared with the experimental values in Ref. [12]. For the parameters, μ in the parameter α is the reduced mass of two interacting particles, and the value of $C_{c,b}$ are tuned from those in Tables 4.1 and 5.2. For the quark and S, A diquark masses, we use the value summarized in Tables 4.2 and 6.2.

Parameters ($AP1$)		Masses (MeV)		
		Mesons	$AP1$ [122]	(exp.) [12]
$\breve{\alpha}$	0.4242	$D(0^-)$	1881	1868.04
$\breve{\lambda}$ (GeV$^{5/3}$)	0.3898	$D^*(1^-)$	2033	2009.12
$\breve{C}$ (GeV)	-1.1313	$D_s(0^-)$	1955	1968.34
$\breve{\kappa}$	1.8025	$D_s^*(1^-)$	2107	2112.20
$\breve{A}$ (GeV$^{\breve{B}-1}$)	1.5296	$B(0^-)$	5311	5279.44
$\breve{B}$	0.3263	$B^*(1^-)$	5367	5324.70
M_n (GeV)	0.277	$B_s(0^-)$	5356	5366.88
M_s (GeV)	0.553	$B_s^*(1^-)$	5418	5415.40
M_c (GeV)	1.819	$\eta_c(0^-)$	2982	2983.90
M_b (GeV)	5.206	$J/\psi(1^-)$	3103	3096.90
		$B_c(0^-)$	6269	6274.90
		$\eta_b(0^-)$	9401	9398.70
		$\Upsilon(1^-)$	9461	9460.30

Table6.2 Parameters and quark masses of the $AP1$ potential in Eq. (6.5), and the calculated masses of ground-state heavy mesons compared with the experimental values in Ref. [12].

S or A anti-diquark with color **3**, whose masses are summarized in Table 4.2 and we use those values given by Y-potential. We then compute the lightest T_{QQ} tetraquark masses $M_{T_{QQ}}$ for each quark component, and compare with those lowest strong-decay threshold $M_{\rm th}$ to give those binding energies defined as $M_{T_{QQ}} - M_{\rm th}$.

Furthermore, we explain the partial spin by two heavy quarks inside a T_{QQ} tetraquark, s_{QQ}. For T_{cc} and T_{bb} tetraquarks in the lowest ground state, the quantum number s_{cc} and s_{bb} is restricted to $s_{cc} = s_{bb} = 1$ because of the Pauli principle between two same heavy quarks. However, for T_{cb} tetraquarks, there are no restrict by the Pauli principle, so that the quantum number s_{cb} can take both 0 and 1. Hence, we consider two types of T_{cb} tetraquarks with different partial spins, $s_{cb} = 0$ and 1.

6.2 Existence and structure of T_{QQ} tetraquark bound states

In this section, we show the computed masses of T_{QQ} tetraquark ground states based on each meson-meson threshold. The stability of T_{QQ} tetraquarks against strong decays are also discussed by comparing with other previous researches based on various theoretical methods. Moreover, for the bound states of T_{QQ} tetraquarks in our research, we also calculate the root-mean-square (RMS) distances between two constituent particles from those density distributions, and predict the structures of those tetraquark bound states.

At first, we show the binding energies of the lowest states for each T_{QQ} tetraquark, as summarized in Table 6.3. About the states of tetraquarks, we can find that the lowest-lying T_{QQ} tetraquarks with strangeness $S = 0$ or $+1$ have a S anti-diquark, since S diquarks are lighter than A diquarks as Table 4.2 and it also affects to T_{QQ} tetraquark masses. However, the $T_{QQ;\bar{s}\bar{s}}$ tetraquarks including two strange anti-quarks have an A anti-diquark for those constituents, because there are no S diquark with two s quarks.

About the numerical results of binding energies represented in the right side of Table 6.3, we can find the stable states for non-strange and singly anti-strange T_{bb} tetraquarks, whose values of binding energies are negative and are written as boldface characters. For both two types of thresholds, the $T_{bb;\bar{u}\bar{d}}$ tetraquark ground state is below the $B - B^*$ threshold

Tetraquark	Anti-diquark	State		Threshold	Binding energy (MeV)	
$T_{QQ;\bar{q}\bar{q}}$	$\bar{\mathcal{D}}$	$[s_{QQ}]$	$I(J^P)$	$M-M$	type-exp	type-AP1
$T_{bb;\bar{u}\bar{d}}$	$\bar{\text{S}}$	[1]	$0(1^+)$	$B-B^*$	**−115**	**−189**
$T_{bb;\bar{n}\bar{s}}$	$\bar{\text{S}}$	[1]	$1/2(1^+)$	B_s-B^*	**−28**	**−59**
$T_{bb;\bar{s}\bar{s}}$	$\bar{\text{A}}$	[1]	$0(0^+)$	B_s-B_s	180	203
$T_{cc;\bar{u}\bar{d}}$	$\bar{\text{S}}$	[1]	$0(1^+)$	$D-D^*$	86	47
$T_{cc;\bar{n}\bar{s}}$	$\bar{\text{S}}$	[1]	$1/2(1^+)$	D_s-D^*	166	153
$T_{cc;\bar{s}\bar{s}}$	$\bar{\text{A}}$	[1]	$0(0^+)$	D_s-D_s	439	466
$T_{cb;\bar{u}\bar{d}}$	$\bar{\text{S}}$	[0]	$0(0^+)$	$D-B$	81	32
$T_{cb;\bar{n}\bar{s}}$	$\bar{\text{S}}$	[0]	$1/2(0^+)$	$D-B_s$	170	165
$T_{cb;\bar{s}\bar{s}}$	$\bar{\text{A}}$	[0]	$0(1^+)$	$D_s-B_s^*$	281	292
$T_{cb;\bar{u}\bar{d}}$	$\bar{\text{S}}$	[1]	$0(1^+)$	$D-B^*$	56	**−3**
$T_{cb;\bar{n}\bar{s}}$	$\bar{\text{S}}$	[1]	$1/2(1^+)$	$D-B_s^*$	143	124
$T_{cb;\bar{s}\bar{s}}$	$\bar{\text{A}}$	[1]	$0(0^+)$	D_s-B_s	335	360

Table6.3 The binding energies of the ground states of T_{QQ} tetraquarks with constituent S or A light anti-diquark clusters. The values of thresholds are based on two types, as "type-exp" from the experimental masses of mesons in Ref. [12], and as "type-AP1" from the theoretical masses of mesons given by the $AP1$ potential in Table 6.2.

more than 100 MeV, so that it is more stabler than the $T_{bb;\bar{n}\bar{s}}$ tetraquark ground state whose binding energy is around −50 MeV. For the other, the non-strange T_{cb} tetraquarks with its partial spin $s_{cb}=1$ is the bound state with the trifle binding energy −3 MeV. However, this result is in the basis of $D-B^*$ threshold with type-AP1, and it is not the bound state based on type-exp. Hence it is insufficient from our work to determine whether this $T_{cb;\bar{u}\bar{d}}$ tetraquark ground state is stable or not.

Unlike the experimental data in Refs. [143, 144], there are no bound state for T_{cc} tetraquarks in Table 6.3. Although it seems to be a contradiction, this implies that the observed T_{cc}^+ tetraquark is in the construction of D^0-D^{*+} meson molecule-like structure, which can be also inferred by its little binding energy with only about 300 keV. Therefore, the T_{cc} tetraquark ground states calculated with our anti-diquark picture is much different from this experimentally discovered T_{cc}^+, since an anti-diquark configuration is far apart from the $D-D^*$ molecule states. This indicates that T_{QQ} tetraquarks with an anti-diquark cluster in Table 6.3 are all irrelevant to the molecule-like T_{QQ}, and they are near to the compact states with quarks and anti-quarks. As a summary, our result shows that some T_{bb} tetraquarks are stable with compact quark and anti-diquark states, but T_{cc} and T_{cb} are mostly not.

For the comparison with other theoretical researches, we introduce the list which represents the stability of low-lying T_{QQ} tetraquark states from some other previous works. Those results are shown in Table 6.5, in which most references indicate the existence of stable state for non-strange $T_{bb;\bar{u}\bar{d}}$ tetraquark, and also for singly anti-strange $T_{bb;\bar{n}\bar{s}}$ tetraquark secondly. For the other tetraquarks with strangeness $S=0$ or $+1$, there are various results and those existence of stable states cannot be determined obviously. For doubly anti-strange tetraquarks $T_{QQ;\bar{s}\bar{s}}$, we can find them to be unstable for the most part.

Finding the existence of stable T_{bb} tetrquark with strangeness $S=0$ and $+1$, and also the stable non-strange T_{cb} tetraquark with $s_{cb}=1$ based on type-AP1 threshold, we then discuss those structures from the density distribution between two constituent particles.

This two-body density distribution is given by the wave function appear by the three-body calculation, expressed as

$$\begin{aligned}\Psi_{JM}(\boldsymbol{r}_c, \boldsymbol{R}_c) = &\sum_c \sum_\beta C_{c,\beta} \\ &\times \left[[\tilde{\phi}^{(c)}_{\nu l}(\boldsymbol{r}_c)\tilde{\psi}^{(c)}_{NL}(\boldsymbol{R}_c)]_\Lambda \otimes \left[[\chi_{1/2}(Q_1)\chi_{1/2}(Q_2)]_{s_{QQ}}\chi_{s_{\bar{\mathcal{D}}}}(\bar{\mathcal{D}})\right]_{s_{QQ\bar{\mathcal{D}}}}\right]_{JM}.\end{aligned} \tag{6.6}$$

Here $\chi_{1/2}$ and $\chi_{s_{\bar{\mathcal{D}}}}$ stand for the spin term of a heavy quark and an anti-diquark in this wave function, respectively. The index β denotes the assembly of quantum numbers which associates to this expression, shown as $\beta = \{\nu, N, l, L, \Lambda, s_{QQ}, s_{QQ\bar{\mathcal{D}}}\}$. The index c denotes the channel number of Jacobi coordinates described in Fig. 3.2. In the wave function, $\boldsymbol{r}_c$ stands for the relative coordinates between two particles in each channel, so that the two-body density distribution is given by

$$\rho(r_c) = \int d\hat{\boldsymbol{r}}_c d\boldsymbol{R}_c |\Psi_{JM}(\boldsymbol{r}_c, \boldsymbol{R}_c)|^2, \tag{6.7}$$

where $r_c = |\boldsymbol{r}_c|$ and $\hat{\boldsymbol{r}}_c$ denote the distance and the angular parts of coordinate $\boldsymbol{r}_c$, respectively. Therefore, we can draw the density distribution between two heavy quarks with channel $c = 3$, and that between a heavy quark and an anti-diquark with channel $c = 1, 2$.

In Figs. 6.2 and 6.3, the density distributions between two constituent particles inside stable tetraquarks are depicted in the form of functions $r^2\rho(r)$. In detail, Fig. 6.2 represents for both non-strange and singly anti-strange T_{bb} tetraquarks, and Fig. 6.3 is for the T_{cb} tetraquark with $s_{QQ} = 1$. From Fig. 6.2, we can see that two bottom quarks $(b - b)$ are nearer than between a bottom quark and an anti-diquark $(b - \bar{\mathcal{D}})$ for both T_{bb} tetraquarks with strangeness $S = 0$ and $+1$. Also, for the density distribution between the $b - \bar{\mathcal{D}}$ pair, its distance of non-strange T_{bb} tetraquark seems to be broader than that of singly anti-strange one. These results come from the suppression of the kinetic energy which is inversely proportional to the reduced mass of two interacting particles, so that its effect decreases by the increase of two particles masses. Same influence of this kinetic energy is confirmed for the density distribution of stable T_{cb} tetraquark in Fig. 6.3, where two interacting particles are approaching by the increase of their masses.

For the distance of two constituent particles, we also calculate the RMS distances from each density distribution $\rho(r)$, given by

$$\sqrt{\langle r_c^2 \rangle} = \sqrt{\left(\int r_c^2 \rho(r_c) r_c^2 dr_c\right) / \left(\int \rho(r_c) r_c^2 dr_c\right)}. \tag{6.8}$$

These numerical results for stable tetraquarks are summarized in Table 6.4. As we predicted from density distributions in Figs. 6.2 and 6.3, the distance of two particles becomes nearer as those masses become heavier. In particular, about the non-strange $T_{bb;\bar{u}\bar{d}}$ and $T_{cb;\bar{u}\bar{d}}$ tetraquarks, we can compare those RMS distances between two heavy quarks $(Q_1 - Q_2)$ with other theoretical results in Refs. [179] and [183] which are given by the four body calculations with quark model. In each previous work, the distance between two bottom quarks inside the $T_{bb;\bar{u}\bar{d}}$ tetraquark bound state is given by 0.285 fm in Ref. [179] and 0.34 fm in Ref. [183], in which our result is 0.30 fm and is between these values. Also, about the distance between a charm quark and a bottom quark inside the low-lying $T_{cb;\bar{u}\bar{d}}$ tetraquark state, it is calculated as 0.357 fm and 0.65 fm in Refs. [179] and [183], respectively, so that our result 0.41 fm is in between these results. However, we note that

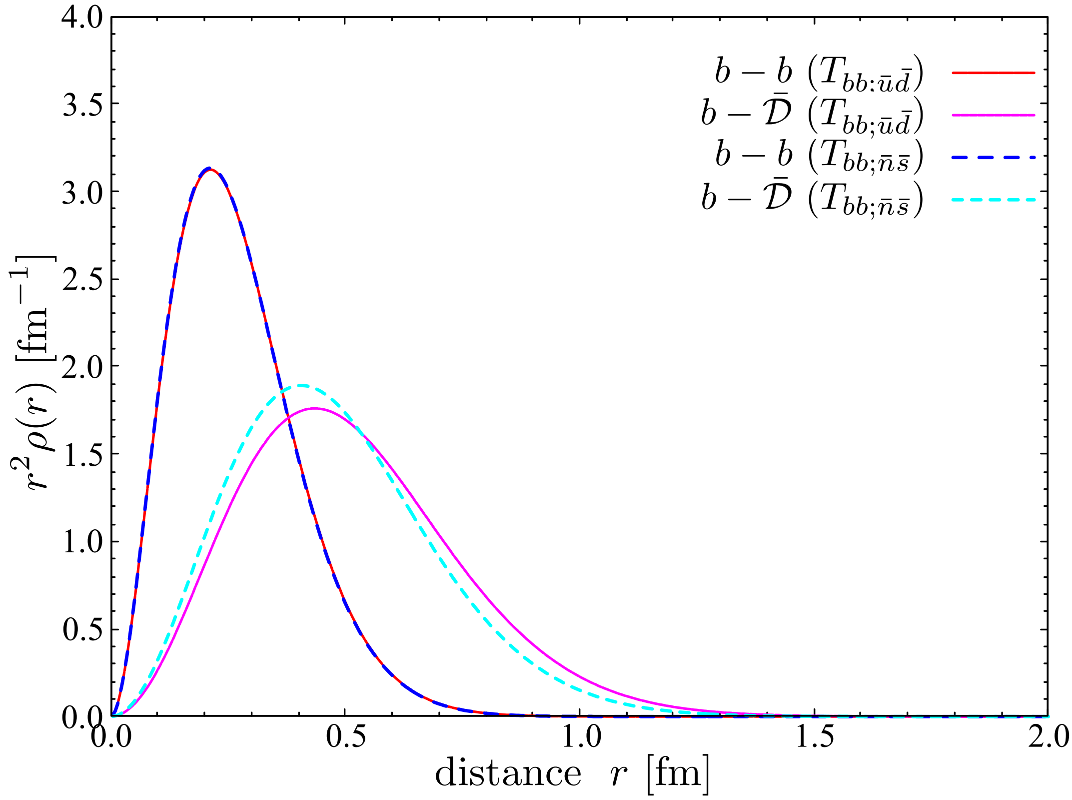

Figure6.2 Density distribution between two bottom quarks ($b-b$) and between a bottom quark and an anti-diquark ($b-\bar{\mathcal{D}}$) inside the stable T_{bb} tetraquarks. The solid lines and dashed lines are for the strangeness $S=0$ and $+1$ tetraquarks, respectively.

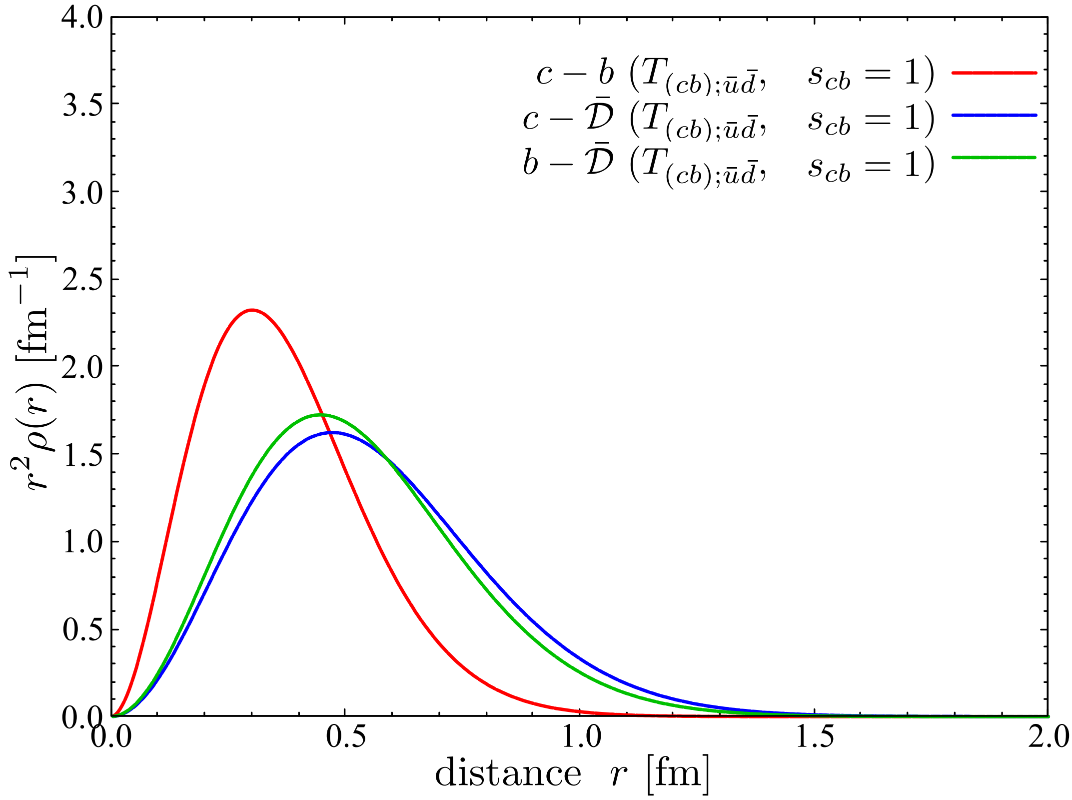

Figure6.3 Density distribution between a charm and a bottom quarks ($c-b$) and between a heavy quark and an anti-diquark ($c-\bar{\mathcal{D}}$, $b-\bar{\mathcal{D}}$) inside the low-lying non-strange T_{cb} tetraquark with $s_{cb}=1$, which is stable in the basis of type-AP1 threshold.

Tetraquark	State		RMS distances $\sqrt{\langle r^2 \rangle}$ (fm)		
$T_{Q_1Q_2;\bar{q}\bar{q}}$	$[s_{QQ}]$	$I(J^P)$	$Q_1 - Q_2$	$Q_1 - \bar{\mathcal{D}}$	$Q_2 - \bar{\mathcal{D}}$
$T_{bb;\bar{u}\bar{d}}$	[1]	$0(1^+)$	0.30	0.56	0.56
$T_{bb;\bar{n}\bar{s}}$	[1]	$1/2(1^+)$	0.30	0.53	0.53
$T_{cb;\bar{u}\bar{d}}$	[1]	$0(1^+)$	0.41	0.61	0.58

Table6.4 RMS distances of the T_{QQ} tetraquarks having negative binding energies.

the state of lowest $T_{cb;\bar{u}\bar{d}}$ tetraquark in Ref. [179] is not the bound state and its spin-parity state is $I(J^P) = 0(0^+)$, which is different from ours and Ref. [183]. Moreover, the RMS distance between two bottom quarks in the singly anti-strange $T_{bb;\bar{n}\bar{s}}$ tetraquark can be compared with the result in Ref. [179], though its tetraquark is not a bound state according to this previous work. Its numerical result is given by 0.284 fm, which is similar to our calculated value 0.30 fm. Furthermore, we can find from our work and Ref. [179] that the RMS distance between two bottom quarks inside the lowest states of non-strange and singly anti-strange doubly bottom tetraquarks, $T_{bb;\bar{u}\bar{d}}$ and $T_{bb;\bar{n}\bar{s}}$, are not much different.

Reference	T_{cc}			T_{bb}			T_{cb}		
(Constituent light anti-quarks)	$\bar{u}\bar{d}$	$\bar{n}\bar{s}$	$\bar{s}\bar{s}$	$\bar{u}\bar{d}$	$\bar{n}\bar{s}$	$\bar{s}\bar{s}$	$\bar{u}\bar{d}$	$\bar{n}\bar{s}$	$\bar{s}\bar{s}$
Quark-level models									
Lipkin (1986) [147]	ND			S					
ZouZou et al. (1986) [148]	S			S			S		
Carlson-Heller-Tjon (1988) [150]	S			S			ND		
Semay–Silvestre-Brac (1994) [152]	ND			S	S		ND		
Pepin et al. (1997) [155]	S			S					
Janc-Rosina (2004) [159]	S			S					
Ebert et al. (2007) [161]	US	US	US	S	US	US	US	US	US
Zhang-Zhang-Zhang (2008) [162]	US		US	S		US			
Vijande-Valcarce-Barnea (2009) [163]	S			S					
Yang et al. (2009) [164]	ND			S					
Feng-Guo-Zou (2013) [165]	S			S			S		
Karliner-Rosner (2017) [166]	US			S			ND		
Eichten-Quigg (2017) [167]	US	US	US	S	S	US	US	US	US
Park-Noh-Lee (2019) [170]	US			S	S		US		
Deng-Chen-Ping (2020) [171]	S	US	US	S	S	US	S	US	US
Yang-Ping-Segovia (2020a) [174]	S			S			S		
Tan-Lu-Ping (2020) [178]	S			S			S		
Lü-Chen-Dong (2020) [179]	US	US	US	S	US	US	US	US	US
Braaten-He-Mohapatra (2021) [180]	US	US	US	S	S	US	US	US	US
Yang-Ping-Segovia (2020b) [181]			US			US			US
Meng et al. (2021) [183, 198, 203]	S			S	S		S		
(This work) (2022) [4]	US	US	US	S	S	US	ND	US	US
Chen et al. (2022) [194]		S	US		S	US		US	US
Praszalowicz (2022) [196]	US	US		S	S				
Wu-Ma (2022) [199]	ND			S					
Song-Jia (2023) [201]	US	US	US	S	US	US	US	US	US
Chromo-magnetic interaction models									
Lee-Yasui (2009) [205]	S	S		S	S		S	US	
Luo et al. (2017) [207]	S	S	US	S	S	US	S	S	US
Cheng et al. (2020) [209]							ND	US	
Cheng et al. (2021) [210]	US	US	US	S	S	US	ND	US	US
Weng-Deng-Zhu (2022) [211]	S	ND	US	S	S	ND	S	ND	ND
Guo et al. (2022) [212]	S	S	US	S	S	ND	S	S	US
Liu-Zhang-Jia (2023) [213]	US			S			S		
QCD sum rules									
Navarra-Nielsen-Lee (2007) [214]	ND			S					
Du et al. (2013) [216]		US	US	S	S	S			
Chen-Steele-Zhu (2014) [217]							ND		S
Wang (2018) [218]	ND	ND		S	S				
Wang-Yan (2018) [219]	ND	ND	ND						
Agaev et al. (2019) [220]				S					
Agaev-Azizi-Sundu (2020) [222]							ND		
Agaev et al. (2020, 2021) [224, 227]					S				
Wang-Chen (2020) [226]								S	
Lattice QCD									
Francis et al. (2017) [242]				S	S				
Francis et al. (2019) [245]				S	S		S		
Junnarkar-Mathur-Padmanath (2019) [246]	S	S	US	S	S	ND			
Leskovec et al. (2019) [247]				S					
Hudspith et al. (2020) [248]				S	S		US	S	
Mohanta-Basak (2020) [249]				S					
Padmanath-Radhakrishnan-Mathur (2023) [253]							S		

Table6.5 The stability list of doubly heavy tetraquarks from other theoretical studies. The symbols "S", "US", and "ND" stand for "stable" (below the threshold), "unstable" (above the threshold), and "not determined" (not conclusive within theoretical uncertainties), respectively. Similar summary is shown in Ref. [210].

Chapter 7

Summary

In this present research, we have mainly studied about the chiral effective model of diquarks, where diquarks in this model are composed of two light quarks such as up (u), down (d), and strange (s). Chiral effective model is a significant way to explain the spontaneous chiral symmetry breaking, which is caused by the chiral condensation and induce the dynamical generation of light quark masses. Also, some chiral effective model can represent the mechanism of chiral symmetry restoration with approach to the environment with high temperature and/or high density. On the other hand, diquarks are often applied to the building blocks of hadrons since the quark model has been proposed. Diquarks are also expected to come out in the color superconducting phase in forms of diquark condensates. Hence, diquarks are the important subject in a wide field of physics.

For the chiral effective model of diquarks, we have applied the $SU(3)$ linear sigma model [112–114]. Three types of chiral effective Lagrangians are discussed in this work: The first Lagrangian $\mathcal{L}_S$ is for spin 0, scalar (S) and pseudoscalar (P) diquarks with color $\bar{\mathbf{3}}$, which is previously created in Ref. [87]. The next one $\mathcal{L}_V$ is for vector (V) and axial-vector (A) diquarks which have the color $\bar{\mathbf{3}}$ and spin 1. Lastly, the effective Lagrangian $\mathcal{L}_{S-V}$ is considered for the interaction between these spin 0 and 1 diquarks. In the effective Lagrangians $\mathcal{L}_S$ and $\mathcal{L}_V$, the dynamical generation of diquark masses from the chiral symmetry breaking is represented by the finite VEV of scalar meson field. In particular, the Lagrangian for spin 0 diquarks $\mathcal{L}_S$ derived the reversed mass relation between non-strange and singly strange P diquarks, and the Lagrangian for spin 1 diquarks $\mathcal{L}_V$ derived the generalized Gell-Mann–Okubo mass formula for A diquarks [116, 117]. On the other hand, the effective Lagrangian $\mathcal{L}_{S-V}$ expressed the interaction between two diquarks with different spins meditated by mesons.

Singly heavy baryons, including one heavy quark such as charm (c) and bottom (b), are expected to form a diquark picture with the remained two light quarks. Assuming those baryons as the diquark–heavy-quark two body systems, we have applied them to give parameters in the chiral effective Lagrangians with using GEM [118, 119] as the method of two body calculation. Quoting the numerical results for some singly heavy baryons from other references such as experimental values [12] and quark model calculation [121], we have numerically derived the parameters in effective Lagrangians, and also the effective diquark masses and the coupling constants related to the energy spectra and the strong decays of singly heavy baryons.

After the forms and parameters in these chiral effective Lagrangians are determined, we have applied the chiral effective model of diquarks with diquark–heavy-quark two body calculation, so as to analyze the singly heavy baryons from the perspective of those energy spectra and strong decays. The theoretical results of mass spectra represented the prediction of non-observed mass data, and there were various features appearing from our chiral effective model of diquarks. Also, the chiral effective model of diquarks induced the interesting prediction between the one pion emission decays of singly heavy baryons and the environmental change from the viewpoints of chiral condensation.

For the additional research, we have investigated about the doubly heavy T_{QQ} tetraquarks with the diquark cluster, which can be regarded as three body systems composed of two heavy quarks and one anti-diquark. Applying the diquark–heavy-quark potential model constructed for the singly heavy baryons with diquark–heavy-quark systems, we have computed the masses of T_{QQ} tetraquarks with using GEM for the three body calculation. Although the given results of those tetraquark bound states were different from the recently observed T_{cc}^{+} tetraquark [143, 144] due to the different hadronic structures, we have found the non-strange and singly anti-strange T_{bb} tetraquark bound states which are stable against strong decays. Similar results are also predicted in previous theoretical researches with various approaches. For more works about the T_{QQ} tetraquarks which are stable or uncertain, we have given those structures from the density distribution between two constituent particles.

The contents in this dissertation are summarized in Refs. [1–4]. In detail, Ref. [1] shows the research about the spectrum of Λ_Q and Ξ_Q baryons, which applies the chiral effective model of S and P diquarks in Ref. [87]. Likewise, Ref. [2] describes the spectrum of singly heavy baryons, developed by the additional V and A diquarks in the chiral effective model and also by the updated diquark–heavy-quark potential model. On the other hand, Ref. [3] is about the strong decays of singly heavy baryons from the perspective of chiral effective diquark model, and Ref. [4] explains the T_{QQ} tetraquarks with an anti-diquark picture.

Acknowledgements

First of all, I, Yonghee Kim, would like to express my sincere gratitude to my supervisors during my graduate school life: Prof. Emiko Hiyama, Prof. Yoichi Ikeda, and Prof. Kazuyuki Ogata. They gave me a lot of valuable comments and led me to think various possibilities for future works through many discussions. Without their guidance, this dissertation would not have been formed. Moreover, I am deeply grateful to Prof. Hiroshi Suzuki for valuable discussions and various objective opinions about this thesis.

As the same, I would like to express my heartfelt gratitude to many of my co-researchers. In particular, Prof. Makoto Oka in JAEA and RIKEN taught me not only the basics of QCD and hadron physics, but also many kinds of courses and strategies of researches related to this thesis. Also, Dr. Kei Suzuki, Prof. Yan-Rui Liu, and Dr. Daiki Suenaga gave me a lot of advices and knowledges through many collaborations and discussions for these researches. Their attitude toward many academic works will be a great support in all the way of my future.

Moreover, I would like to give thanks to all my fellows of the nuclear theory laboratory in Kyushu University. Through all my graduate school life, daily conversations with Dr. Shoya Ogawa gave me encouragements as well as the peace of mind. Many advices from Dr. Kohei Washiyama, Dr. Togashi Hajime, and Dr. Takehiro Hirakida was also helpful to me. Also, I would like to appreciate my former classmates during the master course, Mr. Ryosuke Miyamoto and Mr. Takumi Yamamoto, for their kind cooperation in the common study for each of our research. Moreover, many conversations with my younger grade members, Mr. Koki Sakaibara, Mr. Dongwook Lee, Mr. Yu Kitagawa, Mr. Reiji Matsukawa, Mr. Hibiki Nakada, and Mr. Hiroki Kida, were my delightful times. Had it not been for their kind supports, I could not have been in the same group because of loneliness, and could not keep the motivation for my researches.

Furthermore, I would like to express my hearty thanks to all the members in office of the department of physics, Kyushu University. I owe a lot of my procedures for this research to their assistance.

Finally, I would like to express my deepest appreciation to my family, especially my parents and younger sister, for supporting me all my life.

While all my responsibility, this dissertation was made with many supports by the great people around myself. I would like to express my thanks with all my heart to those people who gave me a lot of kind supports, guidance, and encouragements.

This work was supported by the Research Fellowship of the Japan Society for the Promotion of Science (JSPS) for Young Scientists with No. JP21J20048.

Bibliography

[1] Y. Kim, E. Hiyama, M. Oka, and K. Suzuki, Phys. Rev. D **102**, 014004 (2020), arXiv:2003.03525 [hep-ph] .
[2] Y. Kim, Y.-R. Liu, M. Oka, and K. Suzuki, Phys. Rev. D **104**, 054012 (2021), arXiv:2105.09087 [hep-ph] .
[3] Y. Kim, M. Oka, D. Suenaga, and K. Suzuki, Phys. Rev. D **107**, 074015 (2023), arXiv:2212.08338 [hep-ph] .
[4] Y. Kim, M. Oka, and K. Suzuki, Phys. Rev. D **105**, 074021 (2022), arXiv:2202.06520 [hep-ph] .
[5] E. Rutherford, Phil. Mag. Ser. 6 **21**, 669 (1911).
[6] J. Chadwick, Nature **129**, 312 (1932).
[7] M. Gell-Mann, Phys. Lett. **8**, 214 (1964).
[8] G. Zweig, "An SU(3) model for strong interaction symmetry and its breaking. Version 1," (1964), (See https://inspirehep.net/literature/11881).
[9] G. Zweig, "An SU(3) model for strong interaction symmetry and its breaking. Version 2," in *DEVELOPMENTS IN THE QUARK THEORY OF HADRONS. VOL. 1. 1964 - 1978*, edited by D. B. Lichtenberg and S. P. Rosen (1964) pp. 22–101, (See https://inspirehep.net/literature/4674).
[10] M. Y. Han and Y. Nambu, Phys. Rev. **139**, B1006 (1965).
[11] O. W. Greenberg, Phys. Rev. Lett. **13**, 598 (1964).
[12] R. L. Workman and Others (Particle Data Group), PTEP **2022**, 083C01 (2022 (and 2023 update)).
[13] D. J. Gross and F. Wilczek, Phys. Rev. Lett. **30**, 1343 (1973).
[14] H. D. Politzer, Phys. Rev. Lett. **30**, 1346 (1973).
[15] G. 't Hooft, Nucl. Phys. B **33**, 173 (1971).
[16] G. 't Hooft, Nucl. Phys. B **35**, 167 (1971).
[17] H. Meyer-Ortmanns, Rev. Mod. Phys. **68**, 473 (1996), arXiv:hep-lat/9608098 .
[18] A. V. Smilga, Phys. Rept. **291**, 1 (1997), arXiv:hep-ph/9612347 .
[19] D. H. Rischke, Prog. Part. Nucl. Phys. **52**, 197 (2004), arXiv:nucl-th/0305030 .
[20] K. Fukushima and T. Hatsuda, Rept. Prog. Phys. **74**, 014001 (2011), arXiv:1005.4814 [hep-ph] .
[21] K. Fukushima, J. Phys. G **39**, 013101 (2012), arXiv:1108.2939 [hep-ph] .
[22] K. Fukushima and C. Sasaki, Prog. Part. Nucl. Phys. **72**, 99 (2013), arXiv:1301.6377 [hep-ph] .
[23] M. G. Alford, A. Schmitt, K. Rajagopal, and T. Schäfer, Rev. Mod. Phys. **80**, 1455 (2008), arXiv:0709.4635 [hep-ph] .
[24] A. Manohar and H. Georgi, Nucl. Phys. B **234**, 189 (1984).
[25] D. K. Hong, Y. J. Sohn, and I. Zahed, Phys. Lett. B **596**, 191 (2004), arXiv:hep-ph/0403205 .
[26] C. DeTar and U. M. Heller, Eur. Phys. J. A **41**, 405 (2009), arXiv:0905.2949 [hep-lat] .
[27] W.-j. Fu, J. M. Pawlowski, and F. Rennecke, Phys. Rev. D **101**, 054032 (2020),

arXiv:1909.02991 [hep-ph] .
[28] T. Nishi *et al.* (piAF), Nature Phys. **19**, 788 (2023), arXiv:2204.05568 [nucl-ex] .
[29] K. Suzuki *et al.*, Phys. Rev. Lett. **92**, 072302 (2004), arXiv:nucl-ex/0211023 .
[30] Y. Nambu, Phys. Rev. Lett. **4**, 380 (1960).
[31] J. Goldstone, Nuovo Cim. **19**, 154 (1961).
[32] J. Goldstone, A. Salam, and S. Weinberg, Phys. Rev. **127**, 965 (1962).
[33] S. Weinberg, Phys. Rev. D **11**, 3583 (1975).
[34] Y. Kuroda, M. Harada, S. Matsuzaki, and D. Jido, PTEP **2020**, 053D02 (2020), arXiv:1910.09146 [hep-ph] .
[35] G. Aarts, Acta Phys. Polon. Supp. **16**, 1 (2023), arXiv:2210.06875 [hep-lat] .
[36] J. Kim and S. H. Lee, Phys. Rev. D **103**, L051501 (2021), arXiv:2012.06463 [nucl-th] .
[37] M. Harada and Y.-L. Ma, Phys. Rev. D **87**, 056007 (2013), arXiv:1212.5079 [hep-ph] .
[38] Y. Kawakami and M. Harada, Phys. Rev. D **97**, 114024 (2018), arXiv:1804.04872 [hep-ph] .
[39] Y. Kawakami and M. Harada, Phys. Rev. D **99**, 094016 (2019), arXiv:1902.06774 [hep-ph] .
[40] D. B. Lichtenberg, Phys. Rev. **178**, 2197 (1969).
[41] D. B. Lichtenberg, W. Namgung, E. Predazzi, and J. G. Wills, Phys. Rev. Lett. **48**, 1653 (1982).
[42] K. F. Liu and C. W. Wong, Phys. Rev. D **28**, 170 (1983).
[43] D. Ebert, R. N. Faustov, and V. O. Galkin, Phys. Lett. B **659**, 612 (2008), arXiv:0705.2957 [hep-ph] .
[44] E. Hernandez, J. Nieves, and J. M. Verde-Velasco, Phys. Lett. B **666**, 150 (2008), arXiv:0803.3672 [hep-ph] .
[45] H.-W. Ke, X.-Q. Li, and Z.-T. Wei, Phys. Rev. D **77**, 014020 (2008), arXiv:0710.1927 [hep-ph] .
[46] H.-W. Ke, X.-H. Yuan, X.-Q. Li, Z.-T. Wei, and Y.-X. Zhang, Phys. Rev. D **86**, 114005 (2012), arXiv:1207.3477 [hep-ph] .
[47] D. Jido and M. Sakashita, PTEP **2016**, 083D02 (2016), arXiv:1605.07339 [nucl-th] .
[48] K. Kumakawa and D. Jido, PTEP **2017**, 123D01 (2017), arXiv:1708.02012 [nucl-th] .
[49] K. Kumakawa and D. Jido, PTEP **2022**, 053D01 (2022), arXiv:2107.11950 [hep-ph] .
[50] R. L. Jaffe, Phys. Rev. D **15**, 267 (1977).
[51] D. Black, A. H. Fariborz, and J. Schechter, Phys. Rev. D **61**, 074001 (2000), arXiv:hep-ph/9907516 .
[52] L. Maiani, F. Piccinini, A. D. Polosa, and V. Riquer, Phys. Rev. Lett. **93**, 212002 (2004), arXiv:hep-ph/0407017 .
[53] S. Prelovsek, PoS **LATTICE2008**, 102 (2008), arXiv:0809.5134 [hep-lat] .
[54] G. 't Hooft, G. Isidori, L. Maiani, A. D. Polosa, and V. Riquer, Phys. Lett. B **662**, 424 (2008), arXiv:0801.2288 [hep-ph] .
[55] S. Prelovsek and D. Mohler, Phys. Rev. D **79**, 014503 (2009), arXiv:0810.1759 [hep-lat] .
[56] D. K. Hong and C.-j. Song, Int. J. Mod. Phys. A **27**, 1250051 (2012), arXiv:hep-ph/0407274 .
[57] T. Friedmann, Eur. Phys. J. C **73**, 2298 (2013), arXiv:0910.2229 [hep-ph] .
[58] R. L. Jaffe and F. Wilczek, Phys. Rev. Lett. **91**, 232003 (2003), arXiv:hep-

ph/0307341 .
[59] F. Wilczek, in *Deserfest: A Celebration of the Life and Works of Stanley Deser* (2004) pp. 322–338, arXiv:hep-ph/0409168 .
[60] R. L. Jaffe, Nucl. Phys. B Proc. Suppl. **142**, 343 (2005).
[61] M. Karliner and H. J. Lipkin, Phys. Lett. B **638**, 221 (2006), arXiv:hep-ph/0601193 .
[62] L. Maiani, A. D. Polosa, and V. Riquer, Phys. Lett. B **749**, 289 (2015), arXiv:1507.04980 [hep-ph] .
[63] R. F. Lebed, Phys. Lett. B **749**, 454 (2015), arXiv:1507.05867 [hep-ph] .
[64] R. F. Lebed, Phys. Rev. D **96**, 116003 (2017), arXiv:1709.06097 [hep-ph] .
[65] M. Y. Barabanov *et al.*, Prog. Part. Nucl. Phys. **116**, 103835 (2021), arXiv:2008.07630 [hep-ph] .
[66] U. Özdem and K. Azizi, Eur. Phys. J. A **58**, 171 (2022), arXiv:2202.11466 [hep-ph] .
[67] R.-R. Dong, N. Su, and H.-X. Chen, Eur. Phys. J. C **82**, 983 (2022), arXiv:2206.09517 [hep-ph] .
[68] R. F. Lebed and S. R. Martinez, Phys. Rev. D **106**, 074007 (2022), arXiv:2207.01101 [hep-ph] .
[69] L. Maiani and A. Pilloni (2022) arXiv:2207.05141 [hep-ph] .
[70] H. Mutuk, Phys. Lett. B **834**, 137404 (2022), arXiv:2208.11048 [hep-ph] .
[71] R. F. Lebed and S. R. Martinez, Phys. Rev. D **108**, 014013 (2023), arXiv:2305.09146 [hep-ph] .
[72] M. G. Alford, K. Rajagopal, and F. Wilczek, Phys. Lett. B **422**, 247 (1998), arXiv:hep-ph/9711395 .
[73] R. Rapp, T. Schäfer, E. V. Shuryak, and M. Velkovsky, Phys. Rev. Lett. **81**, 53 (1998), arXiv:hep-ph/9711396 .
[74] M. B. Hecht, C. D. Roberts, and S. M. Schmidt, Lect. Notes Phys. **578**, 218 (2001), arXiv:nucl-th/0012023 .
[75] M. Buballa, Phys. Rept. **407**, 205 (2005), arXiv:hep-ph/0402234 .
[76] K. Nawa, E. Nakano, and H. Yabu, Phys. Rev. D **74**, 034017 (2006), arXiv:hep-ph/0509029 .
[77] A. H. Rezaeian and H. J. Pirner, Nucl. Phys. A **779**, 197 (2006), arXiv:nucl-th/0606043 .
[78] G. Baym, T. Hatsuda, T. Kojo, P. D. Powell, Y. Song, and T. Takatsuka, Rept. Prog. Phys. **81**, 056902 (2018), arXiv:1707.04966 [astro-ph.HE] .
[79] Y. Fujimoto, K. Fukushima, and W. Weise, Phys. Rev. D **101**, 094009 (2020), arXiv:1908.09360 [hep-ph] .
[80] G. Malfatti, M. G. Orsaria, I. F. Ranea-Sandoval, G. A. Contrera, and F. Weber, Phys. Rev. D **102**, 063008 (2020), arXiv:2008.06459 [astro-ph.HE] .
[81] G. Malfatti, *Non-local quark models for description of dense matter in the cores of neutron stars*, Ph.D. thesis, La Plata U. (2020), arXiv:2010.14728 [nucl-th] .
[82] D. Blaschke, O. Ivanytskyi, and M. Shahrbaf, (2022), arXiv:2202.05061 [nucl-th] .
[83] D. Suenaga, K. Murakami, E. Itou, and K. Iida, Phys. Rev. D **107**, 054001 (2023), arXiv:2211.01789 [hep-ph] .
[84] W.-L. Yuan, J. Chao, and A. Li, Phys. Rev. D **108**, 043008 (2023), arXiv:2304.12050 [hep-ph] .
[85] J. Bardeen, L. N. Cooper, and J. R. Schrieffer, Phys. Rev. **106**, 162 (1957).
[86] J. Bardeen, L. N. Cooper, and J. R. Schrieffer, Phys. Rev. **108**, 1175 (1957).
[87] M. Harada, Y.-R. Liu, M. Oka, and K. Suzuki, Phys. Rev. D **101**, 054038 (2020), arXiv:1912.09659 [hep-ph] .

[88] M. Hess, F. Karsch, E. Laermann, and I. Wetzorke, Phys. Rev. D **58**, 111502 (1998), arXiv:hep-lat/9804023 .
[89] K. Orginos, PoS **LAT2005**, 054 (2006), arXiv:hep-lat/0510082 .
[90] C. Alexandrou, P. de Forcrand, and B. Lucini, Phys. Rev. Lett. **97**, 222002 (2006), arXiv:hep-lat/0609004 .
[91] R. Babich, N. Garron, C. Hoelbling, J. Howard, L. Lellouch, and C. Rebbi, Phys. Rev. D **76**, 074021 (2007), arXiv:hep-lat/0701023 .
[92] T. DeGrand, Z. Liu, and S. Schaefer, Phys. Rev. D **77**, 034505 (2008), arXiv:0712.0254 [hep-ph] .
[93] Y. Bi, H. Cai, Y. Chen, M. Gong, Z. Liu, H.-X. Qiao, and Y.-B. Yang, Chin. Phys. C **40**, 073106 (2016), arXiv:1510.07354 [hep-ph] .
[94] K. Watanabe and N. Ishii, Few Body Syst. **62**, 45 (2021), arXiv:2105.07969 [hep-lat] .
[95] K. Watanabe, Phys. Rev. D **105**, 074510 (2022), arXiv:2111.15167 [hep-lat] .
[96] A. Francis, P. de Forcrand, R. Lewis, and K. Maltman, JHEP **05**, 062 (2022), arXiv:2106.09080 [hep-lat] .
[97] A. Francis, P. de Forcrand, R. Lewis, and K. Maltman, Rev. Mex. Fis. Suppl. **3**, 0308082 (2022), arXiv:2201.03332 [hep-lat] .
[98] H. Noumi, PoS **Hadron2013**, 031 (2013).
[99] I. I. Y. Bigi, Y. L. Dokshitzer, V. A. Khoze, J. H. Kuhn, and P. M. Zerwas, Phys. Lett. B **181**, 157 (1986).
[100] N. Isgur and M. B. Wise, Phys. Lett. B **232**, 113 (1989).
[101] N. Isgur and M. B. Wise, Phys. Lett. B **237**, 527 (1990).
[102] H. Georgi, Phys. Lett. B **240**, 447 (1990).
[103] E. Eichten and B. R. Hill, Phys. Lett. B **234**, 511 (1990).
[104] M. Neubert, Phys. Rept. **245**, 259 (1994), arXiv:hep-ph/9306320 .
[105] R. Casalbuoni, A. Deandrea, N. Di Bartolomeo, R. Gatto, F. Feruglio, and G. Nardulli, Phys. Rept. **281**, 145 (1997), arXiv:hep-ph/9605342 .
[106] A. V. Manohar and M. B. Wise, *Heavy Quark Physics*, Cambridge Monographs on Particle Physics, Nuclear Physics and Cosmology (Cambridge University Press, 2000).
[107] M. Gell-Mann and M. Levy, Nuovo Cim. **16**, 705 (1960).
[108] Y. Nambu and G. Jona-Lasinio, Phys. Rev. **122**, 345 (1961).
[109] R. Delbourgo and M. D. Scadron, Mod. Phys. Lett. A **10**, 251 (1995), arXiv:hep-ph/9910242 .
[110] M. D. Scadron, G. Rupp, and R. Delbourgo, Fortsch. Phys. **61**, 994 (2013), arXiv:1309.5041 [hep-ph] .
[111] R. Delbourgo and M. D. Scadron, J. Phys. G **5**, 1621 (1979), [Addendum: J.Phys.G 6, 649 (1980)].
[112] J. Schaffner-Bielich and J. Randrup, Phys. Rev. C **59**, 3329 (1999), arXiv:nucl-th/9812032 .
[113] Y. Kuroda, M. Harada, S. Matsuzaki, and D. Jido, PTEP **2020**, 053D02 (2020), arXiv:1910.09146 [hep-ph] .
[114] B.-J. Schaefer and M. Wagner, Phys. Rev. D **79**, 014018 (2009), arXiv:0808.1491 [hep-ph] .
[115] M. Gell-Mann, R. J. Oakes, and B. Renner, Phys. Rev. **175**, 2195 (1968).
[116] M. Gell-Mann, Phys. Rev. **125**, 1067 (1962).
[117] S. Okubo, Prog. Theor. Phys. **27**, 949 (1962).
[118] M. Kamimura, Phys. Rev. A **38**, 621 (1988).
[119] E. Hiyama, Y. Kino, and M. Kamimura, Prog. Part. Nucl. Phys. **51**, 223 (2003).

[120] E. Eichten, K. Gottfried, T. Kinoshita, J. B. Kogut, K. D. Lane, and T.-M. Yan, Phys. Rev. Lett. **34**, 369 (1975), [Erratum: Phys.Rev.Lett. 36, 1276 (1976)].
[121] T. Yoshida, E. Hiyama, A. Hosaka, M. Oka, and K. Sadato, Phys. Rev. D **92**, 114029 (2015), arXiv:1510.01067 [hep-ph] .
[122] B. Silvestre-Brac, Few Body Syst. **20**, 1 (1996).
[123] T. Barnes, S. Godfrey, and E. S. Swanson, Phys. Rev. D **72**, 054026 (2005), arXiv:hep-ph/0505002 .
[124] K. Tanida *et al.* (Belle), in *18th International Conference on Hadron Spectroscopy and Structure* (2020) pp. 183–187, arXiv:1908.06235 [hep-ex] .
[125] R. Aaij *et al.* (LHCb), Phys. Rev. Lett. **123**, 152001 (2019), arXiv:1907.13598 [hep-ex] .
[126] R. Aaij *et al.* (LHCb), JHEP **06**, 136 (2020), arXiv:2002.05112 [hep-ex] .
[127] Y. Kawakami and M. Harada, Phys. Rev. D **97**, 114024 (2018), arXiv:1804.04872 [hep-ph] .
[128] Y. Kawakami and M. Harada, Phys. Rev. D **99**, 094016 (2019), arXiv:1902.06774 [hep-ph] .
[129] D. Suenaga and A. Hosaka, Phys. Rev. D **105**, 074036 (2022), arXiv:2202.07804 [hep-ph] .
[130] W. Weise, Prog. Theor. Phys. Suppl. **174**, 1 (2008).
[131] D. Suenaga and M. Oka, Phys. Rev. D **108**, 014030 (2023), arXiv:2305.09730 [hep-ph] .
[132] P. Costa, M. C. Ruivo, and Y. L. Kalinovsky, Phys. Lett. B **560**, 171 (2003), arXiv:hep-ph/0211203 .
[133] V. S. Timoteo and C. L. Lima, Braz. J. Phys. **36**, 208 (2006).
[134] H. Nagahiro, M. Takizawa, and S. Hirenzaki, Phys. Rev. C **74**, 045203 (2006), arXiv:nucl-th/0606052 .
[135] M. Cheng *et al.*, Eur. Phys. J. C **71**, 1564 (2011), arXiv:1010.1216 [hep-lat] .
[136] S. Sakai and D. Jido, Phys. Rev. C **88**, 064906 (2013), arXiv:1309.4845 [nucl-th] .
[137] S. Borsanyi, Z. Fodor, J. N. Guenther, R. Kara, S. D. Katz, P. Parotto, A. Pasztor, C. Ratti, and K. K. Szabo, Phys. Rev. Lett. **125**, 052001 (2020), arXiv:2002.02821 [hep-lat] .
[138] G. David, Rept. Prog. Phys. **83**, 046301 (2020), arXiv:1907.08893 [nucl-ex] .
[139] S. K. Choi *et al.* (Belle), Phys. Rev. Lett. **91**, 262001 (2003), arXiv:hep-ex/0309032 .
[140] S. K. Choi *et al.* (Belle), Phys. Rev. Lett. **100**, 142001 (2008), arXiv:0708.1790 [hep-ex] .
[141] M. Ablikim *et al.* (BESIII), Phys. Rev. Lett. **110**, 252001 (2013), arXiv:1303.5949 [hep-ex] .
[142] P. Koppenburg (LHCb collaboration), "List of hadrons observed at the LHC," LHCb-FIGURE-2021-001 (2021), (See 2022 update online).
[143] R. Aaij *et al.* (LHCb), Nature Phys. **18**, 751 (2022), arXiv:2109.01038 [hep-ex] .
[144] R. Aaij *et al.* (LHCb), Nature Commun. **13**, 3351 (2022), arXiv:2109.01056 [hep-ex] .
[145] J. P. Ader, J. M. Richard, and P. Taxil, Phys. Rev. D **25**, 2370 (1982).
[146] J. l. Ballot and J. M. Richard, Phys. Lett. B **123**, 449 (1983).
[147] H. J. Lipkin, Phys. Lett. B **172**, 242 (1986).
[148] S. Zouzou, B. Silvestre-Brac, C. Gignoux, and J. M. Richard, Z. Phys. C **30**, 457 (1986).
[149] L. Heller and J. A. Tjon, Phys. Rev. D **35**, 969 (1987).
[150] J. Carlson, L. Heller, and J. A. Tjon, Phys. Rev. D **37**, 744 (1988).

[151] B. Silvestre-Brac and C. Semay, Z. Phys. C **57**, 273 (1993).
[152] C. Semay and B. Silvestre-Brac, Z. Phys. C **61**, 271 (1994).
[153] C.-K. Chow, Phys. Rev. D **51**, 3541 (1995), arXiv:hep-ph/9411221 .
[154] C.-K. Chow, Phys. Rev. D **51**, 6327 (1995), arXiv:hep-ph/9412242 .
[155] S. Pepin, F. Stancu, M. Genovese, and J. M. Richard, Phys. Lett. B **393**, 119 (1997), arXiv:hep-ph/9609348 .
[156] D. M. Brink and F. Stancu, Phys. Rev. D **57**, 6778 (1998).
[157] B. A. Gelman and S. Nussinov, Phys. Lett. B **551**, 296 (2003), arXiv:hep-ph/0209095 .
[158] J. Vijande, F. Fernandez, A. Valcarce, and B. Silvestre-Brac, Eur. Phys. J. A **19**, 383 (2004), arXiv:hep-ph/0310007 .
[159] D. Janc and M. Rosina, Few Body Syst. **35**, 175 (2004), arXiv:hep-ph/0405208 .
[160] J. Vijande, A. Valcarce, and K. Tsushima, Phys. Rev. D **74**, 054018 (2006), arXiv:hep-ph/0608316 .
[161] D. Ebert, R. N. Faustov, V. O. Galkin, and W. Lucha, Phys. Rev. D **76**, 114015 (2007), arXiv:0706.3853 [hep-ph] .
[162] M. Zhang, H. X. Zhang, and Z. Y. Zhang, Commun. Theor. Phys. **50**, 437 (2008), arXiv:0711.1029 [nucl-th] .
[163] J. Vijande, A. Valcarce, and N. Barnea, Phys. Rev. D **79**, 074010 (2009), arXiv:0903.2949 [hep-ph] .
[164] Y. Yang, C. Deng, J. Ping, and T. Goldman, Phys. Rev. D **80**, 114023 (2009).
[165] G. Q. Feng, X. H. Guo, and B. S. Zou, (2013), arXiv:1309.7813 [hep-ph] .
[166] M. Karliner and J. L. Rosner, Phys. Rev. Lett. **119**, 202001 (2017), arXiv:1707.07666 [hep-ph] .
[167] E. J. Eichten and C. Quigg, Phys. Rev. Lett. **119**, 202002 (2017), arXiv:1707.09575 [hep-ph] .
[168] X. Yan, B. Zhong, and R. Zhu, Int. J. Mod. Phys. A **33**, 1850096 (2018), arXiv:1804.06761 [hep-ph] .
[169] A. Ali, Q. Qin, and W. Wang, Phys. Lett. B **785**, 605 (2018), arXiv:1806.09288 [hep-ph] .
[170] W. Park, S. Noh, and S. H. Lee, Nucl. Phys. A **983**, 1 (2019), arXiv:1809.05257 [nucl-th] .
[171] C. Deng, H. Chen, and J. Ping, Eur. Phys. J. A **56**, 9 (2020), arXiv:1811.06462 [hep-ph] .
[172] T. F. Caramés, J. Vijande, and A. Valcarce, Phys. Rev. D **99**, 014006 (2019), arXiv:1812.08991 [hep-ph] .
[173] E. Hernández, J. Vijande, A. Valcarce, and J.-M. Richard, Phys. Lett. B **800**, 135073 (2020), arXiv:1910.13394 [hep-ph] .
[174] G. Yang, J. Ping, and J. Segovia, Phys. Rev. D **101**, 014001 (2020), arXiv:1911.00215 [hep-ph] .
[175] M. A. Bedolla, J. Ferretti, C. D. Roberts, and E. Santopinto, Eur. Phys. J. C **80**, 1004 (2020), arXiv:1911.00960 [hep-ph] .
[176] M.-T. Yu, Z.-Y. Zhou, D.-Y. Chen, and Z. Xiao, Phys. Rev. D **101**, 074027 (2020), arXiv:1912.07348 [hep-ph] .
[177] P. C. Wallbott, G. Eichmann, and C. S. Fischer, Phys. Rev. D **102**, 051501 (2020), arXiv:2003.12407 [hep-ph] .
[178] Y. Tan, W. Lu, and J. Ping, Eur. Phys. J. Plus **135**, 716 (2020), arXiv:2004.02106 [hep-ph] .
[179] Q.-F. Lü, D.-Y. Chen, and Y.-B. Dong, Phys. Rev. D **102**, 034012 (2020), arXiv:2006.08087 [hep-ph] .

[180] E. Braaten, L.-P. He, and A. Mohapatra, Phys. Rev. D **103**, 016001 (2021), arXiv:2006.08650 [hep-ph] .
[181] G. Yang, J. Ping, and J. Segovia, Phys. Rev. D **102**, 054023 (2020), arXiv:2007.05190 [hep-ph] .
[182] Q. Qin, Y.-F. Shen, and F.-S. Yu, Chin. Phys. C **45**, 103106 (2021), arXiv:2008.08026 [hep-ph] .
[183] Q. Meng, E. Hiyama, A. Hosaka, M. Oka, P. Gubler, K. U. Can, T. T. Takahashi, and H. S. Zong, Phys. Lett. B **814**, 136095 (2021), arXiv:2009.14493 [nucl-th] .
[184] Q. Meng, M. Harada, E. Hiyama, A. Hosaka, and M. Oka, Phys. Lett. B **824**, 136800 (2022), arXiv:2106.11868 [hep-ph] .
[185] X. Chen and Y. Yang, Chin. Phys. C **46**, 054103 (2022), arXiv:2109.02828 [hep-ph] .
[186] Y. Jin, S.-Y. Li, Y.-R. Liu, Q. Qin, Z.-G. Si, and F.-S. Yu, Phys. Rev. D **104**, 114009 (2021), arXiv:2109.05678 [hep-ph] .
[187] K. Chen, R. Chen, L. Meng, B. Wang, and S.-L. Zhu, Eur. Phys. J. C **82**, 581 (2022), arXiv:2109.13057 [hep-ph] .
[188] O. Andreev, Phys. Rev. D **105**, 086025 (2022), arXiv:2111.14418 [hep-ph] .
[189] C. Deng and S.-L. Zhu, Phys. Rev. D **105**, 054015 (2022), arXiv:2112.12472 [hep-ph] .
[190] L. M. Abreu, H. P. L. Vieira, and F. S. Navarra, Phys. Rev. D **105**, 116029 (2022), arXiv:2202.10882 [hep-ph] .
[191] H.-W. Ke and Y.-L. Shi, Phys. Rev. D **105**, 114019 (2022), arXiv:2202.13380 [hep-ph] .
[192] C.-R. Deng and S.-L. Zhu, Sci. Bull. **67**, 1522 (2022), arXiv:2204.11079 [hep-ph] .
[193] L. M. Abreu, Nucl. Phys. B **985**, 115994 (2022), arXiv:2206.01166 [hep-ph] .
[194] X. Chen, F.-L. Wang, Y. Tan, and Y. Yang, Chin. Phys. C **47**, 023102 (2023), arXiv:2206.10917 [hep-ph] .
[195] L. Maiani, A. Pilloni, A. D. Polosa, and V. Riquer, Phys. Lett. B **836**, 137624 (2023), arXiv:2208.02730 [hep-ph] .
[196] M. Praszalowicz, Phys. Rev. D **106**, 114005 (2022), arXiv:2208.08602 [hep-ph] .
[197] L. M. Abreu, F. S. Navarra, M. Nielsen, and H. P. L. Vieira, in *25th International Conference in Quantum Chromodynamics* (2022) arXiv:2209.03862 [hep-ph] .
[198] J.-M. Richard, A. Valcarce, and J. Vijande, in *25th International Conference in Quantum Chromodynamics* (2022) arXiv:2209.07372 [hep-ph] .
[199] T.-W. Wu and Y.-L. Ma, Phys. Rev. D **107**, L071501 (2023), arXiv:2211.15094 [hep-ph] .
[200] J. Hoffmann, A. Zimermmane-Santos, and M. Wagner, PoS **LATTICE2022**, 262 (2023), arXiv:2211.15765 [hep-lat] .
[201] Y. Song and D. Jia, Commun. Theor. Phys. **75**, 055201 (2023), arXiv:2301.00376 [hep-ph] .
[202] V. Montesinos, M. Albaladejo, J. Nieves, and L. Tolos, Phys. Rev. C **108**, 035205 (2023), arXiv:2306.17673 [hep-ph] .
[203] Q. Meng, E. Hiyama, M. Oka, A. Hosaka, and C. Xu, Phys. Lett. B **846**, 138221 (2023), arXiv:2308.05466 [nucl-th] .
[204] S. H. Lee, S. Yasui, W. Liu, and C. M. Ko, Eur. Phys. J. C **54**, 259 (2008), arXiv:0707.1747 [hep-ph] .
[205] S. H. Lee and S. Yasui, Eur. Phys. J. C **64**, 283 (2009), arXiv:0901.2977 [hep-ph] .
[206] T. Hyodo, Y.-R. Liu, M. Oka, K. Sudoh, and S. Yasui, Phys. Lett. B **721**, 56 (2013), arXiv:1209.6207 [hep-ph] .
[207] S.-Q. Luo, K. Chen, X. Liu, Y.-R. Liu, and S.-L. Zhu, Eur. Phys. J. C **77**, 709

(2017), arXiv:1707.01180 [hep-ph] .
[208] T. Hyodo, Y.-R. Liu, M. Oka, and S. Yasui, (2017), arXiv:1708.05169 [hep-ph] .
[209] J.-B. Cheng, S.-Y. Li, Y.-R. Liu, Y.-N. Liu, Z.-G. Si, and T. Yao, Phys. Rev. D **101**, 114017 (2020), arXiv:2001.05287 [hep-ph] .
[210] J.-B. Cheng, S.-Y. Li, Y.-R. Liu, Z.-G. Si, and T. Yao, Chin. Phys. C **45**, 043102 (2021), arXiv:2008.00737 [hep-ph] .
[211] X.-Z. Weng, W.-Z. Deng, and S.-L. Zhu, Chin. Phys. C **46**, 013102 (2022), arXiv:2108.07242 [hep-ph] .
[212] T. Guo, J. Li, J. Zhao, and L. He, Phys. Rev. D **105**, 014021 (2022), arXiv:2108.10462 [hep-ph] .
[213] X.-Y. Liu, W.-X. Zhang, and D. Jia, Phys. Rev. D **108**, 054019 (2023), arXiv:2303.03923 [hep-ph] .
[214] F. S. Navarra, M. Nielsen, and S. H. Lee, Phys. Lett. B **649**, 166 (2007), arXiv:hep-ph/0703071 .
[215] J. M. Dias, S. Narison, F. S. Navarra, M. Nielsen, and J. M. Richard, Phys. Lett. B **703**, 274 (2011), arXiv:1105.5630 [hep-ph] .
[216] M.-L. Du, W. Chen, X.-L. Chen, and S.-L. Zhu, Phys. Rev. D **87**, 014003 (2013), arXiv:1209.5134 [hep-ph] .
[217] W. Chen, T. G. Steele, and S.-L. Zhu, Phys. Rev. D **89**, 054037 (2014), arXiv:1310.8337 [hep-ph] .
[218] Z.-G. Wang, Acta Phys. Polon. B **49**, 1781 (2018), arXiv:1708.04545 [hep-ph] .
[219] Z.-G. Wang and Z.-H. Yan, Eur. Phys. J. C **78**, 19 (2018), arXiv:1710.02810 [hep-ph] .
[220] S. S. Agaev, K. Azizi, B. Barsbay, and H. Sundu, Phys. Rev. D **99**, 033002 (2019), arXiv:1809.07791 [hep-ph] .
[221] H. Sundu, S. S. Agaev, and K. Azizi, Eur. Phys. J. C **79**, 753 (2019), arXiv:1903.05931 [hep-ph] .
[222] S. S. Agaev, K. Azizi, and H. Sundu, Nucl. Phys. B **951**, 114890 (2020), arXiv:1905.07591 [hep-ph] .
[223] L. Tang, B.-D. Wan, K. Maltman, and C.-F. Qiao, Phys. Rev. D **101**, 094032 (2020), arXiv:1911.10951 [hep-ph] .
[224] S. S. Agaev, K. Azizi, B. Barsbay, and H. Sundu, Phys. Rev. D **101**, 094026 (2020), arXiv:1912.07656 [hep-ph] .
[225] S. S. Agaev, K. Azizi, B. Barsbay, and H. Sundu, Eur. Phys. J. A **56**, 177 (2020), arXiv:2001.01446 [hep-ph] .
[226] Q.-N. Wang and W. Chen, Eur. Phys. J. C **80**, 389 (2020), arXiv:2002.04243 [hep-ph] .
[227] S. S. Agaev, K. Azizi, B. Barsbay, and H. Sundu, Chin. Phys. C **45**, 013105 (2021), arXiv:2002.04553 [hep-ph] .
[228] S. S. Agaev, K. Azizi, B. Barsbay, and H. Sundu, Eur. Phys. J. A **57**, 106 (2021), arXiv:2008.02049 [hep-ph] .
[229] S. S. Agaev, K. Azizi, and H. Sundu, Nucl. Phys. B **975**, 115650 (2022), arXiv:2108.00188 [hep-ph] .
[230] K. Azizi and U. Özdem, Phys. Rev. D **104**, 114002 (2021), arXiv:2109.02390 [hep-ph] .
[231] T. M. Aliev, S. Bilmis, and M. Savci, Phys. Rev. D **105**, 074038 (2022), arXiv:2111.01081 [hep-ph] .
[232] U. Özdem, Phys. Rev. D **105**, 054019 (2022), arXiv:2112.10402 [hep-ph] .
[233] S. Bilmiş, Turk. J. Phys. **45**, 390 (2021), arXiv:2201.06109 [hep-ph] .
[234] W. Detmold, K. Orginos, and M. J. Savage, Phys. Rev. D **76**, 114503 (2007),

arXiv:hep-lat/0703009 .
[235] M. Wagner (ETM, Y), PoS **LATTICE2010**, 162 (2010), arXiv:1008.1538 [hep-lat] .
[236] G. Bali and M. Hetzenegger (QCDSF), PoS **LATTICE2010**, 142 (2010), arXiv:1011.0571 [hep-lat] .
[237] P. Bicudo and M. Wagner (European Twisted Mass), Phys. Rev. D **87**, 114511 (2013), arXiv:1209.6274 [hep-ph] .
[238] Z. S. Brown and K. Orginos, Phys. Rev. D **86**, 114506 (2012), arXiv:1210.1953 [hep-lat] .
[239] Y. Ikeda, B. Charron, S. Aoki, T. Doi, T. Hatsuda, T. Inoue, N. Ishii, K. Murano, H. Nemura, and K. Sasaki, Phys. Lett. B **729**, 85 (2014), arXiv:1311.6214 [hep-lat] .
[240] P. Bicudo, K. Cichy, A. Peters, B. Wagenbach, and M. Wagner, Phys. Rev. D **92**, 014507 (2015), arXiv:1505.00613 [hep-lat] .
[241] P. Bicudo, K. Cichy, A. Peters, and M. Wagner, Phys. Rev. D **93**, 034501 (2016), arXiv:1510.03441 [hep-lat] .
[242] A. Francis, R. J. Hudspith, R. Lewis, and K. Maltman, Phys. Rev. Lett. **118**, 142001 (2017), arXiv:1607.05214 [hep-lat] .
[243] P. Bicudo, J. Scheunert, and M. Wagner, Phys. Rev. D **95**, 034502 (2017), arXiv:1612.02758 [hep-lat] .
[244] P. Bicudo, M. Cardoso, A. Peters, M. Pflaumer, and M. Wagner, Phys. Rev. D **96**, 054510 (2017), arXiv:1704.02383 [hep-lat] .
[245] A. Francis, R. J. Hudspith, R. Lewis, and K. Maltman, Phys. Rev. D **99**, 054505 (2019), arXiv:1810.10550 [hep-lat] .
[246] P. Junnarkar, N. Mathur, and M. Padmanath, Phys. Rev. D **99**, 034507 (2019), arXiv:1810.12285 [hep-lat] .
[247] L. Leskovec, S. Meinel, M. Pflaumer, and M. Wagner, Phys. Rev. D **100**, 014503 (2019), arXiv:1904.04197 [hep-lat] .
[248] R. J. Hudspith, B. Colquhoun, A. Francis, R. Lewis, and K. Maltman, Phys. Rev. D **102**, 114506 (2020), arXiv:2006.14294 [hep-lat] .
[249] P. Mohanta and S. Basak, Phys. Rev. D **102**, 094516 (2020), arXiv:2008.11146 [hep-lat] .
[250] P. Bicudo, A. Peters, S. Velten, and M. Wagner, Phys. Rev. D **103**, 114506 (2021), arXiv:2101.00723 [hep-lat] .
[251] M. Padmanath and N. Mathur, in *38th International Symposium on Lattice Field Theory* (2021) arXiv:2111.01147 [hep-lat] .
[252] P. Bicudo, Phys. Rept. **1039**, 1 (2023), arXiv:2212.07793 [hep-lat] .
[253] M. Padmanath, A. Radhakrishnan, and N. Mathur, (2023), arXiv:2307.14128 [hep-lat] .